January 2009

Investigations into the Ulnar Response to Mechanical Stimuli Activating Lamellar and Woven Bone Formation

Jennifer McKenzie
Washington University in St. Louis

WASHINGTON UNIVERSITY IN ST. LOUIS

School of Engineering and Applied Science

Department of Biomedical Engineering

Dissertation Examination Committee:
Matthew Silva, Chair
Fanxin Long
Shelly Sakiyama-Elbert
Linda Sandell
Larry Taber
Stavros Thomopoulos

INVESTIGATIONS INTO THE ULNAR RESPONSE TO MECHANICAL STIMULI ACTIVATING LAMELLAR AND WOVEN BONE FORMATION

by

Jennifer Ann McKenzie

A dissertation presented to the
Graduate School of Arts and Sciences
of Washington University in
partial fulfillment of the
requirements for the degree
of Doctor of Philosophy

December 2009

Saint Louis, Missouri

ABSTRACT OF THE DISSERTATION

Investigations into the Ulnar Response to Mechanical Stimuli Activating Lamellar and Woven Bone Formation

by

Jennifer Ann McKenzie

Doctor of Philosophy in Biomedical Engineering

Washington University in St. Louis, 2009

Professor Matthew Silva, Chairperson

Woven and lamellar bone formation can be stimulated using mechanical loading. Woven bone forms rapidly in response to damaging loading in a disorganized manner with low mineral density. In contrast, lamellar bone formation can be induced in the absence of damage, and is characterized by its slow, organized deposition and high density. In this dissertation, we first examined the molecular response to woven and lamellar bone formation using damaging and non-damaging dynamic loading protocols, respectively. We observed a significant increase in gene expression related to angiogenesis, cell proliferation and osteogenesis prior to woven bone formation, with significantly lower levels of expression associated with lamellar bone formation. To fully characterize the molecular responses of woven and lamellar bone we used a whole genome microarray. The micorarray results brought to light many inflammatory factors not previously investigated in our model, expanded previous findings about angiogenesis, and strengthened our understanding of the role of osteogenic pathways. Our investigations suggested that angiogenesis is required for successful woven bone formation. We used several angiogenic inhibitors, but were unable to prove the dependence of woven bone formation on angiogenesis. Finally, we sought to separate the effects of static and dynamic strains on bone formation. These findings demonstrate that in the absence dynamic strain, bone damage triggers a woven bone response that leads to a functional repair of whole-bone strength. Overall, the work done in this thesis has enhanced our understanding of bone formation. Future studies will expand on the microarray findings and clarify the role of angiogenesis in woven bone formation.

Acknowledgements

I would first like to thank my advisor, Matt Silva, for helping me develop into a research scientist. I would also like to thank all the current and former members of the Silva/Thomopoulos lab who assisted me on these projects, in particular Brian Uthgenannt, who helped me learn about rat forelimb loading, and especially Michael Brodt, Greg Wohl and Rosalina Das, who taught me nearly every technique I used in this thesis. Additionally, I would like to thank Elise Bixby for her enthusiasm and optimism when approaching analysis of the microarray data. I would like to acknowledge the National Institutes of Health/NIAMS (grant AR050211) and ASBMR for funding these projects.

Jenny McKenzie

Washington University in St. Louis

November, 2009

Contents

List of Tables

List of Figures

List of Equations

1 Introduction

1.1 Bone Fragility

All materials, including bone, are subject to failure if loaded to a force that exceeds the materials ultimate strength. Skeletal fragility and osteoporosis are common in our nations aging population and lead to an increased risk for hip, spine and wrist fracture (2000, Pramer 1999). The link between vasculature and bone has emerged as critical to bone formation (Brandi 2006, Fang 2005), and it has been hypothesized that vascular dysfunction may contribute to age-related osteoporosis (Alagiakrishnan 2003, Burkhardt 1987). Novel interventions to enhance bone mass could improve the quality of life and reduce mortality rates commonly associated with skeletal fragility (Cooper 1997) and osteoporotic fractures. In order to accomplish this, it is essential that we have a better understanding of the mechanisms that relate mechanical loading, angiogenesis and new bone formation.

1.2 Ex Vivo and In Vivo Bone Fatigue/Creep

Bone fatigue is characterized by diminished mechanical properties after repeated loading at a force well below the materials failure load. It causes loss of stiffness and strength and plays an important role in stress fractures (Burr 1997, Jones 1989, Shaffer 2001, Sterling 1992). Both the fatigue and creep behaviors of *ex vivo* compact bone have been well characterized (Carter 1985, Carter 1976, 1977, Pattin 1996). Bone exhibits three phases of fatigue (or creep) (Bowman 1994, Caler 1989, Carter 1977). The primary stage has an initial rapid increase in displacement followed by a gradually decreasing slope. The secondary stage follows with a relatively constant displacement rate. The tertiary stage begins with a rapid acceleration in displacement rate leading to fracture. This reproducible change in displacement (and associated mechanical property degradation) can be used as a functional assessment of damage level (Carter 1977, Danova 2003, Pattin 1996, Uthgenannt 2007b). Not only is this behavior applicable to *ex vivo* bone samples, *in vivo* bones behave in the same manner (Uthgenannt 2007b). Thus, through monitoring the *in vivo* displacement of a bone we have the ability to control the level of imposed

structural damage.

1.3 Strain and Fluid Flow Induced Using External Stimuli

Mechanical loading is required to maintain bone volume, as signaling cues trigger bone formation. According to the mechanostat theory, interactions between bone modeling (by osteoblasts forming bone) and bone remodeling (by osteoclasts resorbing bone) results in a net equilibrium in bone, which acts to maintain the mechanical integrity of the bone (Frost 1982, 2000). Low magnitude bone strain (smaller than typical strains) will result in a state of disuse and will cause a net loss of bone mass and strength, while high bone strain magnitudes (larger than typical strains) will result in an increase of bone mass and strength. Strain magnitude and location is highly correlated with changes in bone architecture (Frost 1982, Goodship 1979, Lanyon 1979, Lanyon 1984, Rubin 1984, 1985, 1987, Smith 1996). Pathological overload (supraphysiological strain magnitudes) results in microdamage or bone fracture. Fortunately, the bone's ability to adapt to the changes in the strain environment activates a repair process that initiates bone formation to restore the structural integrity of the bone.

The complex mechanisms used to induce bone formation following mechanical loading are not clearly defined. The level of bone strain is one of the determinants of bone formation. Load-induced fluid flow may be an additional important factor in bone metabolism (Cowin 1995, Turner 1994a, Weinbaum 1994). It has been postulated that load-induced fluid flow contributes to the movement of interstitial fluid through cortical bone tissue (Knothe Tate 2000a, Knothe Tate 1998, Knothe Tate 2000b). This fluid movement may activate signaling cues (though application of sheer stresses on the osteocytic cell processes) or enhance transport of cells and nutrients.

1.4 Bone Formation Response to Mechanical Loading

Studies have demonstrated formation of woven and lamellar bone in response to mechanical loading as a result of supraphysiological (overload) or physiological (normal) strains (Frost 1987a, Frost 1992, Hsieh 2002, Robling 2006a, Tami 2003). Woven bone is created in areas of the bone where large amounts of damage have been inflicted. In this case, woven bone forms rapidly to repair the structural competence of the damaged bone. In contrast, lamellar

bone typically forms after mild overload (Frost 1987a, Frost 1992) and is characterized by the organized manner in which new layers of bone are deposited. It has been hypothesized that strain magnitude determines whether woven or lamellar bone forms (Frost 1987a, Frost 1992, Hsieh 2001b, Turner 1994b). However, studies have disproved this notion by using lower, physiological strains to induce woven bone formation (Rubin 1995). Consequently, strain magnitude is not the only factor to distinguish between woven and lamellar bone formation.

1.5 Dynamic Loading

Dynamic loading has been widely used to stimulate bone formation. A forelimb loading model, initially developed by Torrance et al. in 1994 has been used by many investigators as a means to apply mechanical strain to the ulna (Figure 1.1). A strong benefit of this loading model is that the points of applied load are far away from the region undergoing the greatest response (Torrance 1994). This model has been used to characterize the bone response after multiple (Hsieh 2001a, Mosley 2002, Mosley 1997, Robling 2001b), as well as a single bout bouts of loading (Bentolila 1998, Kotha 2004, Lynch 2008, Matsuzaki 2007, Silva 2006a, Tami 2003, Uthgenannt 2007a, Uthgenannt 2007b, Verborgt 2000, Wohl 2009).

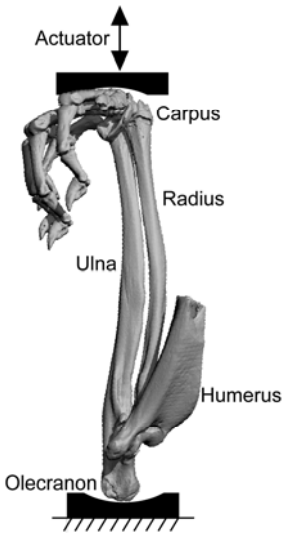

Figure 1.1. Medial view of bones in a right forelimb of a rat during simulated loading (image obtained by microCT). The majority of the load is transferred through the ulna (Kotha 2004), from the flexed carpus to the olecranon process. The natural curvature of the ulna allows for bending, which leads to increased strains on the medial side of the ulna near the midpoint. Image taken from (Uthgenannt 2007b).

1.5.1 Damaging Loading

By applying cyclic compression (fatigue loading) to the rat forelimb, an ulnar stress fracture can be created that triggers the two main tissue-level responses seen in humans – intracortical resorption and periosteal woven bone formation (Hsieh 2002, Tami 2003). A single bout of high strain fatigue loading has been used by our lab for a number of years. This model can generate several distinct levels of fatigue damage (as defined by loss of stiffness)(Danova 2003, Uthgenannt 2007b), but my investigations have focused on a moderate damage level (65% of the displacement to fracture; 2 Hz hsine, constant peak force). Damaging loading leads to a loss of stiffness and ultimate force following the loading event. The structural properties are restored within 2 weeks due to the rapid deposition of woven bone within the first 7 days, followed by densification of the newly laid bone (Hsieh 2002, Uthgenannt 2007a). The damaging fatigue loading model can be used to stimulate woven bone in a very controlled manner and is an excellent research tool to help characterize woven bone formation.

1.5.2 Non-damaging Loading

Dynamic loading that does *not* produce damage is a powerful stimulus for lamellar bone formation. Loading protocols have been established that produce lamellar bone (Castillo 2006, Forwood 1995, Robling 2000, Srinivasan 2003, Turner 1994b). Historically these loading protocols involve multiple days of loading(Forwood 1995) or form lamellar bone only on the endosteal surface of the bone while forming woven bone on the periosteal surface. Unlike other multi-day models, in order to tease out the differences between woven and lamellar bone formation, we wanted to only load the forelimbs only once. Not only would this ensure that the stimulus for bone formation occurred only once, but complications arising from multiple rounds of anesthesia, pain medication or loading stress would not complicate the healing response. Examining the stimulation of lamellar bone in the absence of woven bone will help characterize the mechanisms that separate these distinct two types of bone formation. In order to accomplish this goal we needed to develop a single-bout non-damaging loading protocol to stimulate lamellar but not woven bone formation. The non-damaging loading protocol should not compromise the structural integrity of the bone following loading (which would presumably lead to woven bone formation).

1.6 Static Loading

Creep loading, in contrast to fatigue, involves application of a static force. As with fatigue loading, bone can sustain progressive displacement and damage under creep loading (Caler 1989, Carter 1985). Previous studies of the bone response to creep loading have reported mixed findings. Positive osteogenic effects have been reported in dog femora (Meade 1984) and rabbit calvariae (Hassler 1980) after long term continuous loading studies. However, the majority of static loading has not shown the same osteogenic response as commonly seen in dynamic loading. Comparisons between static versus dynamic loading protocols applied to the rabbit tibia (Hert 1969), the turkey ulna (Lanyon 1984) and the rat ulna (Robling 2001b) demonstrated that static loading produced no osteogenic response whereas dynamic loading was osteogenic. In

growing rats, brief-duration static loading had an inhibitory effect on appositional bone formation while dynamic loading triggered an adaptive formation response. While non-damaging static loading is generally believed to be non-osteogenic (Lanyon 1984, Robling 2001b), to our knowledge the response of bone to creep loading that produces measurable bone damage has not been reported. Thus, we sought to develop a static creep loading model that could produce bone damage without dynamic loading and thereby provide a useful experimental tool to separate the effects of dynamic strain and damage.

1.7 Molecular Response to Loading

The molecular responses associated with mechanical stimulation of bone are not fully understood, but some pathways are known and others are emerging (Armstrong 2007, Dean 2009, Dimitriou 2005, Glowacki 1998, Liedert 2006, Turner 2009, Wohl 2009). Mechanical stimulation can lead to enhanced proliferation and differentiation of osteoblasts (Lau 2006) that increase bone mass. Gene expression studies using quantitative reverse transcriptase polymerase chain reaction (RT-PCR) have begun confirming physiological roles for many genes. Murine tibial bending has been shown to upregulate bone formation genes, including bone sialoprotein (*Bsp*) and osteocalcin (*Osc*)(Kesavan 2005). In the rat ulnar loading model, upregulation of genes related to angiogenesis, cell proliferation and osteogenesis (including *Bsp* and *Osc*) were found (Wohl 2009). In addition to qRT-PCR, microarrays have recently been used to evaluate changes in gene expression from studies using mechanical loading. Four days of tibial bending in mice led to differential expression of 346 genes compared to control, with evidence for upregulation of angiogenesis and growth factor signaling (Xing 2005). Although many gene expression studies have been completed, further studies are needed to clarify the molecular responses to mechanically stimulated woven and lamellar bone formation.

1.8 Vascular Response to Loading

There has been strong evidence linking bone formation (osteogenesis) and blood vessel formation (angiogenesis) (Brandi 2006, Matsuzaki 2007). Angiogenesis plays a role in skeletal

development (Gerber 1999, Pechak 1986) as well as fracture (Glowacki 1998, Hausman 2001) and stress fracture healing (Matsuzaki 2007, Wohl 2009). In these situations, angiogenesis precedes osteogenesis. In further support of the vascular response to loading, there is an increase in ^{18}F-fluoride uptake using positron emission tomography (PET) (Li 2005, Silva 2006a). Fluoride uptake is influenced by factors that expose mineral surface or increase blood flow (Blau 1972, Genant 1974). These studies suggest a strong link between angiogenesis and osteogenesis in the rat ulna following induction of a stress fracture. However, it has not been shown that in the absence of angiogenesis bone does not form after mechanical loading.

1.9 Scope and Procedure of the Dissertation

In this dissertation, we studied the effects of dynamic and static loading on the rat ulna. We used dynamic loading protocols that were damaging and non-damaging, leading to the formation of woven and lamellar bone, respectively. We also used a damaging static loading protocol to produce woven bone. First, we compared the molecular responses between damaging and non-damaging dynamic loading. For this study, we created a non-damaging loading protocol, a novel method for forelimb loading to stimulate lamellar bone formation in the ulnar mid-diaphysis. We performed a comprehensive mechanical analysis of non-damaging loading to ensure it caused no degradation of mechanical properties, did not stimulate woven bone and led to an increase in lamellar bone formation. We compared the early molecular responses of select genes between damaging and non-damaging loading (using quantitative real time PCR). Following that study, we expanded our findings using a microarray. Next, we investigated the importance of angiogenesis on woven and lamellar bone formation. Finally, we examined the effects of static loading on rats *in vivo*. For this study, we compared and contrasted two damaging loading protocols, in the absence and presence of dynamic strain.

In summary, we wanted to explore the molecular pathways associated with woven and lamellar bone, thereby identifying the mechanical and molecular factors that promote bone formation in the adult skeleton. Furthermore, we examined the link between angiogenesis and

osteogenesis for both woven and lamellar bone formation. Lastly, we investigated the roles of damage and dynamic strain on woven bone formation.

2 Differences in Angiogenesis and Cell Proliferation Distinguish Woven and Lamellar Bone Formation Following Mechanical Loading in the Rat Ulna

2.1 Abstract

Bone formation in the post natal skeleton can be induced using external mechanical stimuli. Comparisons were made between the responses of bone to damaging and non-damaging loading, promoting the formation of woven and lamellar bone, respectively. Bone formation was initiated using forelimb compression, a non-contact loading model. Damaging fatigue loading of the rat forelimb stimulates formation of robust periosteal woven bone at sites of ulnar damage. The objectives of our research were to develop a single-bout "lamellar" loading protocol, enabling synchronization of the timelines for damaging and non-damaging loading groups, and to study the gene expression changes caused by the stimulation of woven and lamellar bone. We hypothesized that 1) lamellar bone is stimulated in a single loading bout without creating bone damage, and 2) stimulation of woven bone formation (using damaging loading) induces abundant over-expression of genes associated with cell proliferation, angiogenesis and osteogenesis compared to stimulation of lamellar bone (using non-damaging loading). Our study demonstrated that a single bout of loading could produce increased lamellar bone formation in the absence of damage. Gene expression data gathered using quantitative real time PCR and immunohistochemistry demonstrated increases in cell proliferation and angiogenesis after damaging loading, but not for non-damaging loading. Damaging loading also increased vascularity, whereas non-damaging loading did not change vascularity compared to control. As time progressed, bone formation markers were higher in fold change for woven (between 4 and 89-fold) than for lamellar bone (near 2-fold), consistent with the differences in total bone volume formed ten days after loading. In summary, the early molecular changes in cell proliferation and angiogenesis distinguish loading-induced woven from lamellar bone formation in the adult skeleton.

2.2 Key terms

Woven bone, lamellar bone, gene expression, ulna, loading, angiogenesis

2.3 Introduction

Osteogenesis occurs by formation of woven or lamellar bone. In the post natal skeleton, woven bone forms under conditions that require rapid mineral deposition such as in distraction osteogenesis, fracture healing and stress fracture repair (Jazrawi 1998, Johnson 1963, Mori S 2001, Tami 2003). Histologically, woven bone is characterized by relatively poor organization, low mineral density and high cellularity (Mori S 2001). By contrast, lamellar bone forms at a slower rate during normal skeletal growth and in response to mild anabolic stimuli. It is more highly organized, denser and has fewer cells compared to woven bone. The underlying mechanisms that trigger woven versus lamellar bone formation have been addressed by several authors (Forwood 1994, Komori 2008, Maruyama 2007, Turner 1994b), but remain poorly understood. Because in vivo mechanical loading can stimulate either woven or lamellar bone formation (Turner 1994b), it provides an experimental approach to study the processes that lead to these two distinct types of bone.

Mechanical loading that generates hyperphysiological bone strain and/or damage leads to woven bone formation (Frost 1987b). Fatigue loading of the rat forelimb has been used to generate bone damage resulting in an ulnar stress fracture. After a single bout of damaging fatigue loading, there is a robust repair response characterized by periosteal woven bone formation at the stress fracture site (Danova 2003, Tami 2003, Uthgenannt 2007b). Prior to woven bone formation there is an increase in expression of genes related to cell proliferation, angiogenesis and osteogenesis (Wohl 2009). Other models of woven bone formation have also reported increased proliferation (Ai-Aql 2008, Wang 2003), vascularity (Carvalho 2004, Fang 2005, Gerstenfeld 2003b, Hausman 2001), and osteogenic gene expression (Ai-Aql 2008, Gerstenfeld 2003a).

Mechanical loading that generates modest levels of bone strain without creating damage can stimulate lamellar bone formation (Turner 1994b). The cell and molecular responses that precede lamellar bone formation have not been extensively studied, although some work has been done. Cell proliferation was increased three days after stimulation of endocortical lamellar bone formation using tibial bending (Turner 1998). Increases in angiogenic and osteogenic gene

expression were reported after four days of tibial bending in mice (Xing 2005). However, it was not clear whether the loading protocol induced lamellar or a combination of woven and lamellar bone formation, because tibial bending protocols often form lamellar bone only on the endosteal surface, with woven bone on the periosteal surface (Akhter 1998, Robling 2000, Turner 1994b). To better characterize the cell and molecular changes associated with lamellar bone formation requires a loading protocol that does not induce woven bone formation. Forelimb compression and tibial bending protocols that stimulate lamellar bone formation have been reported (Forwood 1995, Hsieh 2001b, Robling 2000, Srinivasan 2003), however these protocols typically involve multiple days of loading. A limitation of multi day protocols for studies of gene expression is that events triggered by the first bout of loading cannot be separated from events triggered by subsequent bouts. To overcome this limitation, we wanted to develop a single-bout loading protocol that stimulated a significant increase in lamellar bone formation in the rat ulna.

The first goal of our project was to establish a loading protocol to stimulate *only* lamellar bone. The lamellar loading protocol needed to satisfy the following requirements: 1) loading in a single bout, 2) non-damaging, 3) no woven bone formation as a result of loading, and 4) a significant increase in lamellar bone formation on the loaded ulna compared to control. We hypothesized that lamellar bone is stimulated in a single bout of non-damaging loading. Our second goal was to compare the formation of lamellar bone induced by this protocol to the formation of woven bone induced by the previously established damaging fatigue protocol (Uthgenannt 2007a). We hypothesized that stimulation of woven bone formation (using damaging loading) induces abundant over-expression of genes associated with cell proliferation, angiogenesis and osteogenesis compared to stimulation of lamellar bone (using non-damaging loading).

2.4 Methods

The right forelimbs of 155 adult male rats (F344, Harlan) age 4 ½ - 5 ½ mo (337.1 ± 21.9 g), were loaded in axial compression to stimulate woven or lamellar bone formation at the ulnar mid-diaphysis (Tables 2.1 and 2.2). Contralateral left forelimbs served as non-loaded controls.

With the animals anesthetized (1-3% isofluorane), right forelimbs were positioned in a loading fixture connected to a servohydraulic materials testing machine (Instron 8841) and a 0.3 N compressive pre-load applied. Rats designated for damaging loading (fatigue protocol) had the right forelimbs cyclically loaded in a single bout (2 Hz, 18 N) to a total displacement of 1.3 mm (avg. cycles 5279 ± 4544), a protocol shown to cause a 70% decrease in ulnar stiffness (Uthgenannt 2007b) and to induce abundant woven bone formation (Uthgenannt 2007a). A second loading protocol was used to stimulate lamellar bone formation as described below. After loading the animals received analgesia (i.m., 0.05 mg/kg buprenorphine) and were returned to their cages. All animals recovered well from anesthesia and mechanical loading. They were allowed normal cage activity and ad libitum access to water and chow. Rats were euthanized by carbon dioxide asphyxia at 1 hr (day 0), 1 day, 3 days, or 10 days after loading. Right and left ulnae were dissected. This study was approved by our animal studies committee.

Table 2.1. Waveforms tested for use in a single-bout lamellar loading protocol. Woven bone formation (day 10) was used as the primary exclusion criterion. Ultimately, a 15 N rest-inserted (100 cycle) waveform was chosen based on low cycle number, low total displacement and absence of woven bone formation.

	Haversine waveform (2 Hz)					Rest-inserted waveform (0.5 s load-unload followed by 9.5 sec rest)		
Number of animals loaded	7	7	10	13	10	12	2	6
Peak loading force (N)	14	15	16	17	18	15	15	18
Loading cycles	230	230	230	230	230	100	200	100
Total disp. (mm)	0.413 ± 0.015	0.399 ± 0.047	0.365 ± 0.028	0.407 ± 0.04	0.392 ± 0.036	0.087 ± 0.051	0.173 ± 0.062	0.108 ± .042
Loading-induced woven bone formation?	No (0/7)	Yes (1/7)	Yes (2/10)	Yes (3/13)	Yes (5/10)	No (0/12)	No (0/2)	Yes (2/6)

Table 2.2. Forelimb loading parameters used for damaging (woven) and non-damaging (lamellar) loading for gene expression, immunohistochemistry and vascular perfusion outcomes.

	Gene Expression		Immunohistochemistry		Vascular Perfusion	
	Woven	Lamellar	Woven	Lamellar	Woven	Lamellar
Initial animal number	18	20	9	10	8	6
Final animal number	18	18	7	8	4	5
Applied force (N)	18	15	18.4 ± 0.7	15	18	15
Loading cycles	5279 ± 1071	100	8868 ± 8490	100	13,604 ± 7126	100
Displacement (mm)	1.30	0.10 ± 0.06	1.30	0.10 ± 0.06	1.30	0.18 ± 0.08

2.4.1 Development of a Single Bout Loading Protocol to Stimulate Lamellar Bone Formation

In a preliminary experiment, we investigated two waveforms and a range of peak forces from 14-18 N (1900-2400 microstrain) (Uthgenannt 2007b). Our goal was to determine a suitable single-bout loading protocol that did not cause bone damage and stimulated only lamellar bone formation (Table 2.1). The first waveform was a 2 Hz hsine, the same as used in damaging loading. The second waveform was a rest-inserted trapezoid. In this waveform the load/unload period is the same as in the fatigue waveform, but with a 9.5 second delay between loading cycles. Five of the loading conditions were rejected because woven bone was observed on at least one histological section. There were three loading protocols that did not result in woven bone formation. The option using a 2 Hz hsine waveform (14 N) was rejected because the total displacement was close to loading protocols that did stimulate woven bone formation. Of the two remaining protocols, we chose a 100 cycle, 15 N rest-inserted waveform for further characterization.

The right forelimbs of 29 rats were loaded in cyclic compression for a single bout of 100 cycles using the 15 N rest-inserted waveform. We assessed the effects of loading on mechanical properties, bone damage and bone formation. Twelve rats were euthanized immediately after loading for three-point bending tests (Instron 8841). Ulnae were positioned on supports 15 mm apart and a displacement ramp (0.5 mm/s) was applied on the medial surface at the midpoint. Structural properties were determined from force-displacement curves (Labview 7.0). Five additional rats were euthanized immediately after loading to assess damage with basic fuchsin

staining (Burr 1995). Briefly, upon dissection ulnae were placed into 10% formalin for 24 hours. Bones were then subjected to graded fuchsin (80%, 90% and 100%) in a vacuum for 2 hr intervals before being embedded in plastic. Forelimbs were sectioned 1 mm distal to the midpoint (100 μm thick) and imaged using a confocal microscope (Carl Zeiss, LSM 510). Twelve rats were euthanized on day 10 to measure bone formation using dynamic histomorphometry. Rats were given intraperitoneal injections of calcein green (5 mg/kg, Sigma) on day 3 and alizarin-complexone (30 mg/kg, Sigma) on day 8 before being euthanized on day 10. Ulnae were then embedded in methylmethacrylate (Sigma) using standard procedures. Sections (100 μm thick) were cut 1 mm distal to the midpoint (D1) (Leica Microsystems, SP 1600). Each section was mounted on a glass slide and imaged on a microscope (Olympus, DP-30) using fluorescein isothiocyanate (Jacobsen) and tetramethylrhodamine isothiocynate (TRITC) filters for calcein and alizarin, respectively. The sections were analyzed (Bioquant) for bone area, bone surface (BS), mineralizing surface (MS), bone formation rate (BFR) and mineral apposition rate (MAR).

2.4.2 Gene Expression

Forelimbs were loaded using a single-bout protocol to stimulate woven or lamellar bone formation (Table 2.2). Rats were euthanized on day 0 (1 hr), day 1 or day 3 for assessment of ulnar gene expression using quantitative real time PCR (qRT-PCR) as described (Wohl 2009). Both the loaded (right) and non-loaded control (left) ulnae were frozen in liquid nitrogen immediately upon dissection. A central 5 mm piece of each ulna was pulverized, suspended in trizol, and mixed with chloroform before separating the nucleic acid phase (phase lock gel tube, Eppendorf). The total RNA was isolated using an RNeasy mini kit (Qiagen). RNA integrity was quantified (Nanodrop, ND-1000) and verified (Agilent 2100 bioanalyzer). First strand cDNA was synthesized (Superscript III, Invitrogen) from total RNA (500 ng). qRT-PCR reactions were carried out at 20 μL total volume and measured with *Power* SYBR® green (7300 Real-Time PCR System, Applied Biosystems). Samples were run in triplicate and the average was used for further analysis. Primers were validated previously (Wohl 2009) or purchased as predesigned sets (QuantiTect Primer Assays, Qiagen). Eleven target genes were evaluated including histone

cluster 1, H4b (*Hist4*; marker for cell proliferation), cyclin D1 (*Ccnd1*; cell cycle protein); vascular endothelial growth factor A (*Vegf*; angiogenic morphogen), hypoxia-inducible factor 1, alpha subunit (*Hif1a*; hypoxia marker), platelet/endothelial cell adhesion molecule 1 (*Pecam*; endothelial cell marker), bone morphogenetic protein 2 (*Bmp2*; osteogenesis-angiogenesis coupling factor), bone sialoprotein (*Bsp*; matrix glycoprotein mediating cell adhesion), runt related transcription factor 2 (*Runx2*; required for osteoblast differentiation), bone gamma-carboxyglutamate (gla) protein (osteocalcin) (*Bglap*; marker for fully differentiated osteoblasts), osterix (*Osx*; required for osteoblast formation), and patched homolog 1 (*Ptch*; marker of activated hedgehog pathway). Data were analyzed using relative quantification ($2^{-\Delta\Delta C_T}$) comparing loaded to non-loaded ulnae by normalizing to glyseraldehyde-3-phosphate dehydrogenase (*Gapdh*).

2.4.3 Immunohistochemistry

BMP2, HIF1a and proliferating cell nuclear antigen (PCNA) proteins were localized using immunohistochemistry. Following dissection, forelimbs (ulna and radius with some muscle tissue left intact) were dissected, fixed overnight in 4% paraformaldehyde at room temperature and decalcified in 14% EDTA. Specimens were embedded in paraffin and 5 µm sections were cut 1 mm distal to the midpoint. Primary antibodies for BMP2 (Santa Cruz, sc-6895) and HIF1a (Santa Cruz, sc-22538) were diluted to 1:50 and 1:100, respectively. Sections were deparaffinized and rehydrated then washed in dH_20, treated with H_20_2 (10 min). Antigen retrieval for BMP2 was performed using a decloaking chamber (Biocare Medical, 95°C, 10 min) containing sodium citrate buffer (pH 6.0). Antigen retrieval for HIF1a was performed in an oven (37 deg, 15 min) using 5% pepsin. After antigen retrieval specimens were cooled and washed in PBS. Sections were blocked with 10% of the appropriate serum (room temperature, 1 hr) and then incubated overnight (4°C) with the optimized dilution of primary antibody. The next day, slides were washed, incubated with a 1:400 dilution of streptavidin (Sigma), washed, incubated with 1:400 of the appropriate secondary antibody, washed, then visualized using 3,3'-diaminobenzidine (DAB) for a predetermined time. Slides were dehydrated, counterstained lightly with Mayer's hematoxylin, coverslipped, and examined under light field microscopy. PCNA immunohistochemistry was done

according to the manufacturer's protocol (Invitrogen). The antibody was visualized with DAB after exposure for 5 minutes.

2.4.4 Vascular Perfusion

Vascular perfusion was performed as previously described (Matsuzaki 2007). Three days after loading the rats were anesthetized by intraperitoneal injection of ketamine (87 mg/kg) and xylazine (13 mg/kg). Heparin (10 mL, 100 USP units/mL) was injected (18-gauge catheter in left ventricle) to inhibit clotting. The vasculature was irrigated with 100 mL saline and 60 mL of a silicone rubber solution was injected (MICROFIL®, MV-122; Flow Tech). Following injection, the specimens were stored at 4°C overnight to allow the rubber to cure. The forelimbs were dissected and placed in 10% formalin overnight. MicroCT (uCT 40, Scanco Medical, 45 kV, 200 ms, 16 μm resolution) was used to image 1.6 mm of the central ulna starting 1 mm distal to the midpoint and ending 0.4 mm proximal to the midpoint. The forelimbs were then decalcified in 14% EDTA for 3 weeks. Thin (5 μm) sections were cut 1 mm distal to the midpoint from paraffin embedded blocks and mounted on glass slides. Slides were stained with hematoxylin and eosin (H&E) before being analyzed for vessel number and area (Bioquant). A number of animals (n=4 for damaging loading and n=1 for non-damaging loading) were excluded from analysis due to poor perfusion.

2.4.5 Statistics

Two-way analysis of variance (ANOVA) was used to compare across treatment groups and timepoints. Differences between individual timepoints were assessed using Fisher's protected least significant difference test. Differences between right and left ulnae were assessed using paired t-tests. Significance was defined at $p<0.05$.

2.5 Results

2.5.1 A Single Bout of Loading Stimulates Increased Lamellar Bone Formation in the Absence of Damage

We subjected forelimbs to a single bout of loading using a rest-inserted trapezoidal waveform (0.5 s triangle load-unload to 15 N followed by 9.5 s rest; 100 cycles). Results indicate that the loading protocol was non-damaging and stimulated lamellar bone formation. Three-point bending tests demonstrated no significant differences in structural properties between loaded and control ulnae (Table 3). There was no obvious difference in basic fuchsin staining between loaded and control ulnae. In contrast, ulna loaded by a damaging fatigue protocol had diffuse staining, indicating extensive damage (Figure 2.1). Dynamic histomorphometry revealed that ten days after "non-damaging" loading, there was no woven bone observed on loaded or control specimens, while lamellar bone formation was increased on loaded ulnae. Mineralized surface (MS/BS) was increased by 50% in loaded ulnae vs. control, while MAR and BFR/BS were increased 24 and 92%, respectively ($p<0.05$) (Figure 2.1, Table 2.3). In summary, the rest-inserted trapezoidal waveform (15 N, 100 cycles) satisfied all of the criteria for a non-damaging, single-bout induction of lamellar bone formation.

Table 2.3. Mechanical property (day 0) and bone formation (day 10) outcomes from non-damaging loading (n=12/group). Non-damaging loading does not reduce mechanical properties in the loaded ulna. Histological variables (mean ± SD) showed increased lamellar bone formation after loading. Mineralizing surface per bone surface (MS/BS), bone formation rate per bone surface (BFR/BS) and mineral apposition rate (MAR) were measured 1 mm distal to the midpoint of the ulna. *$p<0.05$ vs. non-loaded

	Ultimate Force (N)	Stiffness (N/mm)	Energy to Fracture (N*mm)	MS/BS (%)	BFR/BS (μm/day)	MAR (μm/day)
Non-loaded (Left ulna)	12.9 ± 1.4	20.9 ± 3.0	22.7 ± 4.1	47.3 ± 16.2	0.68 ± 0.32	1.41 ± 0.45
Loaded (Right ulna)	12.8 ± 0.9	20.2 ± 1.7	26.4 ± 5.2	74.0* ± 11.7	1.30* ± 0.30	1.75* ± 0.20

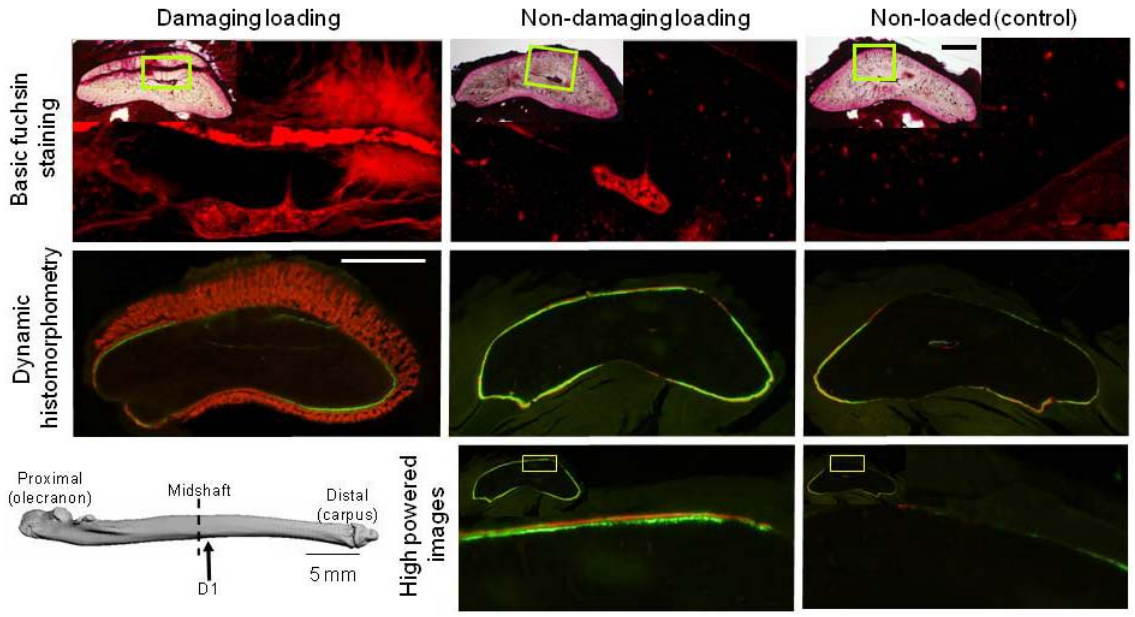

Figure 2.1. Damaging loading (18 N hsine; 1.3 mm accumulated disp.) led to formation of woven bone, while non-damaging loading (15 N rest-inserted waveform; 100 cycles) led to formation of lamellar bone. Basic fuchsin staining on day 0 (immediately after loading) was used to assess damage on bright field [inset] and fluorescent images. Damaging fatigue loading had high amounts of diffuse ulnar staining while both non-damaging and non-loaded ulnae had no diffuse damage. Bone formation (assessed by dynamic histomorphometry) 10 days after loading from representative histological sections illustrate extensive woven bone formation after damaging loading. There is increased labeled surface around the periosteum after non-damaging loading compared to non-loaded control. A high powered view of double labeled surface on medial side of ulnae demonstrate increased lamellar bone formation in non-damaging loaded compared to controls. All sections were taken 1 mm distal to the midpoint (D1). (scale bar 500 micron unless otherwise indicated)

2.5.2 Cell Proliferation is Upregulated Early After Damaging Loading, but Not for Non-Damaging Loading

Cell proliferation marker *Hist4* was upregulated 5- and 13-fold on days 1 and 3, respectively, for damaging loading but was unchanged for non-damaging loading bone compared

to controls (Table 2.4, Figure 2.2). Damaging loading also strongly upregulated the cell cycle marker *Ccnd1* (5- and 17-fold on days 1 and 3, respectively), whereas non-damaging loading led to only a modest increase on day 3 (2-fold). Histologically, there was a clear periosteal expansion seen on H&E stained sections on day 1 after damaging loading, but no qualitative differences between controls and ulna loaded with the non-damaging protocol (Figure 2.2). Consistent with qRT-PCR, PCNA staining was absent on sections from control and ulnae loaded with the non-damaging protocol on days 1 and 3. In contrast, consistent with a recent report (Wohl 2009), there was PCNA staining after damaging loading on the medial and lateral sides of the ulna on days 1 and 3 (not shown).

Table 2.4. Fold change in gene expression (loaded/control) were greater for woven than for lamellar bone formation. A fold change of 1 indicates no change from control. * $p<0.05$ vs. control, [a] $p<0.05$ vs Day 0, [b] $p<0.05$ vs Day 1, [#] $p<0.05$ vs. lamellar

Gene Name	Gene Symbol	Damaging loading (woven bone)			Non-damaging loading (lamellar bone)		
		Day 0 (1 hr)	Day 1	Day 3	Day 0 (1 hr)	Day 1	Day 3
Histone H4	*Hist4*	0.87 ± 0.46	5.69*[a#] ± 4.15	13.41*[ab#] ± 4.71	0.98 ± 0.33	1.06 ± 0.65	0.75 ± 0.35
Cyclin D1	*Ccnd1*	1.37 ± 0.39	4.99*[#] ± 1.51	16.86*[#ab] ± 5.31	1.42 ± 0.57	1.69 ± 1.28	1.86* ± 0.51
Vascular endothelial growth factor	*Vegf*	1.69*[#] ± 0.26	3.03*[a#] ± 1.24	3.57*[a#] ± 0.50	1.08 ± 0.14	1.15 ± 0.22	1.20* ± 0.11
Hypoxia-inducible factor 1, alpha subunit	*Hif1a*	1.60* ± 0.40	9.19*[a#] ± 3.14	15.18*[ab#] ± 3.83	1.23 ± 0.30	1.26 ± 0.44	1.44* ± 0.34
Platelet/endothelial cell adhesion molecule 1	*Pecam*	1.15 ± 0.29	2.54*[a#] ± 0.54	4.73*[ab#] ± 0.88	1.14 ± 0.29	1.15 ± 0.36	1.58*[ab] ± 0.33
Bone morphogenetic protein 2	*Bmp2*	2.53* ± 0.46	6.50*[a#] ± 4.03	6.98*[a#] ± 2.49	1.94* ± 0.51	1.70 ± 0.84	1.90* ± 0.44
Bone sialoprotein	*Bsp*	1.16 ± 0.25	13.57*[#] ± 4.92	88.98*[#ab] ± 28.84	1.10 ± 0.38	1.57 ± 0.74	1.93*[a] ± 0.31
Runt related transcription factor 2	*Runx2*	1.03 ± 0.31	2.55*[#] ± 0.78	8.18*[ab#] ± 2.57	1.05 ± 0.42	1.31 ± 0.51	1.61*[a] ± 0.35
Osteocalcin	*Bglap*	0.99 ± 0.31	0.39*[#] ± 0.10	3.85*[ab#] ± 1.09	1.03 ± 0.42	1.43 ± 0.67	2.24*[ab] ± 0.64
Osterix	*Osx*	0.5*[#] ± 0.17	3.81*[#] ± 2.03	24.01*[ab#] ± 9.53	1.00 ± 0.35	1.61 ± 0.76	2.14*[a] ± 0.45
Patched homolog 1	*Ptch*	0.86 ± 0.33	1.97* ± 0.97	6.65*[ab#] ± 2.92	0.94 ± 0.32	1.46 ± 0.69	1.56*[a] ± 0.30

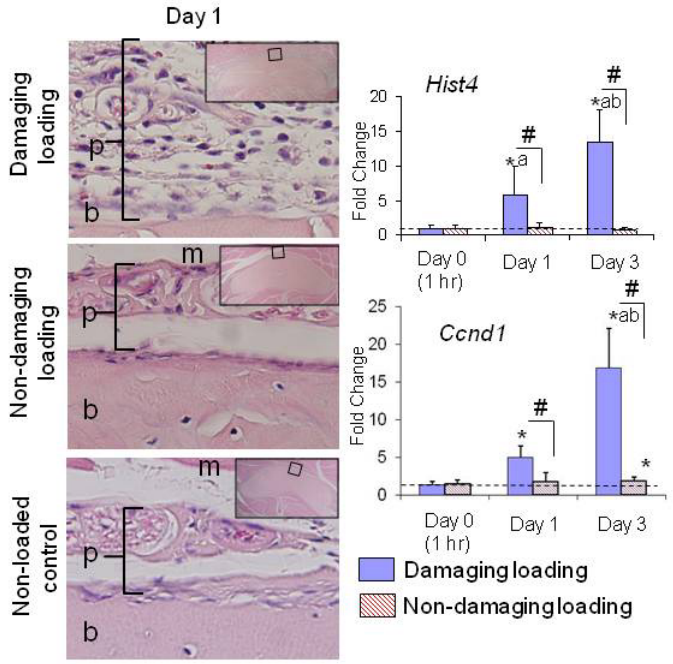

Figure 2.2. Damaging loading (stimulating woven bone) led to periosteal expansion and increased cell proliferation on day 1, while non-damaging loading (stimulating lamellar bone) was unchanged from control. Hematoxylin and eosin (H&E) staining of sections demonstrate cortical bone cracks [inset] following damaging loading. Damaging loading increased expression of cell proliferation markers compared to non-damaging loading and control. Gene expression for *Hist4* and *Ccnd1* (qRT-PCR) demonstrate a significant increase (loaded/non-loaded) on days 1 and 3 only in the ulnae stimulated to produce woven bone. There was no increase in *Hist4* after non-damaging loading at any timepoint. All histological sections are taken 1 mm distal to the midpoint (scale bar 50 μm). b–original cortical bone; p-periosteum; m-muscle; $^{a}p<0.05$ vs Day 0; $^{b}p<0.05$ vs. Day 1; * $p<0.05$ Loaded vs. non-loaded; $^{\#}p<0.05$ Non-damaging vs damaging loading

2.5.3 Early Angiogenesis Distinguishes Damaging from Non-Damaging Loading

Expression of *Vegf* and *Hif1a* were upregulated 1.6 fold one hour after damaging loading (Table 2.4), indicating an early angiogenic stimulus. Expression of *Hif1a* increased to 9- and 15-fold on days 1 and 3 after damaging loading, whereas non-damaging loading led to a small but significant increase on day 3 (1.4-fold). Damaging loading upregulated *Vegf* and *Pecam* expression on days 1 and 3 (between 3- and 5-fold) while non-damaging loading only increased

expression on day 3 (less than 1.6-fold). Consistent with RT-PCR, histological staining of HIF1a was increased in ulnar sections after damaging loading, but not after non-damaging loading on days 1 (Figure 2.3) and 3 (not shown). Bone morphogenetic protein 2 (*Bmp2*), known as an osteogenic-angiogenic coupling factor (Wozney 1998), was upregulated at all timepoints after both types of loading (between 2- and 7-fold), with the exception of non-damaging loading at day 1 (1.7 fold, $p=0.11$). The fold changes were consistently near 2-fold following non-damaging loading and 6-fold (days 1 and 3) after damaging loading ($p<0.05$). Immunohistochemistry for BMP2 showed protein localized to some periosteal lining cells as well as the interior lining (intima) of most blood vessels (Figure 2.3), consistent with a previous report (Wohl 2009). Results for BMP2 on day 3 were similar to day 1 (not shown).

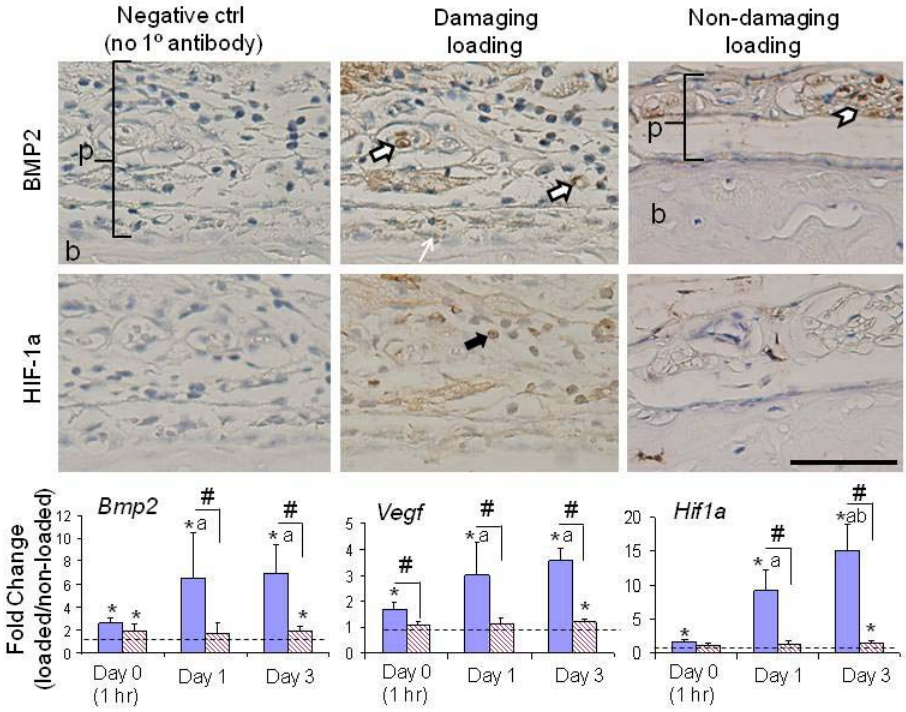

Figure 2.3. Immunohistochemistry staining at day 1 show increased localized protein expression of BMP2 and HIF1a following stimulation of woven compared to lamellar bone formation. Both loading protocols increased BMP2 staining on day 1 in a small number of lining cells (thin arrow), as well as neuro-vascular bundles (arrowhead). There was additional staining in connective tissue and blood vessels were outlined both in the periosteum (block arrow) and muscle (not

shown) after damaging loading. HIF-1a staining is present in small amounts after non-damaging loading, and is much more prominent in neutrophils after damaging loading (black arrow). Staining for BMP2 and HIF1a is absent in the negative control (damage-loaded ulna, no primary antibody). Gene expression (qRT-PCR) confirms a significant increase in the loaded limb at nearly all timepoints for *Bmp2*, regardless of loading group. *Vegf* is upregulated one hour after loading (day 0) for woven bone formation and the upregulation is sustained through day 3. *Hif-1a* is upregulated on days 1 and 3 for woven bone, over 10-fold higher than lamellar bone at day 3. All sections are taken 1 mm distal to the midpoint. b–original cortical bone, p-periosteum ; scale bar 50 microns. Legend for gene expression plots is shown in Figure 2.2.

Woven bone formation increased vascularity assessed using perfusion followed by microCT and histological analysis on day 3 (Figure 2.4). The vessel number, area and volume were all increased significantly when comparing damaging to non-damaging loading, with no differences between non-damaging loading and control.

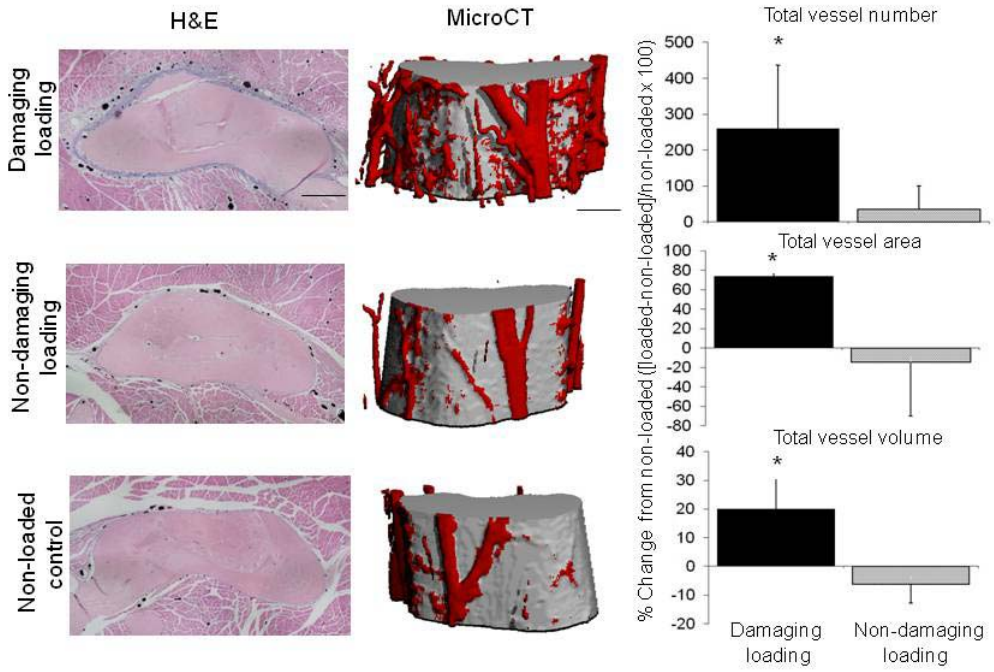

Figure 2.4. Vascularity increased in response to damaging loading. The vascular response was assed using histological sections (stained with H&E) and microCT imaging. H&E stained sections for control and lamellar bone formation are qualitatively different from sections where woven bone formation is occurring (vessels are black dots). Similarly on microCT the appearance of blood vessels is increased after damaging loading. Quantitatively, there is an increase in the number, area and volume of vessels associated with woven bone formation when calculating a percentage change between loaded and control. There is no difference in vessel number, area or volume between ulnae loaded with the non-damaging protocol and controls. (n=4-5/group; scale bar 500 micron)

2.5.4 Genes Associated with Osteogenesis are Highly Upregulated on Days 1 and 3 After Damaging Loading and Only Moderately Upregulated on Day 3 After Non-Damaging Loading

Expression of *Osx* was reduced 2-fold one hour after damaging loading, but upregulated 3.8- and 24-fold by days 1 and 3, respectively (Figure 2.5). Damaging loading also upregulated *Runx2* expression (3- and 8-fold on days 1 and 3, respectively). Furthermore, *Bglap* was

upregulated 4-fold on day 3. In addition, damaging loading upregulated *Bsp* expression 14- and 89-fold on days 1 and 3. The fold changes for osteogenic gene expression markers were significantly higher as a result of damaging loading (compared to non-damaging loading). Nevertheless, gene expression was significantly upregulated when comparing non-damaging loading to control ulnae (between 1.6 and 2.5-fold increase) on day 3. With regard to bone development, the hedgehog pathway was activated as evidenced by increased *Ptch* expression on day 3 for both damaging and non-damaging loading (7- and 1.5-fold, respectively). On day 3 formation of new bone was evident on histological images (Figure 2.1).

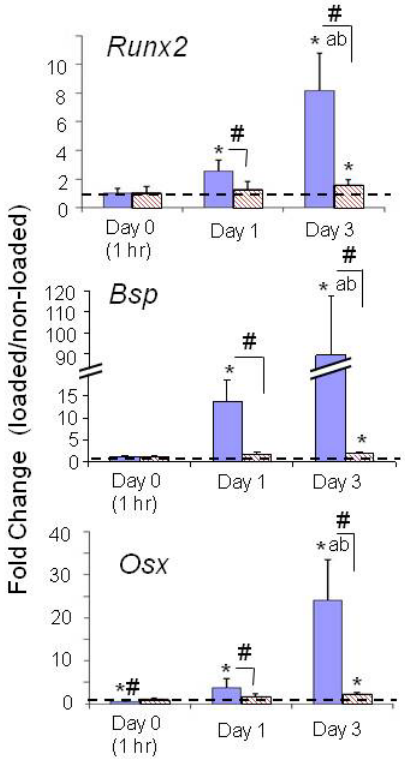

Figure 2.5. Gene expression of osteogenic markers show increased expression at days 1 and 3 for woven bone, with a significant increase at day 3 for lamellar bone. The changes for woven bone were 5 and 11 times larger than lamellar bone at day 3 for *Runx2* and *Osx*, respectively. The upregulation in *Bsp* was over 8 and 45 times larger than lamellar bone on days 1 and 3, respectively. Legend for gene expression plots is shown in Figure 2.2.

2.6 Discussion

The objectives of our research were to establish a loading protocol to stimulate only lamellar bone, and compare the processes associated with lamellar and woven bone formation. In support of our first hypothesis, lamellar bone formation was stimulated by a single bout of non-damaging loading. The single-bout loading protocol did not induce woven bone formation, stimulated a significant increase in bone formation of the loaded ulna, and did not produce structural damage. In support of our second hypothesis there were dramatic differences in gene expression levels between loading protocols that produced woven and lamellar bone. In particular, upregulation of angiogenic genes *Vegf* and *Hif1a* was seen on all days for woven bone, but only a modest upregulation was reported on day 3 for lamellar bone. In addition, vessel number, area and volume were all significantly increased following damaging loading, but not after non-damaging loading. Taken together, these results indicate the importance of vascular support for woven, but not for lamellar bone formation.

Induction of lamellar bone formation in the rat skeleton by mechanical loading has been documented previously, although most studies have used multi-day loading protocols (Chen 2008, Hsieh 2001b, Robling 2001a, Turner 1994b). For the purposes of our study, we needed a one-day protocol because we wanted to document effects relative to a single time-zero, rather than additive effects of multiple days as has been described previously (Kesavan 2005, Xing 2005). There is one report describing endortical lamellar bone formation in the rat tibia after a single bout of loading, although that report also described woven bone periosteally (Forwood 1994).For the purposes of our study, we needed to use a single-day loading protocol, with no woven bone formation. It is not clear if the protocols from previous studies satisfied these criteria. To our knowledge, a single-day loading protocol stimulating lamellar bone formation has not been developed in the rat ulna. A single loading session also minimizes the number of procedures the animal is subjected to; including loading, anesthesia and injections. The development of a single day loading protocol has allowed for synchronization of bone formation timelines between woven

and lamellar bone, to further characterize the mechanisms associated with these two types of bone.

Cellular proliferation is increased following mechanically induced stress fractures (Wohl 2009) and in fracture repair (Heiner 2006, Rundle 2006). Our study also saw a large increase cellular proliferation prior to woven bone formation, as early as one day after loading. Three days after loading there is a 17-fold upregulation of cell cycle marker *Ccnd1*. In contrast, there was only a slight increase in lamellar cell proliferation on day 3. Only *Ccnd1* was upregulated with a relatively moderate fold change of 1.7 above non-loaded control at day 3. Similar to our lamellar results, one study reported an increase in osteoblast proliferation three days after tibial bending (Turner 1998). In their study, lamellar bone was formed on the endosteal surface of the tibia, while perosteal bone formation was not analyzed. Taken together, these two studies indicate that an early increase cell proliferation is not necessary for formation of lamellar bone. This may indicate that active osteoblasts are able to form lamellar bone without additional proliferation of new osteoblasts.

The role of angiogenesis has been documented in skeletal development (Colnot 2001, Ferrara 2001, Pechak 1986), fracture repair (Glowacki 1998, Hausman 2001, Street 2002), and distraction osteogenesis (DO) (Fang 2005, Jazrawi 1998). Fracture studies have shown the importance of angiogenesis for bone formation (Pacicca 2003) by inhibiting vessels using small molecules or a drug (TNP 470). Additionally, DO has been shown to be dependent on both VEGFR1 and VEGFR2 signaling (Jacobsen 2008). These studies demonstrate the importance of angiogenesis in a healing setting where large amounts of bone are required to help stabilize the injury. A stress fracture healing response is characterized by rapid, non-endochondral woven bone formation (Uthgenannt 2007a), which makes it different than fracture healing and DO that include intramembraneous and endochondral bone formation (Einhorn 1998, Gerstenfeld 2003a). Thus, using a fracture repair or DO model, it is difficult to isolate woven bone formation from other processes occurring at the site of new bone formation. In stress fracture repair, the spatial pattern of vascular changes matched the subsequent pattern of woven bone formation (Matsuzaki 2007), suggesting that the vasculature was a template for bone formation. Our study

showed an early angiogenic gene expression response to damaging loading, and an increase in vascularity at day 3. In sharp contrast, we did not detect an increase in vascularity for lamellar bone formation. Lamellar bone formation induced by treadmill running in young rats did lead to increase in *Vegf* expression, vascularity and bone formation in the tibia after several weeks of training (Yao 2004). This study is not consistent with our results, but they used younger rats (9 weeks old) and analyzed bone formation in the trabecular compartment, which differs from the periosteal lamellar bone formation we were investigating in adult rats (19-24 weeks old).

Increased expression of *Bmp2* was seen in response to both damaging and non-damaging loading. This supports the finding that *Bmp2* is mechanresponsive (Sato 1999). The early upregulation seen after damaging loading is consistent with previous findings from stress fractures (Wohl 2009) and fracture repair (Cho 2002, Tsuji 2006). Unexpectedly, our results also demonstrated a significant increase (near 2-fold) in *Bmp2* after non-damaging loading. *Bmp2* has been shown to stimulate angiogenesis by upregulation and secretion of *Vegf* by osteoblasts (Deckers 2002). This is consistent with our woven bone results, but not with our results for lamellar bone formation. Loading-induced *Bmp2* expression is three-times larger following damaging loading (compared to non-damaging loading) and supports an osteogenic-angiogenic coupling for woven bone formation with increased *Vegf* expression at all timepoints. Non-damaging loading led to an increase in *Bmp2* associated with osteogenesis, but did not activate angiogenic coupling, as there was no coordinated increase in *Vegf* expression.

The upregulation of bone formation genes seen in our study are similar to other studies. Murine tibial bending studies induced upregulation of bone formation genes (Kesavan 2005, Lau 2006), consistent with our result that bone sialoprotein and osteocalcin were upregulated by day 3 after damaging and non-damaging loading. Although the bone formation was not detailed, tibial bending likely produced endosteal lamellar and periosteal woven bone formation. In our study, separation of woven and lamellar bone demonstrated that the gene expression responses were different in magnitude. There were larger fold changes associated with woven bone formation, and the upregulation of these genes happened earlier. Our results showed upregulation of 10 genes on day 1 for woven bone formation (fold changes ranging between 2 and 13.5), in contrast

to lamellar bone, which did not have any significant increases at day 1. Moreover, by day 3 we are able to see a large upregulation of osteogenic genes for woven (4- to 89-fold increase) compared to lamellar (1.5- to 2.25 fold increase) bone formation.

One of the strengths of our study was the synchronization of the timelines for induction of woven and lamellar bone formation. The development of a single-bout lamellar loading protocol ensured that only one loading event occurred before the tissue was extracted for analysis. In addition, the damaging and non-damaging loading protocols lead to the formation of two distinct types of bone formation, woven and lamellar. Having the ability to separate the bone formation responses using different initial loading protocols allowed us to compare and contrast the gene expression and vascular responses of woven and lamellar bone.

There were a few limitations to our study. First, only three discrete early timepoints (1 hr, 1 day and 3 days after loading) were evaluated based on previous studies that showed early changes in gene expression and vascularity following damaging fatigue loading (Matsuzaki 2007, Silva 2006b, Wohl 2009). Second, although our data suggests that woven bone is dependent on angiogenesis, we have yet to prove that in the absence of angiogenesis, woven bone is inhibited. Finally, one consideration in our damaging loading scenario is the accumulation of lamellar bone adjacent to woven bone formation. In an attempt to reduce the amount of lamellar bone formation in the samples evaluated after damaging loading we confined our gene expression region of interest to 5 mm near the site of stress fracture formation, an area shown to produce predominantly woven bone (Uthgenannt 2007a). Furthermore, woven bone was absent in our lamellar bone protocol. This ensured that any differences in gene expression observed were from the formation of woven bone in our damaging loading model.

In conclusion, lamellar bone formation can be initiated using a single, non-damaging bout of loading in the rat ulna. We showed dramatic differences in gene expression levels between loading protocols that stimulated woven and lamellar bone formation. Damaging loading increased expression of genes related to cell proliferation and angiogenesis while increasing vascularity at day 3. In addition, there were considerable fold-increases in osteogenic gene expression, and this upregulation is consistent with the large amount of woven bone formation

observed histologically on day 10. Non-damaging loading did not increase upregulation of cell proliferation or angiogenic gene expression at early timepoints, and did not result in an increase in vascularity. There was a modest upregulation of osteogenic gene expression at day 3 that is consistent with the amount of lamellar bone formation seen histologically. In summary, the cell proliferation and angiogenic responses at the molecular level distinguish loading-induced woven from lamellar bone formation in the adult skeleton.

2.7 Acknowledgements: NIH/NIAMS AR050211; ASBMR

3 Differential gene expression from microarray analysis distinguishes woven and lamellar bone formation in the rat ulna following mechanical loading

3.1 Abstract

Formation of woven and lamellar bone in the adult skeleton can be induced through mechanical loading. Although much is known about the morphological appearance and structural properties of the newly formed bone, the molecular responses are still not well understood. Recent studies have made use of microarrays to help characterize the molecular responses to loading. The objective of our study was to distinguish the molecular responses between woven and lamellar bone formation using a microarray. Rat forelimb loading was completed in a single bout. Woven bone was induced using a damaging fatigue loading protocol. In contrast, lamellar bone was induced using a non-damaging loading protocol. Microarrays were performed at three timepoints after loading: 1 hr, 1 day and 3 days. Microarray results were analyzed using two commercial software packages, Partek and GeneGo. Confirmation of microarray results was done for a select group of genes using quantitative real-time PCR. There were a higher number of differentially regulated genes for woven compared to lamellar bone formation. A total of 395 genes were differentially expressed between formation of woven and lamellar bone 1 hr after loading, while 5883 and 5974 genes were differentially expressed on days 1 and 3, respectively. Microarray data demonstrated increased expression of many inflammation factors 1 hr after loading. Specifically, interleukin-6 (*Il6*) was upregulated over 500-fold (by qRT-PCR) after damaging loading, but was not differentially regulated after non-damaging loading compared to control. There was evidence of vasodilation, with increased expression of prostaglandind-endoperoxide synthase 2 (*Ptgs2/Cox2*) at all timepoints for woven bone (8- to 16-fold upregulation by qRT-PCR). Bone formation markers were also expressed. For example, sclerostin (encoded by the *Sost* gene), which inhibits bone formation, was downregulated at all timepoints for woven bone (almost 20-fold on day 1). Moreover, *Sost* expression was nearly significantly downregulated following non-damaging loading on day 1 (1.6-fold; p=0.055). The micorarray results brought to light many inflammatory factors in our model, expanded our

previous findings about angiogenesis, and strengthened our understanding of the role of osteogenic pathways.

3.2 Key Terms

Mechanical loading, microarray, rat, woven bone, lamellar bone, angiogenesis

3.3 Introduction

Mechanical loading can induce woven or lamellar bone formation at the histological level. Woven bone is characterized by its rapid deposition, disorganization and low density. In contrast, lamellar bone deposits more slowly, is more organized and has a higher bone mineral density. Rat forelimb loading can be performed in a single bout to induce the formation of woven bone using damaging fatigue loading (Bentolila 1998, Tami 2003, Uthgenannt 2007a), or lamellar bone using a non-damaging loading protocol (McKenzie 2009). Although many structural and mechanical aspects between woven and lamellar bone are well described, the molecular mechanisms associated with these two bone formation processes are not fully understood. A better understanding of these molecular events could be the basis for future developments of novel therapeutics to accelerate bone formation.

Previous studies investigating damaging loading in the rat ulna found early increases in cell proliferation (Wohl 2009) and angiogenesis (Matsuzaki 2007, Wohl 2009) prior to woven bone formation. A follow up study found that lamellar bone formation did not increase cell proliferation, vessel volume or expression of angiogenic genes at early timepoints (McKenzie 2009). However, these studies only examined select target genes related to angiogenesis, cell proliferation and osteogenesis. Thus, further study is required to broaden our understanding of the overall expression differences between woven and lamellar bone formation.

A microarray allows simultaneous measurement of the expression values in thousands of genes (Trevino 2007). A more traditional analysis of selecting a limited number of genes using quantitative PCR cannot study thousands of coordinately expressed genes in a timely manner. Therefore, expression profiling is an efficient experiment that can reveal previously unrecognized

roles for genes. A whole genome analysis of gene expression can help us to understand the complex process of bone formation.

The objective of our study was to identify gene expression differences between woven and lamellar bone formation using a whole genome microarray. We first induced woven and lamellar bone formation using mechanical loading of the rat forelimb. Damaging fatigue loading resulted in an ulnar stress fracture and subsequent healing through the formation of woven bone. A rest-inserted non-damaging loading protocol induced the formation of lamellar bone in the ulna. We set out to expand our current knowledge about the similarities and differences between woven and lamellar bone formation through the exploration of microarray data.

3.4 Methods

3.4.1 Forelimb Loading

The right forelimbs of 42 anesthetized adult male rats (5 mo., 337 ± 24 g) were loaded in axial compression (Table 3.1). Rats were anesthetized (1-3% isoflourane) prior to loading. The forelimb was positioned between two loading fixtures on a servohydraulic testing machine (Instron 1331) and a 0.3 N compressive preload was applied. Rats designated for damaging fatigue loading had the right forelimbs cyclically loaded in a single bout (2 Hz, 18 N) to a 1.3 mm increase in displacement (avg. cycles 7501 ± 5676), a protocol shown to cause a 70% decrease in ulnar stiffness (Uthgenannt 2007b) and to induce abundant woven bone formation (Uthgenannt 2007a). Rats designated for non-damaging loading had the right forelimbs loaded using a trapezoidal waveform (0.5 s triangle load-unload to 15 N followed by 9.5 s rest; 100 cycles), a protocol which does not induce any bone damage, but significantly increases lamellar bone formation (McKenzie 2009). After loading, rats received analgesia (i.m. 0.05 mg/kg buprenorphine) and were allowed normal cage activity and ad libitum access to food and water. Rats were euthanized at 1 hr, 1 or 3 days after loading corresponding to timepoints that were previously investigated (McKenzie 2009, Wohl 2009). An additional six age-matched rats served as normal controls and were not loaded. This study was approved by the Washington University Animal Studies Committee.

Table 3.1. Summary of the number of rats loaded for each timepoint. The loading parameters for stimulation of woven and lamellar bone formation differed.

	Non loaded	Num. of rats loaded			Applied force (N)	Loading cycles	Increase in disp. (mm)
		1 hr	Day 1	Day 3			
Woven		7	7	7	18	7501 ± 5676	1.3
Lamellar		7	7	7	15	100	0.099 ± 0.062
Normal	6						

3.4.2 RNA Extraction and Preparation

Immediately upon dissection the right ulna was frozen in liquid nitrogen, and recently described RNA extraction methods were followed (Wohl 2009). A 5 mm piece of the central ulna was pulverized and suspended in trizol. Total RNA was isolated using an RNeasy mini kit (Qiagen) and quantified (Nanodrop, ND-1000). RNA from each rat (48 rats total) was run on a microarray by the Washington University Genome Sequencing center (Illumina, RatRef-12; 48 arrays total). The total RNA quality was determined by Agilent 2100 bioanalyzer (Agilent Technologies) according to manufacturer's recommendations. At the Genome Sequencing center, RNA transcripts were amplified by T7 linear amplification (MessageAmp TotalPrep amplification kit; ABI-Ambion). 400 ng of each total cellular RNA sample (11 μl) was mixed with an oligo-dT T7 primer (1 μl), 10x reaction buffer (2 μl), dNTP mix (4 μl), Rnase Inhibitor (1 μl), and Arrayscript RT enzyme (1 μl). Reverse transcription was carried out for 2 hours at 42 ºC. After a three minute incubation on ice, the cDNA underwent second strand synthesis by adding water (63 μl), 10x second strand buffer (10 μl), dNTP mix (4 μl), DNA polymerase (2 μl) and Rnase H (1 μl). This cocktail was incubated at 16 ºC for 2 hours. Following a column cleanup using DNA columns provided in the MessageAmp TotalPrep kit, in vitro-transcription was carried out by adding 10x T7 reaction buffer (2.5 μl), T7 biotin-NTP mix (2.5 μl), and T7 RNA polymerase enzyme mix (2.5 μl) and incubated at 37 ºC. The IVT reaction was carried out for 14 hours. Following reaction termination with water (75 μl), the amplified RNAs (Li) were cleaned with RNA columns provided in the MessageAmp TotalPrep kit. The aRNAs were quantitated on a spectrophotometer and quality determined by Agilent 2100 bioanalyzer (Agilent Technologies) according to manufacturer's recommendations.

3.4.3 Microarray Hybridization, Detection and Analysis

750 µg of each aRNA in water (5 µl) was suspended in Illumina "HYB" buffer (10 µl) and heated to 65 ºC for five minutes, then allowed to cool to room temperature. The samples were applied to RatRef-12 Expression BeadChips and hybridized at 58 ºC for 16-20 hours at high humidity. Arrays were washed according to Illumina standard protocol. Immobilized, biotinylated aRNAs were then detected by staining with cy3 Streptavidin (1 µg cy3-SA per 1 ml of Illumina "Block E1") for 10 minutes at room temperature. Arrays were washed and dried according to Illumina standard protocol, then scanned on an Illumina BeadArray Reader. Laser power and PMT voltage were kept constant for cy3 scans. After image quantitation (Illumina Beadscan, v3) data were imported into Beadstudio software. On-slide spot replicates were averaged by Beadstudio and individual spot data were reported.

3.4.4 Microarray Analysis Using Partek Genomics Suite

Quantile normalized microarray data was retrieved from the Washington University Genome Sequencing Center and imported into Partek Genomics Suite (Partek Incorporated, 6.4). First, data were filtered to include only data points which had a detection p-value less than 0.01 in all microarrays. This excluded data points which were not significantly different from the background of the chip. Next, the average signal data were log transformed. Principal component analysis revealed one outlier in the day 3 lamellar group. This sample was excluded from all further analysis. Using the Partek "gene expression workflow" to detect differentially expressed genes, an ANOVA was performed. ANOVA factors included sentrix position, chip number, treatment, timepoint, and all contrasts between treatment and timepoint. Next, to determine if expression of a gene was significantly different between the two loading conditions we used a false discovery rate (FDR) of 0.05 in a step up analysis. From this analysis, gene lists were created comparing each treatment group and timepoints for a total of 9 comparisons (i.e. lamellar day 1 vs. normal; woven day 3 vs. lamellar day 3). Exported files included significant genes, fold changes and p-values for comparisons between groups and timepoints. These lists were then imported into GeneGo for further analysis.

3.4.5 Data Mining Using GeneGo

The files where uploaded into GeneGo (version 5.4) by accession number. A workflow for each comparison (i.e. lamellar 1 hr over normal) was generated using GeneGo's "Analyze Single Experiment" feature with thresholds of 0.99 and 0.0001 for p-value and fold change, respectively. Non-stringent filters were used in this step as all non-significant expression changes had been excluded by Partek analysis. The top ten "Statistically Significant Maps" from each workflow, as well as canonical GeneGo Pathway Maps (associated with angiogenesis, bone development, inflammatory response, hypoxia response etc.) were investigated. In addition, relevant pathways presented in the surveyed literature were examined for genes or pathways of interest, i.e genes with expression changes above 2-fold or with unique temporal patterns, or several genes in a single pathway being differentially regulated.

3.4.7 Quantitative Real-Time PCR

Following microarray analysis, quantitative real-time PCR (qRT-PCR) was used to validate expression patterns for select genes including interleukin-6 (*Il6*; a pro-inflammatory cytokine), nuclear factor of kappa light polypeptide gene enhancer in B-cells 1 (*Nfkb1*; a transcription factor), nuclear factor of kappa light polypeptide gene enhancer in B-cells inhibitor, alpha (*Nfkbia*; an NF-kb inhibitor), toll-like receptor 2 (*Tlr2*; a cell surface receptor implicated in mechanotrandsuction and inflammation), selectin, endothelial cell (*Sele*; a cell adhesion molecule), prostaglandin-endoperoxide synthase 2 (*Ptgs2*, also known as *Cox-2*; a possible indicator of vasodilation and/or mechanotransduction), chemokine (C-X-C motif) ligand 10 (*Cxcl10*; an angiostatic factor), sclerostin (*Sost*; an inhibitor of the Wnt pathway), matrix metalloproteinase 13 (*Mmp13*; a proteinase capable of cleaving collagen), and cathepsin K (*Ctsk*; a protease involved in bone remodeling). First strand cDNA was synthesized (Superscript III, Invitrogen) from total RNA (500 ng). qRT-PCR reactions were carried out at 20 µL total volume and measured with *Power* SYBR® green (7300 Real-Time PCR System, Applied Biosystems). All primers were purchased as pre-validated sets from Qiagen (QuantiTect Primer Assays; Table 3.4). Samples were run in triplicate and the average was used for further analysis. Data were

analyzed using relative quantification ($2^{-\Delta C_T}$), where gene CT values were normalized to glyseraldehyde-3-phosphate dehydrogenase (*Gapdh*).

3.5 Results

3.5.1 Allocation of Differentially Expressed Genes

The number of differentially expressed genes (DEGs) varied significantly for each comparison group (Table 3.2) at each timepoint. Only five genes (all at 1 hr) were significantly different between normal vs. lamellar groups, whereas many genes were different between woven vs. normal and woven vs. lamellar. We chose to focus on woven vs. lamellar comparisons (Figure 3.1) because of the apparent similarity between expression levels in lamellar and normal groups and because our main objective was to determine the differences between woven and lamellar bone formation. As illustrated (Figure 3.1), some genes were differentially regulated across multiple timepoints, while other genes were differentially regulated at a single timepoint.

Table 3.2. Comparison of the number of DEGs between groups at 1 hr, day 1 and day 3. The woven vs. lamellar DEGs were further analyzed using GeneGo software.

	1 hr	Day 1	Day 3
Woven vs. Lamellar	395	5883	5974
Woven vs. Normal	749	5869	4916
Lamellar vs. Normal	5	0	0

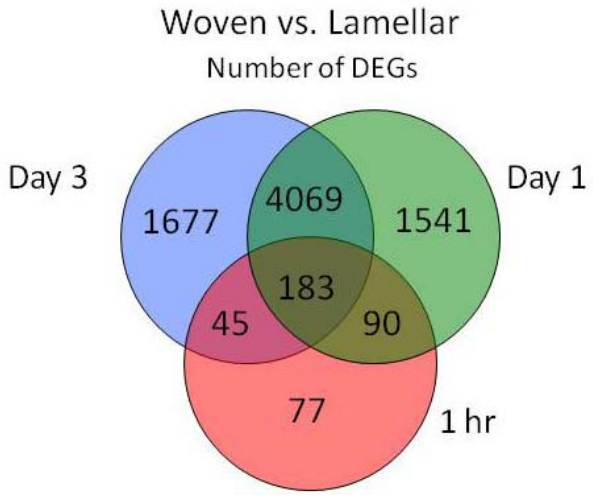

Figure 3.1. A number of genes were differentially regulated at 1 hr, 1 and 3 days post-loading for damaging (woven) vs. non-damaging (lamellar) loading from microarray analysis. Some of the genes were differentially regulated across several timepoints and others were unique to a single timepoint.

3.5.2 Top 10 Canonical Pathways

Analysis of the top ten canonical pathways (GeneGo) activated by woven vs. lamellar loading was completed at each timepoint. At 1 hr after loading the majority of the pathways were related to an inflammatory response (7/10 pathways) with the addition of two pathways related to development. The inflammatory response persisted at day 1 (5/10 pathways) with the addition of cytoskeletal remodeling activation (2/10 pathways). By day 3, the inflammatory response had subsided (0/10 pathways), but cytoskeletal remodeling still played a major role (3/10 pathways) and a development pathway was evident again (1/10 pathways) (Figure 3.2).

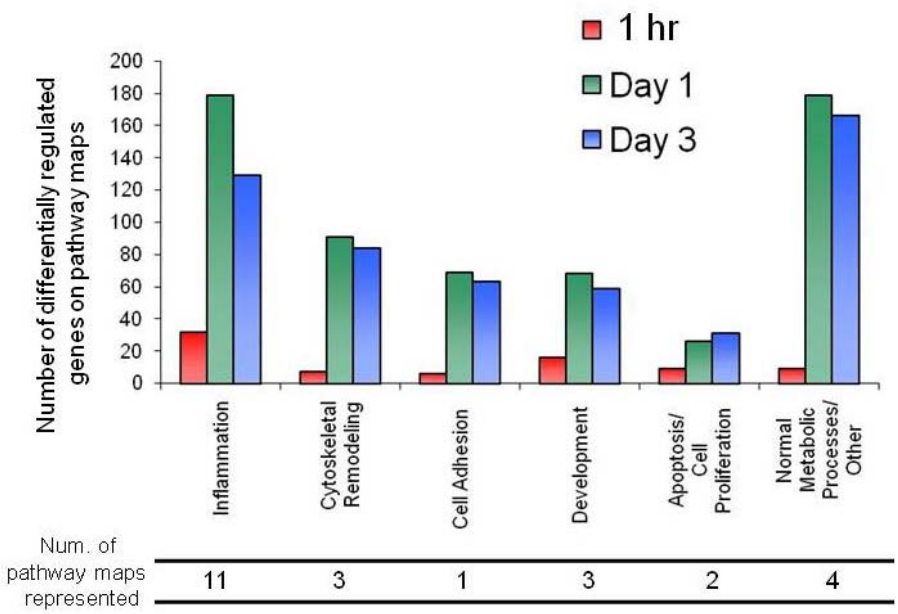

Figure 3.2. The total number of differentially regulated genes shown here is based on overlaying of our data onto predefined canonical pathway maps provided by GeneGo. On each pathway, genes were counted if their expression was significantly different between woven and lamellar bone.

3.5.3 Inflammatory Response

Analysis of microarray data revealed that several components of various innate inflammatory response pathways were upregulated after damaging loading (Table 3.3). As early as one hour after loading there was upregulation of several cell surface proteins/receptors know to function in mechanotransduction (Dinarello 2009), such as integrins, toll-like receptors (TLRs) and interleukin receptors (specifically *Il1r1*). Toll-like receptor 2 (*Tlr2*) was selected as one indicator of this level of inflammation, and its expression was confirmed by qRT-PCR (Figure 3.3; Table 3.4). Both microarray and qRT-PCR data showed *Tlr2* to be upregulated at all timepoints, peaking on day 1. Select intermediate proteins in inflammatory response pathways (such as *Myd88* of TLR pathways) were also upregulated, as were some terminal transcription factors which are responsible for regulating various pro-inflammatory responses, such as NF-kB, AP-1 and NF-AT family members (Ono 2008) (Table 3.3).

NF-κB was of interest as it appeared in a large number of the significant maps produced by GeneGo, and an inhibitor of NF-κB (*Nfkbia*) was one of the five genes to be upregulated in the lamellar to normal comparison. Different combinations of NF-κB subunits form active dimers and several of these subunits (*Nfkb1*, *Nfkb2* and *Rel*) were upregulated in woven as compared to lamellar. *Nfkb1* was chosen for confirmation by qRT-PCR, as it was slightly upregulated at 1 hr, before declining towards normal levels on days 1 and 3 in the microarray. qRT-PCR also showed *Nfkb1* to be upregulated but expression increased on days 1 and 3 (Figure 3.3, Table 3.4). Lamellar expression did not differ from control at any timepoint for *Nfkb1*.

Other components of the NF-κB signaling pathway were also differentially regulated, including members of the I-κB family such as *Bcl3*, *Nkbiz* and *Nkbie* (Renner 2009). *Nfkbia*, which is both an inhibitor and a transcriptional target of NF-κB (Renner 2009), was also upregulated. In the microarray, *Nfkbia* was up at 1 hr in lamellar as compared to normal (fold change 2.0). qRT-PCR did show *Nfkbia* was also upregulated at 1 hr in the lamellar group. However, unlike in the microarray, *Nfkbia* was upregulated in the woven group at all timepoints, most significantly at 1 hr by qRT-PCR.

The microarray also showed the upregulation of transcription factors, as well as several targets of NF- κB including pro-inflammatory cytokines (*Il1a Il1b*, *Il6*) (Dimitriou 2005), chemokines (*Cxcl1*, *2* and *10*) and cell adhesion molecules (*Icam1*, *Sele*). Interleukin 6 and both the alpha and beta subunits of *Il1* were greatly upregulated. Several receptors (*Il1r1* and *Il8rb* for example) were also up. *Socs1*, which takes part in the negative feedback of cytokines (Dimitriou 2008), was also greatly upregulated across all three days suggesting that mechanisms for the attenuation of the inflammatory response were also active in this time range.

Interleukin-6 was chosen as an indicator of pro-inflammatory cytokines. In our study, qRT-PCR confirmed the dramatic upregulation of *Il6* seen in the microarray. Like in the microarray, expression peaked at 1 hr and declined thereafter with levels still well above normal. Expression of *Il6* was upregulated at 1 hr by over 500 fold on qRT-PCR, and near 50 fold on the microarray (Tables 3.3 and 3.4). Expression was not significant for lamellar compared to normal by either method.

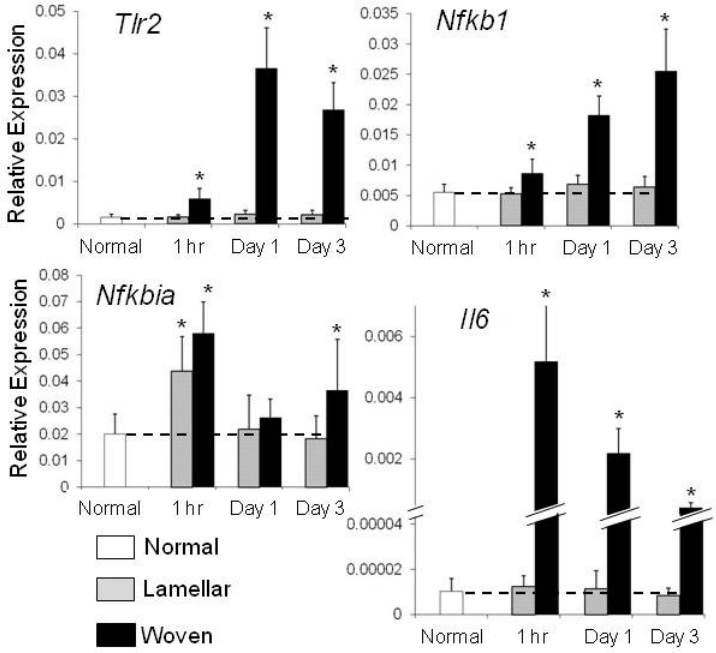

Figure 3.3. qRT-PCR relative expression (delta CT) of genes related to inflammation. Genes were upregulated at all timepoints for woven bone with the exception of *Nfkbia* on day 1. In contrast, only *Nfkbia* at 1 hr was upregulated for lamellar bone. The inflammation marker *Il6* is increased over 500 fold 1 hr after damaging loading. *p<0.05 vs. normal

3.5.4 Angiogenic Response

Angiogenesis is known to respond early to mechanical loading (Matsuzaki 2007, McKenzie 2009, Wohl 2009), and the differential regulation of a variety of angiogenic genes in the microarray supports this. The constitutive beta subunit (*Arnt*) of hypoxia-inducible factor (*Hif1a*, a central component of angiogenesis-osteogenesis coupling) was upregulated, as were the inducible alpha subunit and coactivators found in the nucleus such as *Creb1*. A HIF-1a inhibitor (*Egln1*) was downregulated.

Chemokines also promote angiogenesis (Rosenkilde 2004, Salcedo 2003). In our study, *Cxcl1*, *-2*, *-6* and the receptor *Il8rb* were upregulated while *Ppbp* was downregulated. However, angiostatic chemokines (Rosenkilde 2004, Salcedo 2003) were also differentially regulated, as *Cxcl10* (formerly known as IP-10), -13 and the receptor *Cxcr3* (of *Cxcl10*) were upregulated to

some extent. *Cxcl10* was selected for further confirmation by qRT-PCR (Figure 3.4). Upregulation of *Cxcl10* was significant 1 hr after damaging loading and continued to increase through day 3.

Another chemokine and its receptor, *Ccl20* and *Ccr2* respectively, were upregulated, as were other genes influencing chemotaxis such as *Ccl7* (Ghadjar 2009). *Sele* was chosen to represent chemotaxis in the endothelia (Krishnan 2001) and for further confirmation by qRT-PCR. The microarray showed *Sele* to be upregulated at all three timepoints for woven bone, peaking at 1 hr. The qRT-PCR showed *Sele* to be upregulated significantly in the woven group, but in contrast to the microarray expression peaked on day 1 (Figure 3.4). Expression of *Sele* stayed near control levels in the lamellar group.

Genes associated with blood flow regulation and vasodilation were also differentially expressed. *Ptgs2*/*Cox2* was upregulated in the microarray data, as was *Nos3* (a constitutive form of NOS), and *Ap1* and *Creb1* (two transcription factors for *Ptgs2*/*Cox2*). *Cebpb*, a regulator of COX-2, was upregulated at 1 hr and day 1 but downregulated on day 3. *Ptgs2/Cox2* was selected for further verification by qRT-PCR and was upregulated at all timepoints in the woven group, but declined towards normal by day 3 (Figure 3.4, Table 3.4).

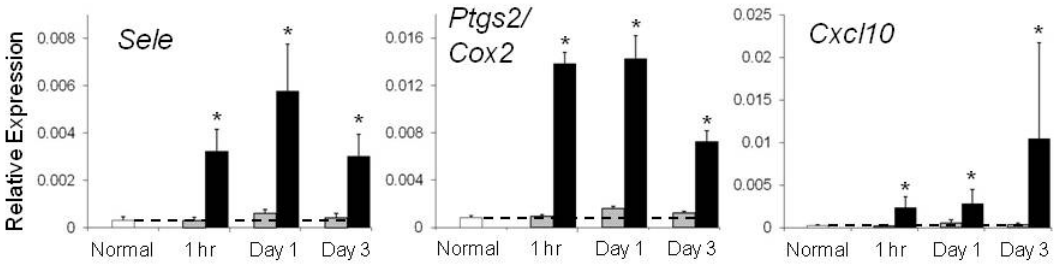

Figure 3.4. Relative expression changes for angiogenic markers. All genes were upregulated at all timepoints for woven bone, but never for lamellar bone. Both *Sele* and *Ptgs2/Cox2* are positively related to increased vasculature with expression peaking on day 1. In contrast, *Cxcl10* is angiostatic and peaks on day 3. *p<0.05 vs. normal; legend in Figure 3.3.

3.5.5 Osteogenic Response

Mechanical loading is known to greatly influence bone modeling (Iqbal 2005, Robling 2006b), and various aspects of this process were differentially regulated in our microarray, starting with mechanoreceptors such as cadherins (for example *Cdh16*, *Fat3* and *Cdh19*) and integrins (*Itgax*, *Itgal*, *Itgam* and *Itgb2*) (Table 3.3). Though several DEGs were part of the canonical Wnt-pathway, the pathway as a whole was not clearly or dramatically regulated in one specific direction. Wnts were not differentially regulated though their receptors were. *Lrp5* was suppressed as was *Fzd8* (slightly), while *Fzd1* was slightly upregulated. *Dkk1* and *Sfrp4* (inhibitors) were downregulated. Both Dishevelled (*Dvl1*) and casein kinase I (*Csnk1a1*) form a complex with beta-catenin, targeting it for ubiquination (i.e. suppressing the pathway). Though *Dvl1* was slightly down, an isoform of *Csnk1a1* was slightly up as was one of its nuclear partners, *Tcf7*. While the direction of regulation of the pathway in general was rather questionable, sclerostin (*Sost)* seemed to be a clear point of Wnt-pathway regulation. Like seen in previous studies (Bonewald 2008, Kubota 2009), *Sost* was greatly suppressed in the microarray after damaging loading. qRT-PCR of *Sost* confirmed this pattern, but with much greater fold changes (down 20-fold on day 1) (Figure 3.5). *Sost* expression was inhibited in the lamellar group on day 1 ($P=0.055$), but was not different from normal at 1 hr or day 3.

BMP pathways were also differentially regulated in woven as compared to lamellar bone formation. TGF-β may initiate BMP synthesis, as well as having chemotactic, proliferative and matrix remodeling effects of its own (Dimitriou 2005). Our data show mixed regulation of three types of TGF-β: *Tgfb1* up, *Tgfb2* down and *Tgfb3* down on day 1 and up on day 3. *Bmp2* itself is upregulated, though only slightly, while *Bmp3*, *-3b (Gdf10)*, - 4, -6 and -7 were downregulated. The receptors for BMP-5, 6, 7, and 8, *Acvr2b* and *Acvr1* were also downregulated, though just slightly for the latter. The downstream transcription factors *Smad1* and *Smad5* were upregulated, though again only slightly. The pathways were most clearly modulated by the downregulation of antagonists (Dean 2009) such as the previously mentioned *Sost*, as well as *Nbl1*, *Bambi*, *Fst*, *Grem1*, *Chrd* and inhibitory SMADs (*Smad6* and *Smad7*) (Table 3.3).

Many genes related to cell proliferation and differentiation were differentially regulated in the microarray. Osteoprotegerin (*Tnfrsf11b*) is an inhibitor of osteoclast differentiation and activation, as is the upregulated *Il6*. *Tnfrs11b* was upregulated on day 1, though neither RANK nor its receptor was differentially regulated. Cell cycle regulation genes such as *Ccnd1*, *Cdk4*, *Cdc2*, and *E2f1* were up, while *E2f6* and members of the Rb family (*Rbl2*, *Rbl1*) were down.

3.5.6 Bone Remodeling Response

Genes associated with matrix remodeling were also differentially regulated, specifically those expressed by osteoclasts. Members of the cathepsin family (*Ctsd*, *Ctsb*, *Ctss* and *Ctsv*) (Lecaille 2008) along with *Csf1* and *Myc* were upregulated to some extent. *Ctsc* and *Ctsk* both localize predominately in osteoclasts (Georges 2009, Zhao 2009), though the first was upregulated and the second downregulated. Cathepsin K was chosen as an osteoclast activity indicator for confirmation with qRT-PCR (Figure 3.5; Table 3.4). *Ctsk* was slightly downregulated on day 1 in the microarray, whereas qRT-PCR showed it to be around normal levels at 1 hr and day 1 but upregulated on day 3. Some inhibitors of *Ctsk* such as *Il6* and *Tnfrsf11b* were upregulated in the microarray, while others such as *Ctsc* were just slightly down.

Matrix degradation is key for remodeling, as well as for increased cell mobility. MMPs in general function in this capacity (Georges 2009, van Hinsbergh 2008) and *Mmp13* was chosen as an indicator of these processes. In the microarray, *Mmp13* was upregulated greatly on day 1, and less so on day 3, a pattern seen again in qRT-PCR (Figure 3.5). Important transcriptional regulators of MMP-13, were also differentially regulated: some subunits of AP-1 were slightly up and others slightly down, while *Etv4* was much more strongly downregulated.

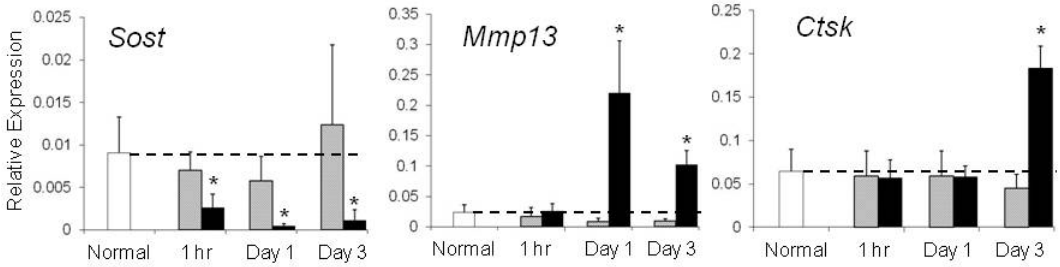

Figure 3.5. Relative expression changes of osteogenic genes associated with matrix modeling and remodeling. *Sost*, a bone formation inhibitor is downregulated at all timepoints for woven bone and neared significance for lamellar bone at day 1 (p=0.055). *Mmp13* and *Ctsk* are markers of bone remodeling and both are upregulated at later timepoints. *p<0.05 vs. normal; legend in Figure 3.3.

Table 3.3. Differential expression of genes from the microarray. Values are fold change difference between woven and lamellar bone formation. An x indicates the fold change between loading conditions was not significant at that timepoint.

			Woven Over Lamellar		
Category	**Gene Name**	**Gene Symbol**	**1 hr**	**Day 1**	**Day 3**
Inflammation	Adaptor-related protein complex 1, beta 1 subunit	*Ap1b1*	x	1.73	1.69
	Adaptor-related protein complex 1, sigma 2 subunit	*Ap1s2*	x	-1.36	
	Activating transcription factor 1	*Atf1*	x	1.65	1.27
	Activating transcription factor 4 (tax-responsive enhancer element B67)	*Atf4*	x	x	-1.26
	Activating transcription factor 5	*Atf5*	x	-2.03	-2.69
	Activating transcription factor 6 beta	*Atf6b*	x	1.54	1.56
	Activating transcription factor 7	*Atf7*	x	x	-1.42
	B-cell CLL/lymphoma 3	*Bcl3*	15.96	17.57	5.37
	FBJ osteosarcoma oncogene	*Fos*	x	3.29	x
	Intercellular adhesion molecule 1	*Icam1*	3.47	2.57	x
	Interleukin 1 alpha	*Il1a*	18.14	x	x
	Interleukin 1 beta	*Il1b*	20.88	7.06	2.45
	Interleukin 1 receptor, type I	*Il1r1*	3.91	7.15	x
	Interleukin 6	*Il6*	53.62	45.97	4.85
	Interleukin 8 receptor, beta	*Il8rb*	x	29.01	x
	Integrin alpha L	*Itgal*	x	79.37	x
	Integrin alpha M	*Itgam*	x	7.69	x
	Integrin alpha X	*Itgax*	x	7.35	x
	Integrin beta 2	*Itgb2*	x	6.66	x

	Jun dimerization protein 2	*Jdp2*	x	1.64	
	Jun oncogene	*Jun*	x	-1.57	-1.74
	Jun B proto-oncogene	*Junb*	5.98	3.93	1.96
	Myeloid differentiation primary response gene 88	*Myd88*	2.54	3.87	2.2
	Nitric oxide synthase 2, inducible	*Nos2*	50.17	7.49	x
	Nuclear factor of activated T-cells, cytoplasmic, calcineurin-dependent 4	*Nfatc4*	x	x	1.33
	Nuclear factor of kappa light polypeptide gene enhancer in B-cells 1	*Nfkb1*	x	2.06	x
	Nuclear factor of kappa light polypeptide gene enhancer in B-cells 2, p49/p100	*Nfkb2*	1.76	1.408	1.33
	Nuclear factor of kappa light polypeptide gene enhancer in B-cells inhibitor, alpha	*Nfkbia*	x	x	-1.41
	Nuclear factor of kappa light polypeptide gene enhancer in B-cells inhibitor, epsilon	*Nfkbie*	x	4.8	6.25
	Nuclear factor of kappa light polypeptide gene enhancer in B-cells inhibitor, zeta	*Nfkbiz*	25.78	6.82	2.81
	Prostaglandin E receptor 2, subtype EP2	*Ptger2*	x	89.6	6.38
	Prostaglandin E receptor 4 (subtype EP4)	*Ptger4*	x	4.39	1.95
	V-rel reticuloendotheliosis viral oncogene homolog (avian)	*Rel*	x	2.48	x
	Suppressor of cytokine signaling 1	*Socs1*	13.29	9.52	6.54
	Toll-like receptor 2	*Tlr2*	3.19	9.82	2.83
	Toll-like receptor 4	*Tlr4*	x	3.79	x
Angiogenesis	Aryl hydrocarbon receptor nuclear translocator	*Arnt*	x	x	1.74
	Chemokine (C-C motif) ligand 12	*Ccl12*	x	26.49	7.78
	Chemokine (C-C motif) ligand 20	*Ccl20*	85.74	3574	150.3
	Chemokine (C-C motif) ligand 7	*Ccl7*	24.49	55.06	6.43
	Chemokine (C-C motif) receptor 2	*Ccr2*	x	3.43	x
	Chemokine (C-C motif) receptor 6	*Ccr6*	x	6.84	2.45
	CCAAT/enhancer binding protein (C/EBP), alpha	*Cebpa*	x	2.63	x
	CCAAT/enhancer binding protein (C/EBP), beta	*Cebpb*	1.64	1.69	-1.5
	cAMP responsive element binding protein 1	*Creb1*	x	1.94	1.71
	Chemokine (C-X-C motif) ligand 1 (melanoma growth stimulating activity, alpha)	*Cxcl1*	61.94	5.7	x
	Chemokine (C-X-C motif) ligand 10	*Cxcl10*	11.67	7.98	9.99
	Chemokine (C-X-C motif) ligand 13	*Cxcl13*	x	5.22	2.84
	Chemokine (C-X-C motif) ligand 2	*Cxcl2*	66.16	16.25	x
	Chemokine (C-X-C motif) ligand 6 (granulocyte chemotactic protein 2)	*Cxcl6*	x	37.59	8.36
	Chemokine (C-X-C motif) receptor 3	*Cxcr3*	x	1.8	x
	EGL nine homolog 1 (C. elegans) [Hif-prolyl hydroxylase]	*Egln1*	x	-2.33	-2.32
	Hypoxia-inducible factor 1, alpha	*Hif1a*	x	x	1.94

	subunit (basic helix-loop-helix transcription factor)				
	Interferon gamma receptor 1	*Ifngr1*	x	1.87	1.21
	Interferon gamma receptor 2	*Ifngr2*	x	1.59	x
	v-Ki-ras2 Kirsten rat sarcoma viral oncogene homolog	*Kras*	x	x	1.48
	Nitric oxide synthase 3, endothelial cell	*Nos3*	1.95	2.26	1.48
	Peroxisome proliferator-activated receptor gamma, coactivator 1 alpha	*Ppargc1a*	x	-14.41	-4.02
	Pro-platelet basic protein (chemokine (C-X-C motif) ligand 7)	*Ppbp*	x	-7.15	-7.91
	Prostaglandin-endoperoxide synthase 2	*Ptgs2/Cox2*	9.06	4.78	1.81
	Selectin, endothelial cell	*Sele*	6.79	3.36	2.06
Osteogenesis	Activin A receptor, type I	*Acvr1*	x	-1.31	x
	Activin A receptor, type IIB	*Acvr2b*	x	-2.02	-2.29
	BMP and activin membrane-bound inhibitor, homolog (Xenopus laevis)	*Bambi*	x	-1.72	x
	Bone morphogenetic protein 2	*Bmp2*	x	1.82	x
	Bone morphogenetic protein 3	*Bmp3*	x	-1.68	x
	Bone morphogenetic protein 4	*Bmp4*	x	-2.31	x
	Bone morphogenetic protein 6	*Bmp6*	x	-3.68	-2.61
	Bone morphogenetic protein 7	*Bmp7*	x	x	-2.64
	Cyclin D1	*Ccnd1*	x	1.46	1.89
	Cell division cycle 2, G1 to S and G2 to M	*Cdc2*	x	x	4.54
	Cadherin 16	*Cdh16*	x	51.56	x
	Cadherin 19, type 2	*Cdh19*	x	-1.56	x
	Cyclin-dependent kinase 4	*Cdk4*	x	1.9	1.83
	Chordin	*Chrd*	x	-2.31	x
	Catenin (cadherin associated protein), beta 1	*Ctnnb1*	x	x	1.72
	Dickkopf homolog 1 (Xenopus laevis)	*Dkk1*	-5.74	-2.75	x
	Dishevelled, dsh homolog 1 (Drosophila)	*Dvl1*	x	-1.94	x
	E2F transcription factor 1	*E2f1*	x	3.86	6.18
	E2F transcription factor 6	*E2f6*	x	-2.22	-3.04
	FAT tumor suppressor homolog 3 (Drosophila)	*Fat3*	x	x	2.25
	Follistatin	*Fst*	x	x	-2.18
	Frizzled homolog 1 (Drosophila)	*Fzd1*	x	1.71	1.61
	Frizzled homolog 8 (Drosophila)	*Fzd8*	-1.56	-1.7	x
	Growth differentiation factor 10	*Gdf10*	x	-1.64	-1.54
	Gremlin 1, cysteine knot superfamily, homolog (Xenopus laevis)	*Grem1*	x	-11.51	-8.98
	Low density lipoprotein receptor-related protein 5	*Lrp5*	x	-1.85	-1.41
	Neuroblastoma, suppression of tumorigenicity 1	*Nbl1*	x	-3.62	-2.68
	Retinoblastoma 1	*Rb1*	x	x	-1.41
	Retinoblastoma-like 2	*Rbl2*	x	-1.48	-1.29
	Secreted frizzled-related protein 4	*Sfrp4*	x	x	-1.476

	SMAD family member 1	*Smad1*	1.32	x	x
	SMAD family member 5	*Smad5*	x	1.56	1.72
	SMAD family member 6	*Smad6*	x	-1.67	x
	SMAD family member 7	*Smad7*	x	-1.89	-1.73
	Sclerosteosis	*Sost*	x	-18.12	-16.24
	Transcription factor 3	*Tcf3*	x	-1.92	x
	Transcription factor 7, T-cell specific	*Tcf7*	x	2.35	3.99
	Transforming growth factor, beta 1	*Tgfb1*	x	x	2.04
	Transforming growth factor, beta	*Tgfb2*	x	x	-1.95
	Transforming growth factor, beta 3	*Tgfb3*	x	-1.72	1.46
	Tumor necrosis factor receptor superfamily, member 11b	*Tnfrsf11b*	x	2.54	x
Bone Remodeling	Colony stimulating factor 1 (macrophage)	*Csf1*	1.9	1.57	x
	Cathepsin B	*Ctsb*	x	2.68	1.7
	Cathepsin C	*Ctsc*	x	2.43	1.82
	Cathepsin D	*Ctsd*	x	2.16	x
	Cathepsin K	*Ctsk*	x	-1.51	x
	Cathepsin L1	*Ctsl1*	x	1.94	x
	Cathepsin S	*Ctss*	x	2.98	x
	Cystatin C	*Cst3*	x	-1.24	x
	Ets variant 4	*Etv4*	x	-12.75	-4.08
	Matrix metallopeptidase 13	*Mmp13*	x	21.04	3.58
	Myelocytomatosis oncogene	*Myc*	4.46	2.45	1.74
Other	Nerve growth factor (beta polypeptide)	*Ngf*	7.58	12.19	3.77

Table 3.4. Relative fold changes (loaded over normal) for gene expression analysis done using qRT-PCR. *p<0.05 vs normal; #p<0.05 vs lamellar.

Gene Name	Gene Symbol	Qiagen primer num.	Lamellar			Woven		
			1 hr	Day 1	Day 3	1 hr	Day 1	Day 3
interleukin 6	*Il6*	*QT00182896*	1.21	1.12	-1.23	504.17*#	212.34*#	38.59*#
toll-like receptor 2	*Tlr2*	*QT00417438*	1.06	1.54	1.46	3.87*#	24.21*#	17.76*#
nuclear factor of kappa light polypeptide gene enhancer in B-cells 1	*Nfkb1*	*QT01577975*	-1.03	1.24	1.16	1.58*#	3.31*#	4.64*#
nuclear factor of kappa light polypeptide gene enhancer in B-cells inhibitor, alpha	*Nfkbia*	*QT01600956*	2.18*	1.09	-1.09	2.90*#	1.31	1.83*#
selectin, endothelial cell	*Sele*	*QT00179018*	-1.08	1.96	1.36	10.37*#	18.52*#	9.63*#
prostaglandin-endoperoxide synthase 2	*Ptgs2 (Cox2)*	*QT00192934*	1.13	1.89	1.43	16.39*#	16.85*#	8.58*#
chemokine (C-X-C motif) ligand 10	*Cxcl10*	*QT01082354*	1.01	2.31	1.47	10.41*#	12.28*#	45.71*#
sclerosteosis	*Sost*	*QT00418558*	-1.30	-1.57	1.37	-3.44*#	-19.77*#	-8.07*#
matrix metallopeptidase 13	*Mmp13*	*QT00385686*	-1.40	-2.66	-2.57	1.08	9.23*#	4.28*#
cathepsin K	*Ctsk*	*QT00375599*	-1.09	-1.09	-1.44	-1.13	-1.11	2.85*#
nerve growth factor	*Ngf*	*QT01800344*	0.85	1.33	1.24	3.24*#	22.63*#	14.07*#

3.6 Discussion

The objective of our study was to identify gene expression differences between woven bone (induced using a damaging fatigue loading protocol) and lamellar bone (induced using a non-damaging loading protocol). Using a microarray we saw a higher number of DEGs for woven compared to lamellar bone formation. A total of 395 genes were differentially expressed between woven and lamellar bone formation 1 hr after loading, while 5883 and 5974 genes were differentially expressed on days 1 and 3, respectively. There were many inflammatory factors upregulated as early as 1 hr after damaging loading, such as toll-like receptors and pro-inflammatory cytokines. We expanded our previous results related to angiogenesis (McKenzie 2009), finding many differentially regulated genes associated with hypoxia and vasodilation. We examined bone-related genes, including Wnt and BMP pathways, to find that stimulation of woven bone formation both activates and attenuates various genes along these pathways. Finally, results demonstrated activation of bone remodeling pathways at later timepoints following damaging loading.

Woven bone formation is an important aspect of fracture repair. In fracture healing, woven bone forms as part of a multi-step process of both intramembranous and endochondral bone formation (Einhorn 1998, Gerstenfeld 2003a). Induction of a stress fracture leads to a more conservative healing response than for fracture repair, where the cartilaginous phase is omitted (Tami 2003, Uthgenannt 2007a). Thus, the stress fracture healing model can be used to study woven bone formation without the complexities involved in fracture healing, and with a reduction in the timeline between injury and repair.

The significance of the inflammatory response during the early stages of woven bone formation (indicated by a number of GeneGo pathway maps) requires further investigation. An inflammatory response is seen as the primary event after fracture healing (Heiner 2006, Khan 2008, Rundle 2006), and our data indicate a similar event for stress fracture healing. Most of the canonical pathways represented by the GeneGo maps focused on innate inflammatory responses and were in general upregulated. This upregulation began with several cell surface proteins/receptors know to function in mechanotransduction such as integrins, toll-like receptors (TLRs) and interleukin receptors (specifically *Il1r1*). In general, TLRs can be activated by PAMPS (pathogen associated molecular patterns found on microbial molecules) but also by mechanical strain and general cellular stress (Dinarello 2009). In woven bone formation *Tlr2* is upregulated at all timepoints but was absent for lamellar bone formation, confirming an inflammatory response for woven but not lamellar bone. These pathways in general lead to transcription factors such as NFκB, which regulates numerous pro-inflammatory responses including cytokines (*Il1*, *Il6*, TNF-alpha), chemokines (IL-8) and cell adhesion molecules (ICAM1, E-selectin). The overall regulation of NF-κB signaling during woven bone formation is complicated by the numerous autoreguatory feedback loops that attenuate the NF-κB response. For example, I-κBα is both an inhibitor and a transcriptional target of NF-κB. In general, a wide range of pro-inflammatory genes known to be targets of these pathways were activated, specifically cytokines. Proinflammatory cytokines such as IL-1, IL-6 and TNF-alpha have been shown to be secreted by macrophages as well as by cells originating from mesenchymal cells located in the periosteum. In previous studies, they peak in expression one day after fracture and decline rapidly to low levels by day three

(Dimitriou 2005). While TNF-alpha was not differentially regulated in the microarray, *Il6* and both *Il1a* and *Il1b* were greatly upregulated. *Socs1*, which takes part in the negative feedback of cytokines, was also upregulated across all three days suggesting that mechanisms for the attenuation of the immune response were also active in this time range. IL-6 and other pro-inflammatory cytokines serve as a central hub for other down-stream responses to tissue damaging, including angiogenesis, ECM synthesis and chemotactic effects on other inflammatory cells (Robling 2006b).

VEGF-A is considered crucial for angiogenesis and our previous qRT-PCR studies have shown its upregulation at all three timepoints (McKenzie 2009, Wohl 2009), although the microarray showed no significant differential regulation of it, nor of its receptors. HIF signaling is central to angiogenesis-osteogenesis coupling in osteoblasts, particularly because of its regulation of VEGF (Berchner-Pfannschmidt 2008, Lohela 2009). Interestingly, recent studies have shown that *Vegf* can be induced independently of *Hif1a*, by *Ppargc1a* (Arany 2008), which was greatly downregulated in this study. VEGF transcription is also promoted under hypoxia conditions by K-ras, as well as JunB and NF-kB. All three were upregulated to some extent. These findings suggest a more complex network of VEGF-A regulation that could be further investigated.

In prior studies we have seen an increase in vasculature on histology (Matsuzaki 2007) and in genes associated with angiogenesis (McKenzie 2009, Wohl 2009) following woven bone formation, but not lamellar bone formation. Microarray results expanded our previous knowledge by reporting prostaglandin signaling and vasodilation factors, such as *Ptgs2/Cox2*. Expression of *Cox2* has also been reported to be required for fracture healing (Simon 2002). However, consistent with our reports, *Cox2* expression is *not* required for lamellar bone formation in the ulna (Alam 2005, Li 2002). Vasodilation is controlled to some extend by the biosynthesis and release of nitric oxide and prostaglandins, controlled by constitutive and inducible forms of nitric oxide synthase (NOS) and cyclooxygenase, respectively (Mollace 2005, Tsuji 2006). The inducible isoforms are sensitive to inflammation, and osteocytes activated by fluid shear stress have been also shown to produce both prostaglandins and nitric oxide (NO) (Robling 2006b),

both of which were highly upregulated in our study. In contrast to our microarray results, which did not suggest a relationship between NO and lamellar bone formation, inhibition of NO was shown to decrease endocortical lamellar bone formation in the rat tibia (Turner 1996). However, the difference may be due to the skeletal site studied, as *Cox2* inhibition experiments in the rat have shown differences in lamellar bone formation between the tibia and ulna (Li 2002).

Microarray findings also pointed to a number of anti-angiogenic genes that were activated. CXCL-10 in particular, it is thought to be involved in (or perhaps triggers) the involution of microvasculature, when angiogenesis stops or even regresses as the nutrient demand of the tissue decreases. Our results demonstrate a significant upregulation of *Cxcl10*, with expression peaking on day 3. Overall, *Cxcl10* may be central to attenuation of the angiogenic response and other anti-angiogenic factors brought to light by the microarray could be further examined to expand our understanding of this part of the response to mechanical loading during woven bone formation.

Prior studies have shown mechanical stimulation, such as the loading done in this experiment, to greatly influence bone formation (Bentolila 1998, Uthgenannt 2007a). Osteocytes are thought to be particularly responsive to mechanical forces, as are osteoblasts, while osteoclasts are affected less directly (Iqbal 2005, Robling 2006b). The canonical Wnt signaling pathway is central to bone remodeling and has been shown to be directly affected by mechanical loading through the suppression of sclerostin (*Sost*) in osteocytes (Robling 2006b). *Sost* normally inhibits the Wnt-pathway, in particular through its interactions with LRP5 (Dinarello 2009). A suppression of *Sost* would therefore lead to an increase in osteogenesis, which was present in our study.

Pathways involving BMPs, specifically that of BMP-2 are critical for osteogenesis, particularly because of their interaction with angiogenic factors such as VEGF. TGF-β may initiate BMP synthesis, as well as having chemotactic, proliferative and matrix remodeling effects of its own (Dimitriou 2005). Although we have seen increased expression in *Bmp2* for both woven and lamellar bone in past experiments (McKenzie 2009), expression of BMP's in the microarray was not dramatic. In agreement with our findings on BMPs, another microarray fracture study also

found weak or no expression of common bone cytokines including BMP2, 4, 6 and 7 (Heiner 2006).

Bone remodeling is an important part of the damage-repair process. The tissue sample used for microarray analysis consisted of both new periosteal bone and original cortical bone. The upregulation of matrix remodeling genes may be due to remodeling at sites of damaged matrix in the cortical bone that are occurring simultaneously with new bone modeling on the periosteal surface. There was evidence of bone remodeling following damaging, but not non-damaging loading. Examining osteoclast function using *Ctsk* (primarily expressed in osteoclasts), demonstrated an overexpression in woven bone at day 3. This likely indicates the activation of osteoclasts to repair cracks in the cortex of the ulna (Hsieh 2002). It is clear from the differential regulation of these genes that osteoclasts play an active role after damaging fatigue loading, but not with non-damaging lamellar loading. MMPs can activate certain cell adhesion molecules, matrix components and cytokines by enzymatic cleavage (Kawamoto 2004). Upregulation of *Mmp13* in our study confirms that the breakdown of matrix components is occurring in woven but not lamellar bone. Promoters of MMP-13 are also known to be upregulated by RUNX2 during osteoblast differentiation, and we've previously shown *Runx2* to be upregulated during woven bone, but not lamellar bone formation (McKenzie 2009).

One additional area of interest is the nervous system response to loading. Our microarray data saw a significant increase in nerve growth factor in response to damaging loading, which was confirmed using qRT-PCR (Tables 3.3 and 3.4). The response was upregulated as early as one hour after loading, but only for woven bone formation. Lamellar bone did not show any increase in nerve growth factor expression. Nerve-related genes have also been seen in fracture healing (Meyer 2004). As opposed to a response localized at the site of damage, an additional aspect of animal loading is the possibility of a whole body nervous system response (Wu 2009). Our loading model demonstrates a significant increase in gene expression at the loading site compared to the contralateral ulna, but additional skeletal sites were not examined for changes in gene expression.

The study was not without limitations. The selected timepoints for expression analysis were based on prior studies and we thought they would give us a good indication of the early molecular events that differentiate woven from lamellar bone formation. Also, our microarray analysis was limited to the canonical pathways available in the GeneGo software. However, this bias was only incorporated into our top ten canonical pathway analysis, as GeneGo has the option to create and study networks generated from user input. Finally, differences in sensitivity between microarray and qRT-PCR were clearly demonstrated in our data. While the fold change differences in expression were not identical, we saw the same general patterns of increasing or decreasing expression using the two methods.

A microarray is an extremely powerful tool that can be used to assess the expression of thousands of genes simultaneously. Using this assay, we were able to distinguish the molecular response between woven and lamellar bone formation. A complete understanding of the molecular mechanisms that regulate bone formation in the adult skeleton will be informative to allow development of drugs or therapies to help promote rapid bone formation in a clinical setting.

3.7 Conclusions

Use of a whole genome microarray has allowed us to confirm the gene expression responses from our prior study (McKenzie 2009) and has identified other genes and pathways that differ between woven and lamellar bone formation. An overview of the major responses associated with woven bone formation depict a strong early inflammatory response, followed by an increase in angiogenesis and finally upregulation of osteogenic genes (Figure 3.6). Validation of these pathways using select target genes (qRT-PCR) confirmed their differential expression in our study. The vast amount of data present in the microarray can be used to show how expression of genes is choreographed to promote the sequential steps in bone formation.

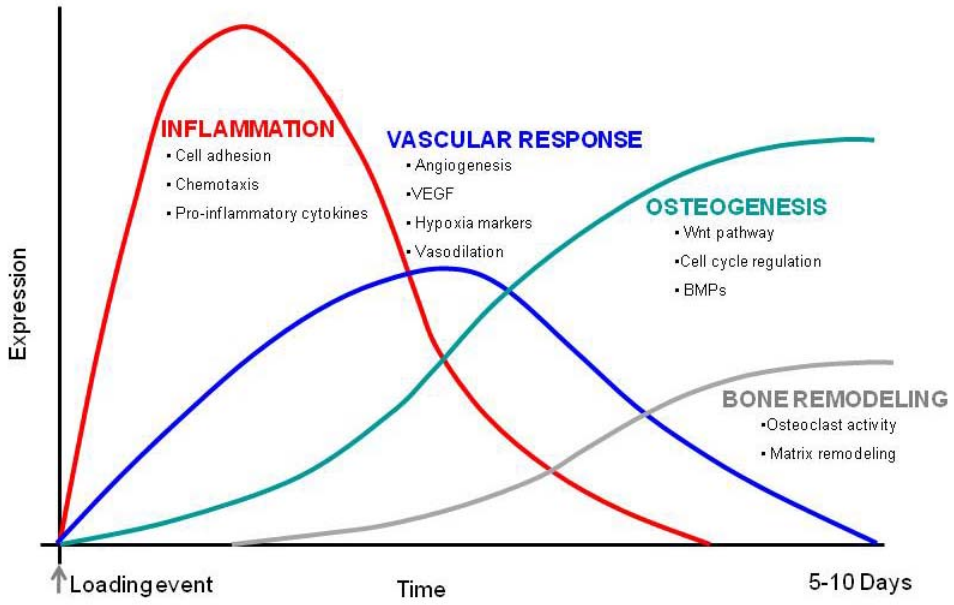

Figure 3.6. In combination with our previous report (McKenzie 2009), we have created an overview of the molecular response comparing woven to lamellar bone formation. There is an early immune response that persists through time but tends to decrease in expression. The vascular response is also a major component of woven bone formation and it precedes osteogenesis. Osteogenic indicators are differentially regulated shortly after loading, but seem to increase over time. Finally, bone remodeling markers are activated later to repair bone damage. Most of these changes likely occur within the first week or two following loading, although our data only goes through day 3.

4 Explorations Into the Use of Angiogenic Inhibitors TNP-470, SU5416 and YC-1 Following Fatigue Loading of the Rat Ulna

4.1 Abstract

In the rat ulna fatigue model, angiogenic gene expression and vascular changes precede osteogenic changes during woven bone repair. Our objective was to determine the effects of angiogenesis on woven bone formation in the rat ulna following fatigue injury using three angiogenic inhibitors. The first inhibitor, TNP-470, acts on methionine aminoptidase-2, and is reported to limit endothelial cell proliferation and vessel formation. The second inhibitor, SU5416, targets VEGF receptor 2. And the third inhibitor, YC-1, acts upstream of VEGF, affecting HIF1a at a transcriptional level. We hypothesized that administration of TNP-470 1) restricts upregulation of angiogenic and osteogenic genes associated with woven bone formation and 2) impairs vessel formation and blood flow. Furthermore, we hypothesized that administration of TNP-470, SU5416 or YC-1 reduces woven bone area following fatigue loading in the rat ulna. Forelimbs of male rats were loaded in a single bout of cyclic (2 Hz) axial compression at a constant peak force. Half of the rats received daily injections of an angiogenic inhibitor (either as a systemic injection or a local injection in the forelimb), while the other half received only the vehicle. TNP-470 administration significantly diminished gene expression of platelet endothelial cell adhesion marker (*Pecam*), and osteogenic markers (bone sialoprotein and osterix) measured three days after loading. Vascular perfusion and [^{15}O] water PET demonstrated increased vascularity and blood flow in loaded forelimbs vs. controls, but TNP-470 did not diminish these loading-induced changes. Nevertheless, there was a 60% reduction in woven bone area seven days after loading ($p<0.001$) in TNP-470 treated ulnae (0.45 mm^2) compared to vehicle alone (1.15 mm^2). Unexpectedly, neither SU5416 nor YC-1 reduced woven bone area. In conclusion, the angiogenic inhibitor TNP-470 impairs osteogenic gene expression and dramatically reduces woven bone formation following fatigue loading, but, surprisingly, did not affect angiogenic outcomes.

4.2 Key Terms

Angiogenesis, rat, woven bone, loading, inhibition, stress fracture

4.3 Introduction

There is an increasing amount of evidence indicating a crucial role for angiogenesis in skeletal development and repair. The role of angiogenesis has been documented in distraction osteogenesis (Fang 2005, Jazrawi 1998), fracture repair (Glowacki 1998, Hausman 2001, Street 2002) and skeletal development (Colnot 2001, Ferrara 2001, Pechak 1986). The increase in angiogenesis at the site of damage has been postulated to introduce additional osteoblast progenitors into the area. These progenitors eventually mature to increase bone formation.

Many different drugs have been taken from the cancer research field and applied to angiogenic inhibition in bone. Fracture studies have shown the importance of angiogenesis on healing in bone formation (Pacicca 2003), by inhibiting vessels using small molecules or a drug. TNP-470, an angiogenic inhibitor, acts by inhibition of methionine aminoptidase-2 (Sin 1997) and has been reported to limit endothelial, but not osteoblast, cell proliferation and vessel formation (Friis 2006, Street 2002, van der Schaft 2004, Wang 2000). Angiogenic inhibition by TNP-470 impairs osteogenesis in fracture repair (Hausman 2001) and distraction osteogenesis (Fang 2005). These studies highlight the importance of angiogenesis in a healing setting where large amounts of bone formation are required to help stabilize the injury.

SU5416 and YC-1 have also been shown to reduce vessel formation. The first inhibitor, SU5416, targets VEGF receptor 2 (Fong 1999, Zhong 2004) and was shown to dramatically reduce vessel formation *in vivo* in wound healing (Haroon 2002) and tumor models (Huss 2003, Katanasaka 2008). The second inhibitor, YC-1, acts upstream of VEGF affecting HIF-1a expression at a transcriptional level (Ko 1994). Similar to SU5416, this drug was shown to reduce vessel formation in several tumor models (Shin 2007, Yeo 2003).

In fracture healing bone forms as part of a multi-step process of both intramembranous and endochondral bone formation (Einhorn 1998, Gerstenfeld 2003a), which makes it difficult to isolate woven bone formation from the cartilaginous repair process. Using a stress fracture healing model, such as the rat ulna loading model (Bentolila 1998, Danova 2003, Tami 2003,

Uthgenannt 2007b) we can study woven bone formation without the complexities involved in fracture healing. Wohl et al. have shown early changes in expression of genes related to angiogenesis and osteogenesis in stress fracture healing (Wohl 2009). Furthermore, the vascular changes seem to correlate in a temporal and spatial pattern to the location of new bone formation (Matsuzaki 2007). These findings suggest that angiogenesis is required for successful woven bone repair.

Our objective was to determine the effects of angiogenic inhibition on woven bone formation in the rat ulna following fatigue injury. We hypothesized that administration of TNP-470 1) restricts upregulation of angiogenic and osteogenic genes associated with woven bone formation and 2) impairs vessel formation and blood flow. Furthermore, we hypothesized that administration of TNP-470, SU5416 or YC-1 reduces woven bone area following fatigue loading in the rat ulna.

4.4 Methods

The Washington University Animal Studies Committee approved all animal protocols.

4.4.1 Forelimb Loading

Male Fischer 344 rats (n=66, 5 mo) were anesthetized (isofluorane) and right forelimbs were loaded in a single bout of cyclic (2 Hz) axial compression at a constant peak force (18 N) as previously described (Uthgenannt 2007b). The left limb was not loaded and served as a control. Force and displacement were continuously monitored (60 Hz; Labview). Fatigue injury was controlled by limiting the cumulative maximal displacement to 65% (1.3 mm) of sub-fracture displacement (Uthgenannt 2007b). After loading, rats were given an analgesic (0.03 mg/kg buprenorphine) and returned to their cages. Rats were euthanized using CO_2 at day 0 (1 hr), day 1, day 3 or day 7 following loading.

4.4.2 Delivery of Angiogenic Inhibition Drugs

All angiogenic inhibitors (or vehicle alone) were administered daily, with the initial dose

prior to the start of loading. Injections were given up to, but not including, the day of euthanasia.

TNP-470

Animals were given TNP-470 (Seedhom) at a dose of 25 mg/kg s.c.. Vehicle animals were given an equivalent volume of saline, with the first injection 1 hr prior to loading. Ulnae were assessed for gene expression, blood vessel formation, blood flow (positron emission tomography), or bone formation (Table 4.1).

Table 4.1. Sixty-six rats were assigned as shown for each time period after a single fatigue loading event. PET imaging was performed serially on 3 rats per group at each time point. Day 0 measures were taken 1 hr after loading.

Outcome (technique)		Rats per time period			
		Day 0	Day 1	Day 3	Day 7
Gene Expression	TNP-470	6	6	6	-
(qRT-PCR)	Vehicle	6	6	6	-
Vessel Formation	TNP-470	-	-	6	-
(Microfil perfusion)	Vehicle	-	-	6	-
Blood Flow	TNP-470	3	→	→	→
(PET [^{15}O] imaging)	Vehicle	3	→	→	→
Woven Bone Area	TNP-470	-	-	-	6
(dynamic histomorphometry)	Vehicle	-	-	-	6

SU5416

SU5416 (Sigma) was given systemically (i.p. injection) at a dose of 12.5 mg/kg/day (Fong 1999). Vehicle rats were given an equivalent dose of dimethyl sulfoxide (DMSO; 350 µl/day). Local injections were given in doses of either 50 µg/day or 500 µg/day in a 5 µl volume (DMSO or inhibitor mixed into DMSO), injected into the forelimb near the periosteum on the medial side of the ulna. Regardless of delivery methods, the first injection was given 10 minutes prior to loading. Ulnae were assessed only for bone formation (n=2-4/gp) at day 7.

YC-1

Rats given treatment with YC-1 (Axxora) were administered injections following the same protocols as SU5416. Daily i.p. injections were given at a dose of 30 mg/kg/day (Yeo 2003) while

local injections were of either 50 µg/day or 500 µg/day (DMSO vehicle for all groups). The first injection was given 10 minutes prior to loading. One rat given YC-1 (i.p. 30mg/kg/day) died on day 3 due to injection complications and was excluded from the study. Ulnae were assessed for bone formation (n= 2-4/gp) at day 7.

4.4.3 Gene Expression – Quantitative Real Time PCR

Changes in gene expression were assessed using quantitative real time PCR (qRT-PCR) using recently described methods (Wohl 2009). Briefly, ulnae were dissected and immediately placed into liquid nitrogen. A 5 mm section from the central ulna was pulverized and RNA extracted (Qiagen). RNA quantity (Nanodrop) and quality (Agilent bioanalyzer) were assessed before making cDNA (Superscript III; Invitrogen). Quantitative real time PCR was run using validated primers (Wohl 2009) on two angiogenic markers, vascular endothelial growth factor (*Vegf*) and platelet endothelial cell adhesion molecular (*Pecam1*). Additional osteogenic markers were also evaluated, including bone morphogenetic protein 2 (*Bmp2*), osterix (*Osx*) and bone sialoprotein (*Bsp*). Measures of real-time PCR cycle to threshold were normalized to the expression of glyseraldehyde-3-phosphate dehydrogenase (*Gapdh*) for each ulna. To obtain a fold change comparison between experimental groups, *Gapdh*-normalized expression from each loaded ulna was divided by the normalized gene expression from the non-loaded contralateral control ($2^{-\Delta\Delta Ct}$).

4.4.4 Analysis of Vasculature

Vessel formation (day 3) was assessed by silicone rubber perfusion of the vasculature followed by routine histology. Using this technique the vessels were easily visualized with the surrounding tissue and cell morphology preserved. The methods have been recently described (Matsuzaki 2007). Rats were anesthetized (87 mg/kg ketamine, 13 mg/kg xylazine, IP) and the heart exposed via a thoracic incision before placing an 18- g catheter into the left ventricle. Heparin (10 ml, 100 USP units/ml) was injected to inhibit clotting. Rats were then euthanized by exsanguination. The vasculature was irrigated with saline prior to injection of a silicone rubber

solution (MICROFIL® MV-122, Flow Tech). Specimens were cured overnight (4 ºC). The ulna was dissected and processed for paraffin embedded histology. Sections (5 μm) were cut 1 mm distal to the mid-diaphysis and were quantitatively assessed. Perfused vessels were segmented from the rest of the image in order to calculate vessel number and total vessel area (Bioquant).

4.4.5 Positron Emission Tomography

To detect changes in blood flow, positron emission tomography (PET) imaging was performed serially on days 0, 1, 3 and 7 using [^{15}O] water. Imaging was performed on a microPET-focus® system (Concorde Microsystems), by the Small Animal Imaging Core at Washington University. Rats were anesthetized (1-3% isofluorane), positioned supine, immobilized and injected with an IV bolus of 30-40 mBq of [^{15}O] water. Dynamic PET data were acquired for 5 min (2 sec × 15 frames, 3 sec × 10 frames, 5 sec × 12 frames, 10 sec × 6 frames, 30 sec × 4) for [^{15}O] water. After imaging, rats were returned to their cages. Regions of interest (Sirois) were drawn on both right and left forelimbs to calculate the standardized uptake value (SUV) of tracer.

4.4.6 Bone Formation

To assess woven bone formation, rats were injected with calcein green (day 0) and alizarin complexone (day 5) before being sacrificed on day 7. Ulnae were imaged using microCT (16 μm resolution) and embedded in plastic (methylmethacrylate). Plastic embedded ulnar sections (100 micron, 1 mm distal to the mid-diaphysis) were analyzed for woven bone area using Bioquant.

4.4.6 Statistics

Data from loaded ulnae were compared to contralateral non-loaded ulnae using a paired t-test (p<0.05). Comparisons between inhibitor and vehicle treatments were made by ANOVA (p < 0.05).

4.5 Results

4.5.1 TNP-470

TNP-470 administration significantly diminished bone formation but did not affect angiogenesis in the fatigue-loaded rat ulna. Bone formation measurements revealed a 60% reduction in woven bone area after TNP-470 treatment (0.45 mm^2) compared to vehicle alone (1.15 mm^2) (Figure 4.1). Additionally, the extent of woven bone (as measured along the length of the ulna by microCT) was reduced (Figure 4.2). Vascular perfusion (Figure 4.3) and [^{15}O] water PET (Figure 4.4) demonstrated increased vascularity/blood flow in loaded forelimbs vs. controls, but TNP-470 did not diminish these loading-induced changes. Osteogenic-angiogenic coupling factors *Bmp2* and *Vegf* were significantly upregulated vs. control at 1 hr along with endothelial cell marker *Pecam* (Figure 4.5). All genes, including bone formation markers *Bsp* and *Osx*, were significantly upregulated on days 1 and 3, regardless of treatment. TNP-470 did not effect gene expression on day 0 or day 1, but expression of *Pecam*, *Osx*, and *Bsp* was significantly reduced in TNP-470 vs. vehicle treated ulnae on day 3.

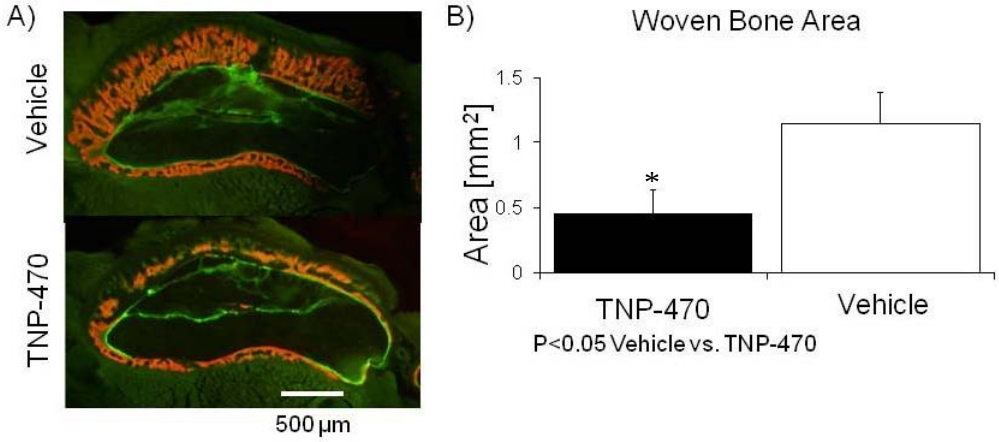

Figure 4.1. Administration of TNP-470 significantly reduced woven bone formation after fatigue loading. (A) Rat ulna cross-sections labeled with calcein (green) and alizarin complexone (red) show differences in periosteal woven bone formation. (B) Quantification of woven bone revealed a reduction in bone area following treatment with TNP-470.

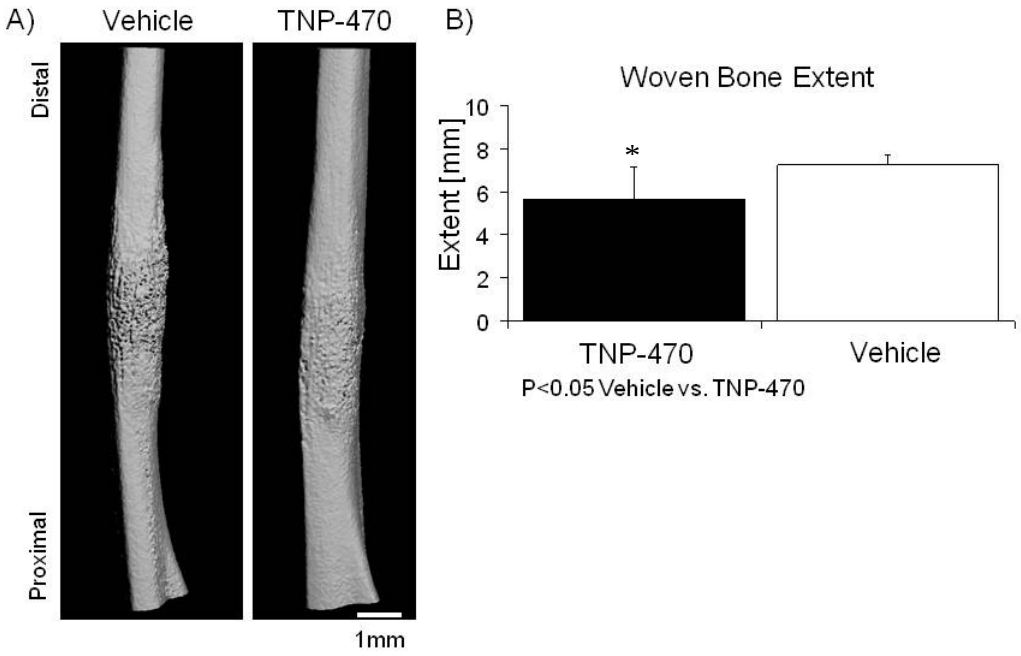

Figure 4.2. Administration of TNP-470 significantly reduced woven bone extent after fatigue loading. (A) MicroCT reconstructions of the central 14 mm of the rat ulna. (B) The woven bone extent was significantly reduced following treatment with TNP-470.

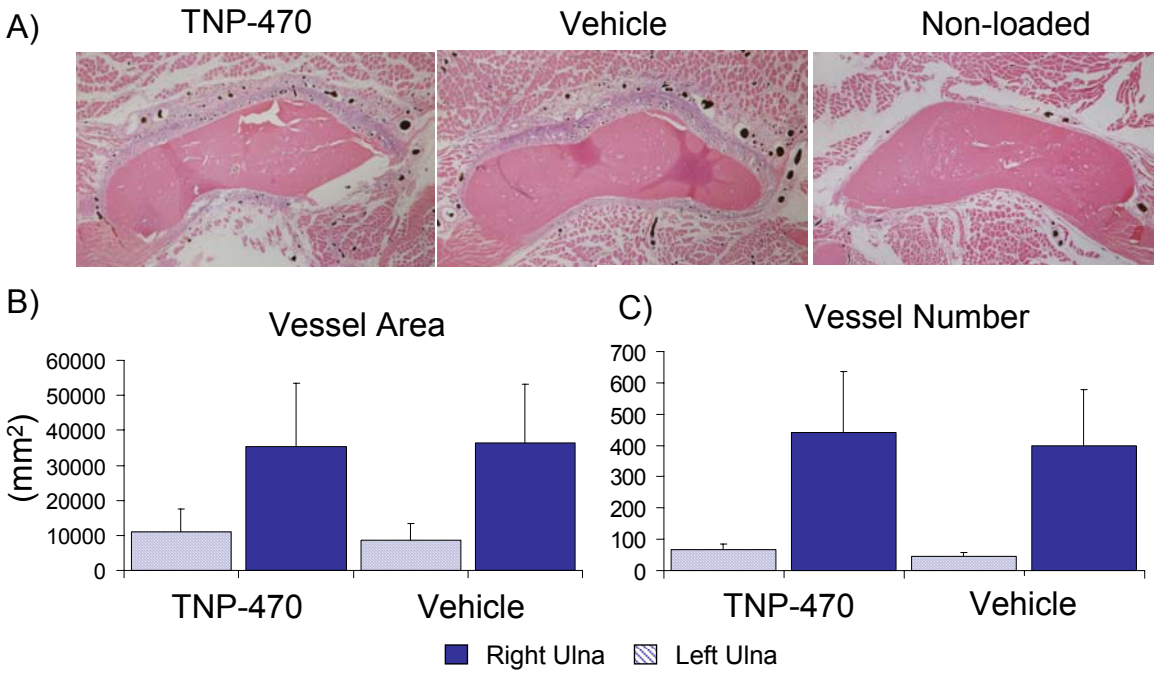

Figure 4.3. Vascularity was increased 3 days after loading. (A) H&E stained sections show increased vessels for both TNP-470 and vehicle treatment groups compared to non-loaded controls. (B,C) Vessel area and number are significantly increased after loading (compared to non-loaded controls), but there was no significant change between treatment groups.

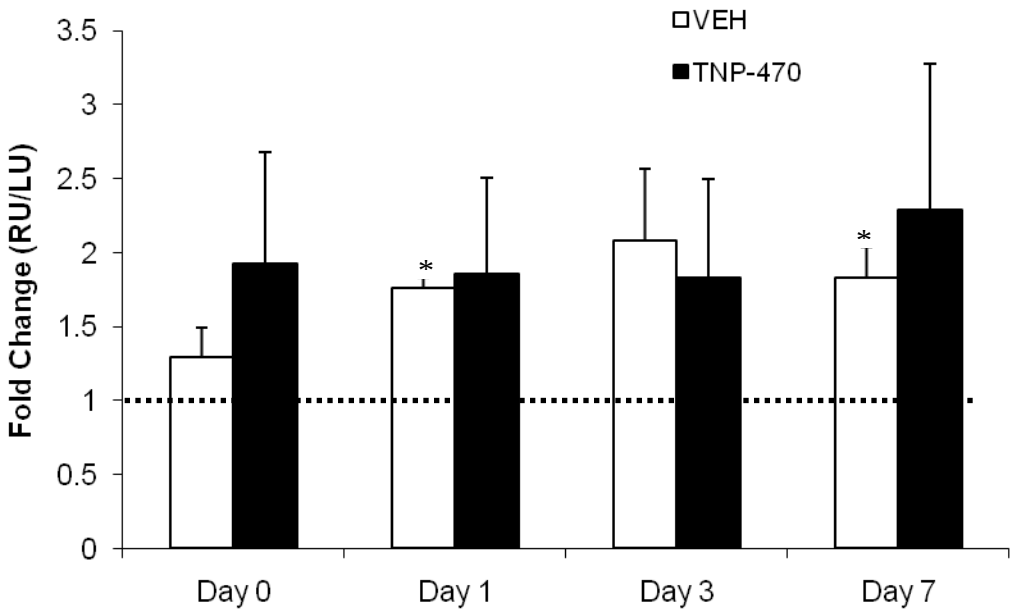

Figure 4.4. Fatigue loading increased blood flow. The fold increase (loaded/non-loaded) in [^{15}O] water standard uptake value (SUV) was assessed by PET imaging. There were no significant differences between TNP-470 and vehicle at any timepoint. (* $p<0.05$ loaded vs. control)

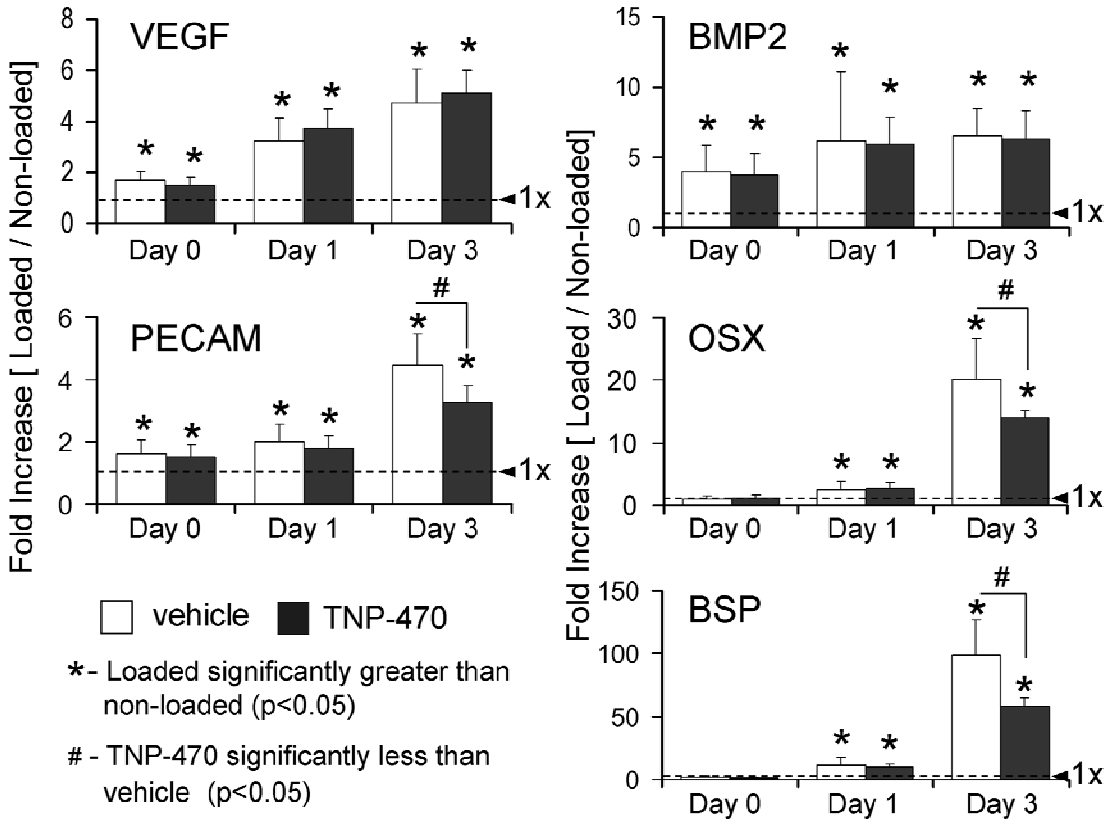

Figure 4.5. Gene expression significantly increased following fatigue loading. Fold increase in gene expression was measured by qRT-PCR at day 0 (1 hr), day 1 and day 3. Angiogenic genes *Vegf* and *Pecam* were significantly increased in both groups at all timepoints, but a treatment effect was seen only at day 3 for *Pecam* expression. Expression of *Bmp2* was unchanged by treatment with TNP-470. Bone formation markers *Osx* and *Bsp* were significantly reduced on day 3 following treatment with TNP-470.

4.5.2 SU5416 and YC-1

Treatment with VEGF inhibitor SU5416 or HIF1a inhibitor YC-1 did not reduce bone formation following forelimb loading. Both systemic and local injections with either vehicle (DMSO) or inhibition drug reduced body weight by more than 5% throughout the duration of the experiment (Figure 4.6). Assessment of systemic injections by microCT demonstrated no change in woven bone area or extent compared to vehicle treatment (Figures 4.7 and 4.8). In contrast, local injections of both SU5416 and YC-1 dramatically increased woven bone formation (Figure 4.9). Additionally, local injection of vehicle (DMSO) increased woven bone extent, but suppressed woven bone formation in localized areas along the medial side of the ulna.

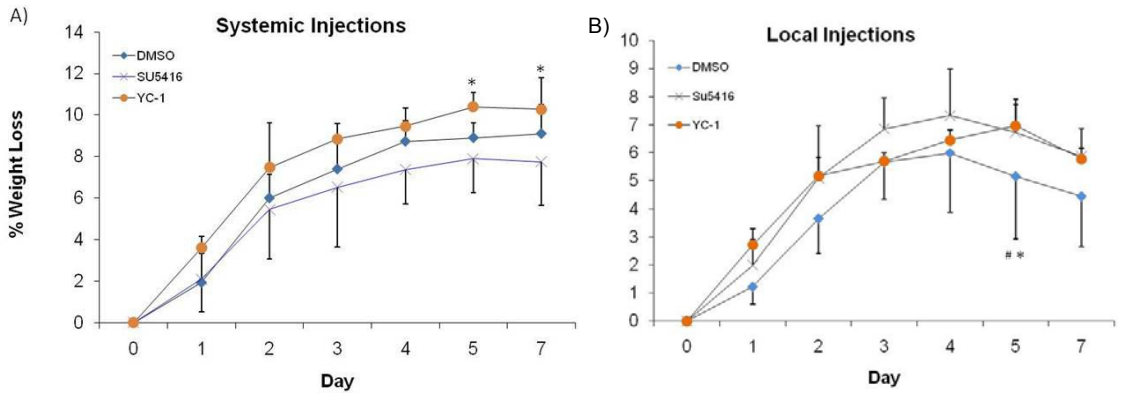

Figure 4.6. Animals treated with vehicle (DMSO), SU5416 or YC-1 lost weight during the experiment. Animals were given (A) systemic injections or (B) local injections. Weight loss peaked around day 4 or 5 for both types of injections. Systemic injection weight loss increased with time whereas local injection weight loss was reduced between days 4 and 7. The animal weight loss was less than 10% of total body weight. (n=3-4/group; *p<0.05 vs. YC-1; # p<0.05 vs. SU5416)

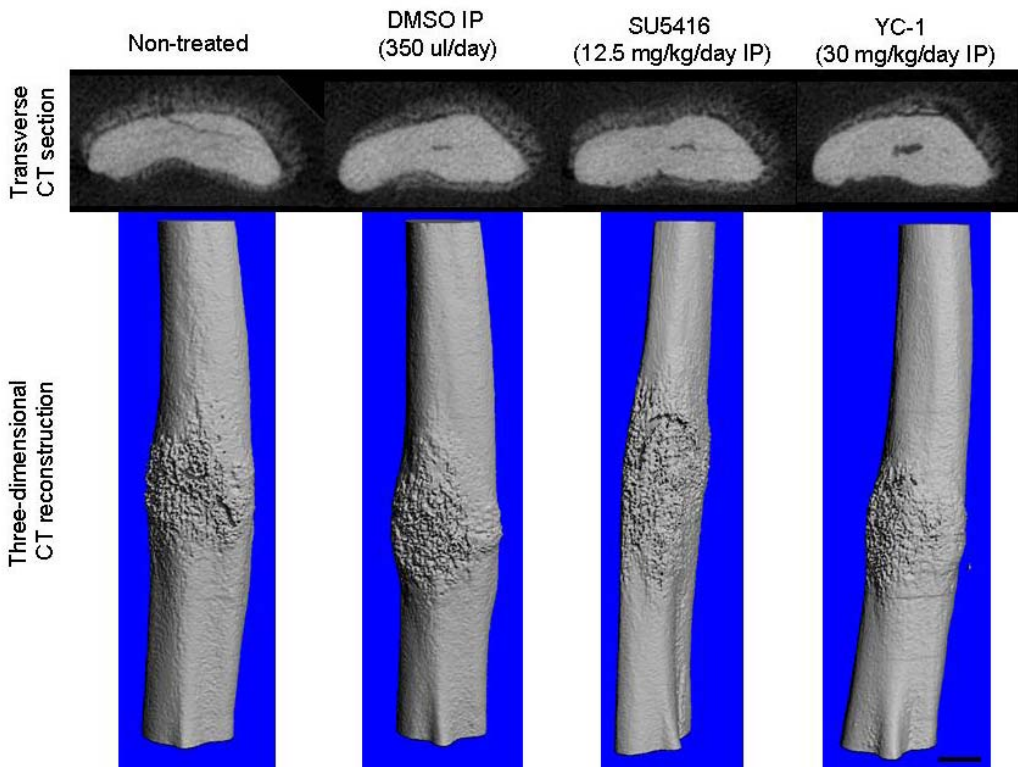

Figure 4.7. Inhibition of angiogenesis using systemic injections of SU5416 or YC-1 did not affect woven bone formation. The non-treated group was not different from vehicle (DMSO), SU5416 or YC-1 treatment. (n=2-4/group; scale bar = 1 mm)

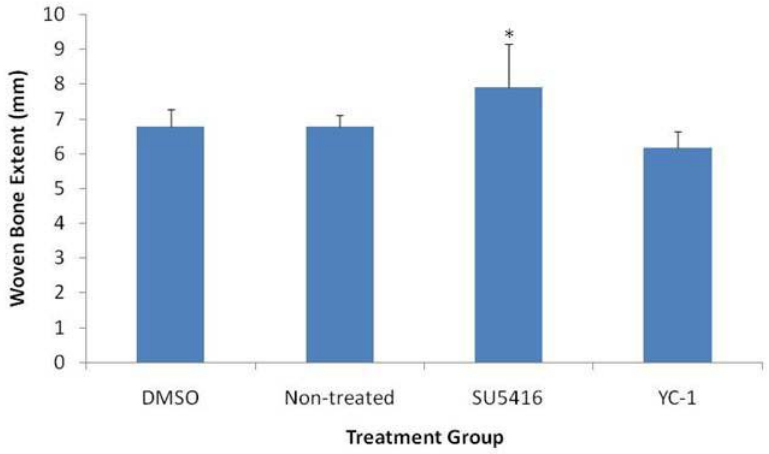

Figure 4.8. Total woven bone extent was not diminished following treatment with angiogenic inhibitors SU5416 or YC-1. The woven bone extent for SU5416 treated animals was significantly higher than those treated with YC-1, but treatment did not reduce woven bone extent compared to vehicle (DMSO) or non-treated animals (n=2-4/group; *p<0.05 vs. YC-1)

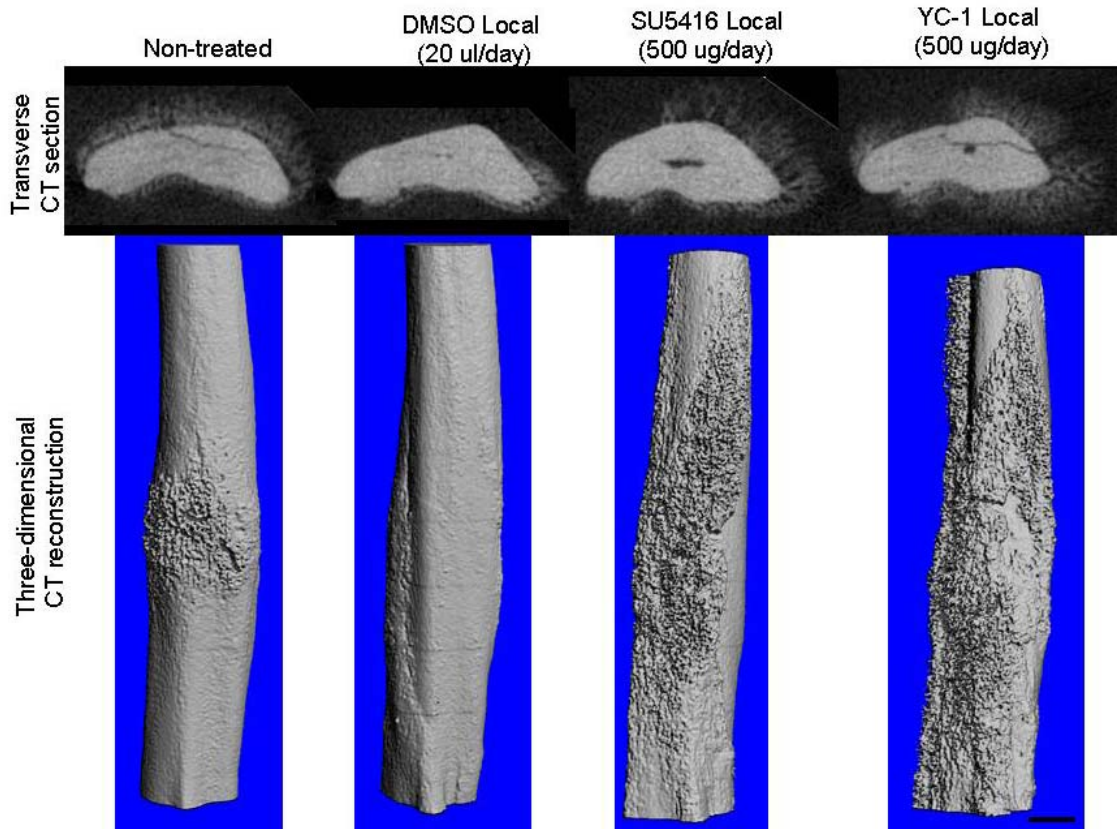

Figure 4.9. Local injections increased woven bone extent. Local injections of vehicle (DMSO), SU5416 and YC-1 all increased the extent of woven bone to greater than 14 mm (total area scanned). Vehicle treatment (with DMSO) diminished bone formation in some areas on the medial surface of the ulna. Bone area increased with treatment of SU5416 and YC-1 compared to non-treated controls. (n=2-4/group; scale bar = 1 mm)

4.6 Discussion

The objective of our study was to determine the effects of angiogenic inhibition on woven bone formation in the rat ulna following fatigue injury. In partial agreement with our first hypothesis, administration of the angiogenic inhibitor TNP-470 significantly impaired upregulation of osteogenic genes *Bsp* and *Osx* and angiogenic marker *Pecam* on day 3. Contrary to our second hypothesis, administration of TNP-470 did not inhibit vascular changes or blood flow following fatigue loading. Third, we hypothesized that angiogenic inhibition would reduce woven bone area. In agreement with this hypothesis, administration of TNP-470 impaired woven bone

formation, however administration of SU5416 and YC-1 did not decrease bone formation. Overall, our attempts to inhibit angiogenesis with the goal of reducing woven bone formation were unsuccessful.

TNP-470 treatment prevented callus formation in fracture repair (Hausman 2001) and bone formation in distraction osteogenesis (Fang 2005), which is similar to our results in stress fracture healing. The increase in *Pecam*, *Osx*, and *Bsp* expression (on day 3) coincides with periosteal thickening and onset of woven bone formation in this model (Silva 2006b, Wohl 2009). TNP-470 inhibited *Pecam* staining (indicator of vascularity) on day 13 of distraction osteogenesis (Fang 2005). In our study, the drop in *Pecam* expression in TNP-470 treated ulnae on day 3 is consistent with inhibition of endothelial cell proliferation. The lack of effect of TNP-470 on growth factors, *Bmp2* and *Vegf*, is also consistent with the mechanism of action of TNP-470, suggesting that TNP-470 acts downstream of both *Vegf* and *Bmp2*. Importantly, the drop in gene expression for osteoblast signaling (*Osx*) and matrix formation (*Bsp*) and the reduction in woven bone area on day 7 demonstrate a significant influence of TNP-470 on osteogenesis, with no affect on angiogenesis.

VEGF is tightly coupled to vascularization and has been a popular target molecule in anti-angiogenic research. Mice lacking VEGF exhibited delayed blood vessel invasion during endochondral bone development (Maes 2002, Zelzer 2002). The early upregulation of *Vegf* and *Pecam* in our study demonstrates a rapid vascular response to fatigue loading. SU5416, which acts on VEGF, has been reported to reduce vessel density (Ma 2003). One difference between administration of TNP-470 and SU5416 is the vehicle (PBS and DMSO, respectively). Treatment with DMSO vehicle has had mixed results in prior tumor models, having no effect (Takamoto 2001), or reducing tumor volume compared to the control (non-treated) (Ma 2003). We saw no vehicle affect with systemic treatment, but local injections reduced woven bone formation on the medial side of the ulna (near the injection site). The anti-angiogenic activity of SU5416 has been reported in vivo, but to our knowledge, has not been used with regard to a bone phenotype. Unfortunately, in our model, administration of SU5416 did not reduce bone formation.

HIF signaling is central to angiogenesis-osteogenesis coupling in osteoblasts, particularly because it regulates VEGF (Berchner-Pfannschmidt 2008, Lohela 2009). Thus, inhibition of HIF has been investigated as a potential cancer drug target (Liao 2007, Powis 2004, Shin 2007). Because of this interest a variety of drugs, such as YC-1, have been produced that target HIF and report a decrease in angiogenesis. Prior research has shown that YC-1 treatment leads to a reduction in migration of cancer cells (Shin 2007), decreased expression of *Hif1a* and *Vegf* (Powis 2004, Yeo 2003) and smaller, less vascularized tumors (Yeo 2003). To our knowledge, no work has been done using YC-1 to inhibit bone formation. Similar to SU5416, we saw no reduction in woven bone formation following administration of YC-1 *in vivo*.

One of the main limitations to this study was the potential lack of localization of the drug to our target area, near the midpoint of the ulna. Although previous studies using other models have shown the efficacy of systemic injections using the same angiogenic inhibitors, it was possible that poor drug delivery played a role in the lack of anti-angiogenic response to loading. An additional limitation to our study was drug dosing. The lack of vascular inhibition by TNP-470 may have been due to sub-optimal dosing or insufficient administration period. In order to limit the amount of drug (and vehicle) the animal was exposed to, we used the lowest effective dose of inhibitor published. Perhaps using a higher dose, as documented in other studies, we could have suppressed angiogenesis. Finally, our local injections seemed to cause a reaction in the periosteum not associated with loading. This technique needs to be improved in order to reduce the injection effect on healing.

Further elucidation of the mechanisms that are responsible for osteogenesis-angiogenesis coupling will deepen our understanding of bone development and homeostasis, and it may also aid in the design of new therapies for accelerating bone regeneration and repair. In order to determine the importance of angiogenesis on woven bone formation we need to expand our angiogenic inhibition work. This can be done with the use of different drugs, better drug targeting or continuous drug delivery. We have shown that bone formation is a complex process that cannot be stopped by inhibition of a single angiogenic target molecule.

In conclusion, the angiogenic inhibitor TNP-470 impairs osteogenic gene expression and dramatically reduces woven bone formation following fatigue loading. Use of VEGF inhibitor SU5416 and HIF1a inhibitor YC-1 did not show any reduction in woven bone formation using local or systemic deliveries. At this point in time we have yet to prove the angiogenic dependence of woven bone formation.

4.7 Acknowledgements

I would like to acknowledge the contribution of Greg Wohl, who assisted in forelimb loading and gene expression studies using TNP-470. Emmanouil Zampiakis performed vascular perfusion on the rats. The PET imaging was done in collaboration with the Small Animal Cancer Imaging Core with Jason Lewis and Jerrel Rutlin. TNP-470 was generously donated by Takeda Industries.

5 In vivo static creep loading of the rat forelimb reduces ulnar structural properties at time-zero and induces damage-dependent woven bone formation

5.1 Abstract

Periosteal woven bone forms in response to stress fractures and pathological overload. The mechanical factors that regulate woven bone formation are poorly understood. Fatigue loading of the rat ulna triggers a woven bone response in proportion to the level of applied fatigue displacement. However, because fatigue produces damage by application of cyclic loading it is unclear if the osteogenic response is due to bone damage (injury response) or dynamic strain (adaptive response). Creep loading, in contrast to fatigue, involves application of a static force. Our objectives were to use static creep loading of the rat forelimb to produce discrete levels of ulnar damage, and subsequently to determine the bone response over time. We hypothesized that 1) increases in applied displacement during loading correspond to ulnae with increased crack number, length and extent, as well as decreased mechanical properties; and 2) in vivo creep loading stimulates a damage-dependent dose-response in periosteal woven bone formation. Creep loading of the rat forelimb to progressive levels of sub-fracture displacement led to progressive bone damage (cracks) and loss of whole-bone mechanical properties (especially stiffness) at time-zero. For example, loading to 60% of fracture displacement caused a 60% loss of ulnar stiffness and a 25% loss of strength. Survival experiments showed that woven bone formed in a dose-dependent manner, with greater amounts of woven bone in ulnae that were loaded to higher displacements. Furthermore, after 14 days the mechanical properties of the loaded limb were equal or superior to control, indicating functional repair of the initial damage. We conclude that bone damage created without dynamic strain triggers a woven bone response, and thus infer that the woven bone response reported after fatigue loading and in stress fractures is in large part a response to bone damage.

5.2 Key Terms

Bone fatigue; bone creep; bone damage; rat ulna; in vivo forelimb loading

5.3 Introduction

Repetitive loading of bone causes fatigue, characterized by the formation and propagation of cracks and the progressive loss of strength and stiffness (Carter 1977, Pattin 1996). Bone fatigue can lead to stress fractures, which are common in athletes and military recruits (Beck 1996, Shaffer 2001). Histologically, stress fractures are associated with localized intracortical remodeling and periosteal woven bone formation (Johnson 1963, Mori S 2001), findings that are also observed in the rat ulna after a bout of damaging fatigue loading (Bentolila 1998, Hsieh 2002, Tami 2003).

The factors that contribute to fatigue-induced woven bone formation are poorly understood, although recent studies using the rat ulna loading model have examined this issue. In this model, dynamic compressive (fatigue) loading is applied to the forelimb, causing bending of the ulna leading to gradients in mechanical strain (Kotha 2004). Peak strains are located on the medial (compressive) surface, 1-3 mm distal to the midpoint of the ulna, corresponding with sites of fatigue crack formations (Danova 2003, Tami 2003, Uthgenannt 2007b) and maximal woven bone formation (Kotha 2004). Woven bone formation is stimulated in areas of high strain (Bentolila 1998, Kotha 2004, Tami 2003). Recently, we used this model to produce discrete levels of ulnar damage in vivo by controlling the level of peak displacement applied during fatigue loading (Uthgenannt 2007b). We observed that 7 days after loading, there was a dose-response in the area of new periosteal woven bone formation, where the amount of new bone was proportional to the level of imposed damage (Uthgenannt 2007a). This finding suggests that the woven bone response to fatigue loading is damage-dependent. However, because fatigue produces damage by application of dynamic loading, it is unclear if the osteogenic response is due to the effects of bone damage or to direct effects of dynamic strain.

Creep loading, in contrast to fatigue, involves application of a static force. As with fatigue loading, bone can sustain progressive displacement and damage under creep loading (Caler 1989, Carter 1985). Thus, static creep loading is a method that can be used to produce bone damage without dynamic loading and thereby provides a useful experimental tool to separate the effects of these two osteogenic stimuli. While non-damaging static loading is generally believed

to be non-osteogenic (Lanyon 1984, Robling 2001b), to our knowledge the response of bone to creep loading that produces measurable bone damage has not been reported.

Our objectives were to use static creep loading of the rat forelimb to produce discrete levels of ulnar damage, and subsequently to determine the in vivo bone response to creep damage. By analogy to the results of recent fatigue experiments (Uthgenannt 2007a, Uthgenannt 2007b), we hypothesized that 1) increases in applied displacement during loading correspond to ulnae with increased crack number, length and extent, as well as decreased mechanical properties; and 2) in vivo creep loading stimulates a damage-dependent dose-response in periosteal woven bone formation.

5.4 Methods

The forelimbs of 134 adult (4 ½ - 5 ½ month old) male Fischer 344 rats (Zimmerman) were loaded in axial compression based on an established rat forelimb loading model (Bentolila 1998, Hsieh 2002, Tami 2003, Uthgenannt 2007b), except rather than applying cyclic loading we applied static loading. Rats were anesthetized using 1-3% isoflorane and loading was applied across the carpus and olecranon process using a servohydraulic materials testing machine (Instron 1321/8500R or 8841). After application of a 0.3 N preload, a force-controlled single ramp (ramp time: 0.25 s) was applied to a pre-determined force level, which was then held constant. Force and displacement data were recorded at 30 Hz (LabView 7.0). In an initial experiment, right and left forelimbs (n = 35) from 18 rats were creep loaded to failure at peak forces between 17 and 30 N. The creep curves were consistent with previous descriptions of bone creep behavior (Figure 5.1). Time to failure (t_f; minutes) correlated moderately well with force (F; newtons): $F = -1.64\text{Log}(t_f) + 25.0$ ($r^2 = 0.66$, $p < 0.05$). The peak force necessary to cause failure after an average of 1 hour of loading was estimated from the force-time to failure equation. Importantly, forelimbs fractured reproducibly (independent of force magnitude or time to failure) when the displacement increased by 2.32 ± 0.46 mm compared to the displacement at 5 seconds.

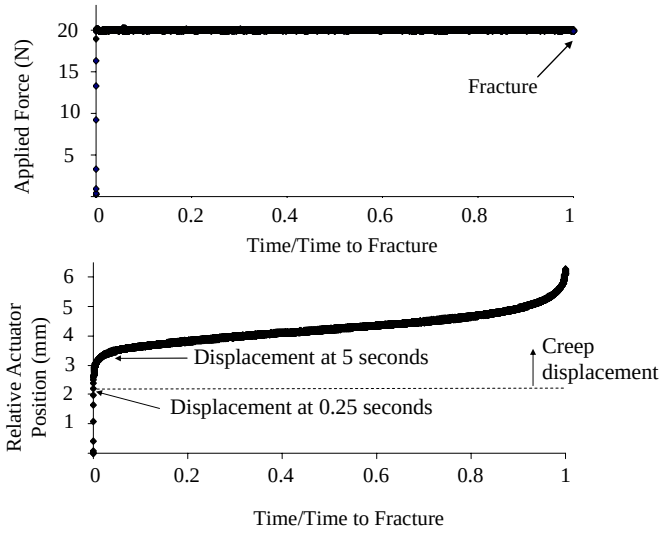

Figure 5.1. Representative creep curves as a function of normalized time. The force is ramped up within 0.25 seconds and held constant for the duration of the test. Displacement changes after 0.25 seconds are considered to be creep displacement. The test shown here ended when fracture occurred (at 6.9 min). The relative actuator position tracks the displacement through three stages of creep (Bowman 1994, Caler 1989, Carter 1977). The primary stage has an initial rapid increase in creep displacement followed by gradually decreasing slope. The secondary creep stage follows with a relatively constant creep rate. The tertiary creep stage begins with a rapid acceleration in creep rate leading to fracture. The average displacement to fracture was 2.32 ± 0.46 mm relative to the displacement at 5 seconds. Five seconds was used as a reference time to match the reference time used in our previous fatigue studies (Uthgenannt 2007b). Displacement in the first 5 seconds of the test is attributed to elastic deformation of the forelimb and soft tissue creep. In subsequent sub-fracture experiments, actuator displacement was monitored and stopped at a percentage of the average fracture displacement.

The right forelimbs of the remaining rats were loaded until the displacement reached a target value less than the average displacement to fracture. Left limbs were not loaded and served as controls. The force applied to the right forelimbs was between 17.3-19.8 N (although constant for each rat; avg. 18.9 ± 0.7 N) resulting in average loading times less than 1 hour. Based on previous strain gage data, these forces were expected to generate initial compressive

strains of 2330 – 2660 με. During loading of approximately one-half of the forelimbs, there were small sinusoidal variations in applied load (0.1 Hz, ±0.1 N) due to servo controller error. Subsequent strain gage tests were performed on three post mortem specimens; full methods were described previously (Uthgenannt 2007b). Briefly, strain gages (SS-080-050-500P-SI; Micron Instruments) were attached near the midpoint of the ulna and the forelimb was creep-loaded. Fluctuations in strain corresponding to the small sinusoidal variations in applied load were recorded. Results indicated that the peak-to-peak strain associated with these variations was < 20 microstrain, or < 1% of the total ulnar strain. For pain relief after loading, rats were administered an intramuscular injection of Buprenex (1.67 mg/kg buprenorphine hydrochloride). All rats were euthanized by CO_2 asphyxiation on day 0, 7 or 14 according to their experimental group. This study was approved by our institutional Animal Studies Committee.

5.4.1 Loading-Induced Damage

Seventy-four rats were used to investigate the effects of a single bout of creep loading on ulnar crack formation and mechanical properties. Rats were assigned to eight sub-fracture displacement groups (20, 30, 40, 50, 60, 70, 80 and 90%; n = 7-11 per group). Right forelimbs were loaded until the displacement reached the prescribed stopping displacement (X% of the average displacement to fracture). Forelimbs of two rats fractured during loading and they were excluded from the study. The loading time ranged from 0.22 min (a rat from the 20% displacement group) to 192.5 min (a rat from the 50% displacement group) (Table 5.1). Rats were euthanized immediately after loading.

Micro-computed tomography (microCT, Scanco Medical μCT40) was used to image and characterize cracks in excised ulnae before mechanical testing. The middle one-third of the ulna was scanned at 16 μm resolution (55 kVp, 172 mA, 200 ms) perpendicular to the long axis of the bone. First, the ulnae were assessed for presence of a crack. The overall crack extent (Cr.E) was measured along the length of the bone as the distance between the first and last transverse CT slice where the crack appeared. The position of the midpoint of the crack relative to the midpoint of the bone was calculated. Finally, using the manufacturer's software (Eval v5.0) a

single user determined the crack number density (Cr.N.D) and length density (Cr.L.D), averaged over four evenly spaced CT slices spanning the crack region.

The mechanical properties of loaded ulnae and non-loaded controls were assessed using three-point bending (Instron 8841). Ulnae were positioned on supports 15 mm apart and the displacement was applied on the medial surface at the midpoint of the ulnar length, producing bending in the same plane as during axial compression. A 0.5 N preload was manually applied followed by a 0.5 mm/s ramp to failure. Standard structural properties were determined from force-displacement curves (Labview 7.0). Ultimate force was calculated as the peak force; stiffness was calculated as the slope of the curve between 25 and 75% of the ultimate force; post-yield displacement was calculated as the displacement from the yield point to the fracture point; fracture energy was calculated as the area under the curve up to the fracture point.

5.4.2 Bone Formation Response

To investigate bone formation after damaging creep loading, survival rats (n=10/group) were assigned to three sub-fracture displacement groups: low (20% of the average displacement to fracture), medium (40%) or high (80%) displacement. The average loading times for the three displacement groups were 1.08 ± 0.4, 9.58 ± 9.4 and 42.12 ± 50.5 minutes, respectively. Rats were given intraperitoneal injections of 5 mg/kg calcein green (Sigma) on day 0 and 30 mg/kg alizarin-complexone (Sigma) on day 5 before being euthanized on day 7. The excised ulnae were imaged using microCT to discern cracks and calculate woven bone extent before being embedded in plastic and sectioned for histology.

Bone area (B.Ar) and bone mineral density (BMD) (calibrated to the manufacturer's hydroxyapatite (HA) mineral phantom) were determined using microCT. Analysis was performed at eight locations spaced longitudinally along the bone from 6 mm proximal to the midpoint (P6) to 8 mm distal to the midpoint (D8) in 2 mm intervals. Using manufacturer's software an average of six CT slices (96 μm total) at each location were analyzed for bone area and BMD (images manually segmented by a single user). Bone mineral content (BMC) was calculated as BMC = B.Ar $\times$ BMD. Ulnae were also analyzed for the presence of a visible crack and woven bone. If

woven bone was present, the extent was computed by determining the beginning and ending CT slices where woven bone was visible. The density of the woven bone at the midpoint was computed for a subset of specimens (n=5).

Ulnae were then embedded in plastic (methylmethacrylate, Sigma) using standard procedures in preparation for measurement of bone formation parameters. Sections (100 μm thick) were cut at five locations along the length of the ulna from 5 mm proximal to the midpoint (P5) to 7 mm distal to the midpoint (D7) in 3 mm intervals using a diamond-tipped saw microtome (Leica Microsystems, SP 1600). Each section was mounted on a glass slide and visualized on an inverted microscope with a 100 W mercury-halogen light source at a 4x objective (DP-30, Olympus). Calcein was imaged using a fluorescein isothiocyanate (Jacobsen) filter, while alizarin was imaged using a tetramethylrhodamine isothiocyanate (TRITC) filter. The images were overlaid using camera software (Olympus). The sections were analyzed (ImageJ) by a single user for woven bone area (Wo.B.Ar), bone area and labeled surfaces, including single-labeled surface, double-labeled surface and woven bone-labeled surface. Contralateral ulnae were pooled from each displacement group (n=4/group; 12 total) to form a common control group.

5.4.3 Recovery of Mechanical Properties

The recovery of mechanical properties was examined 14 days after loading. Rats (n=12) were loaded to high displacement (80% of the average displacement to fracture) and then allowed free cage activity for 14 days before being euthanized. The average loading time was 52.95 ± 35.4 minutes. Ulnae from nine rats were available for mechanical testing, as one forelimb did not reach the necessary displacement within the 3-hour time limit and two forelimbs fractured during loading. Excised ulnae were imaged using microCT before mechanical testing. Identical to the time-zero experiment, the mechanical properties of the loaded and control ulnae were assessed using three-point bending.

5.4.4 Statistics

Differences between right and left ulnae were assessed using paired t-tests, while one-way analysis of variance (ANOVA) was used to compare differences between displacement groups. Significance was defined at $P<0.05$.

5.5 Results

5.5.1 Loading-Induced Damage

Static creep loading of the forelimb created ulnar cracks visible on microCT at time-zero. Each displacement group had examples of loaded ulnae with visible cracks (usually one per ulna), in addition to ulnae with no visible cracks (Table 5.1). The average crack (including all displacement groups) was centered 0.11 ± 0.88 mm distal to the midpoint of the ulna. Generally, crack extent and crack length density increased with increasing displacement, with greater values in the 80 and 90% displacement groups than in most of the lower displacement groups. Left ulnae served as controls and did not have any visible cracks.

Table 5.1. Time-zero crack parameters of loaded (Right) ulnae measured using microCT (mean ± SD; n=7-11/group). The displacement groups were determined as a percentage of the average displacement to fracture (2.32 mm). Each displacement group had examples of ulna with a visible crack, although no group had a visible crack in every ulna.

Displacement Group	Loading Time (min)	Visible crack (% of ulnae)	Crack extent (mm)	Cr.L.D (mm/mm^2)	Cr.N.D. (#/mm^2)	Crack midpoint[1] (mm)
20%	1.05 ± 0.6	22	0.34 ± 0.19	0.32* ± 0.03	0.62* ± 0.04	0.30 ± 1.01
30%	6.65 ± 9.9	33	0.74* ± 0.38	0.47* ± 0.15	0.60* ± 0.03	0.02 ± 0.40
40%	19.33 ± 25.3	44	1.07* ± 0.66	0.58* ± 0.11	0.62* ± 0.07	0.08 ± 0.97
50%	54.21^z ± 65.8	45	0.52 ± 0.32	0.33*^{c} ± 0.09	0.60* ± 0.06	0.29 ± 1.21
60%	17.49 ± 18.1	66	0.58 ± 0.29	0.54*^{d} ± 0.19	0.64* ± 0.05	0.64 ± 0.80
70%	17.78 ± 15.8	56	0.92* ± 0.31	0.64*^{ad} ± 0.11	0.61* ± 0.07	-0.52^e ± 0.82
80%	10.04 ± 10.9	71	1.18*^{ade} ± 0.43	0.75*^{abde} ± 0.11	0.76*^{bcdef} ± 0.08	0.21 ± 0.93
90%	9.19 ± 14.2	56	1.32*^{ade} ± 0.61	0.74*^{abde} ± 0.26	0.78*^{abcdef} ± 0.17	-0.21 ± 0.78

P<0.05: * vs. zero; a vs. 20%; b vs. 30%; c vs. 40%; d vs. 50%; e vs. 60%; f vs. 70%; z vs. all displacement groups
[1]The crack midpoint was measured in the distal direction from the midpoint of the ulna; negative midpoint values are proximal to the ulna midpoint.

Static creep loading caused degradation of ulnar mechanical properties. Three-point bending tests revealed significant reductions in ulnar stiffness (loaded (Right) compared to control (Left)) in displacement groups higher than 20% (Figure 5.2). For example, forelimbs loaded to 60% of fracture had a 60% loss of ulnar stiffness. Beyond 60% displacement there were no further reductions in stiffness. There were similar reductions in ultimate force, although of less magnitude (Table 5.2). Post-yield displacement and energy to fracture did not display a clear decreasing trend with higher displacement groups. Notably, reductions in mechanical properties were observed in both loaded ulnae with and without visible cracks on microCT.

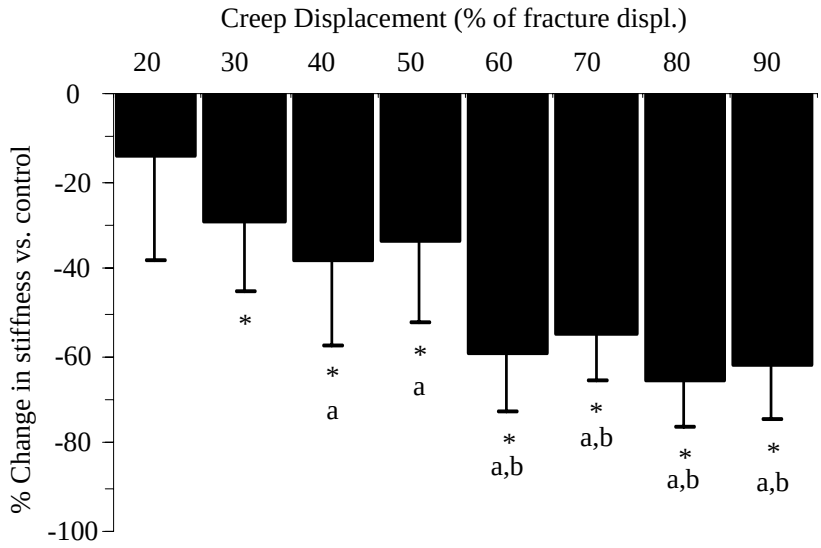

Figure 5.2. Increasing displacement caused progressive loss of time-zero bone stiffness. (The percent change in stiffness for loaded (R) versus control (L) limbs was calculated using (R-L)/L*100.) For all displacement groups beyond 20%, loaded ulnae were significantly less stiff than controls. Beyond 60% displacement there were no further reductions in stiffness. (P<0.05: * vs. control; a vs. 20%; b vs. 30%, 40% and 50%)

Table 5.2. Time-zero mechanical properties of isolated ulnae determined using three-point bending after in vivo creep loading of the right forelimb (mean ± SD; n=7-11/group). Data from the loaded (Right) limbs and control (Left) limbs were evaluated.

Displacement Group	Stiffness (N/mm)		Ultimate force (N)		Fracture energy (Nmm)		Post-yield displacement (mm)	
	Left	Right	Left	Right	Left	Right	Left	Right
20%	19.8 ± 3.4	16.9 ± 4.8	13.3 ± 1.1	12.8 ± 1.6	19.7 ± 3.1	20.7 ± 4.2	1.24 ± 0.26	1.35 ± 0.28
30%	20.9 ± 1.8	14.9* ± 4.2	13.5 ± 1.1	12.6 ± 1.5	24.3^{z} ± 5.2	19.0 ± 3.8	1.66^{z} ± 0.55	1.18 ± 0.31
40%	21.0 ± 2.1	12.8*^{a} ± 3.8	13.3 ± 1.0	11.9 ± 1.4	24.0 ± 3.8	18.1* ± 6.2	1.63^{z} ± 0.27	1.12* ± 0.48
50%	21.3 ± 2.3	13.9* ± 3.5	13.5 ± 1.3	12.7 ± 1.7	24.7^{z} ± 6.1	21.4 ± 5.7	1.68^{z} ± 0.46	1.39 ± 0.51
60%	22.2^{z} ± 2.9	8.90*^{abcd} ± 2.5	13.8 ± 1.4	10.3*^{abcd} ± 1.8	23.4 ± 3.0	14.7*^{ad} ± 5.6	1.51 ± 0.19	0.90^{d} ± 0.57
70%	22.1^{z} ± 2.1	9.86*^{abd} ± 2.3	13.6 ± 1.0	11.1*^{abd} ± 1.0	22.5 ± 4.6	14.2*^{ad} ± 5.9	1.47 ± 0.29	0.79*^{ad} ± 0.58
80%	21.1 ± 1.7	7.27*^{abcd} ± 1.9	13.5 ± 1.1	10.3*^{abd} ± 1.2	24.4^{z} ± 4.3	15.3*^{d} ± 4.8	1.63^{z} ± 0.27	0.82*^{ad} ± 0.50
90%	21.5 ± 2.3	8.06*^{abcd} ± 2.4	13.4 ± 0.82	10.6*^{abd} ± 1.9	23.4 ± 6.3	17.3 ± 6.5	1.58 ± 0.48	1.07 ± 0.62

P<0.05: * vs. control; a vs. 20%; b vs. 30%; c vs. 40%; d vs. 50%; z vs. 20% control group

5.5.2 Bone Formation Response

Micro-computed tomography of loaded ulnae 7 days after loading revealed a displacement-dependent woven bone response (Figure 5.3a, Table 5.3). Total woven bone area (summed over five histomorphometry sections) increased progressively and was significantly different between each of the displacement groups (Figure 5.3b). The same results were seen for woven bone extent. Woven bone was absent from all control specimens.

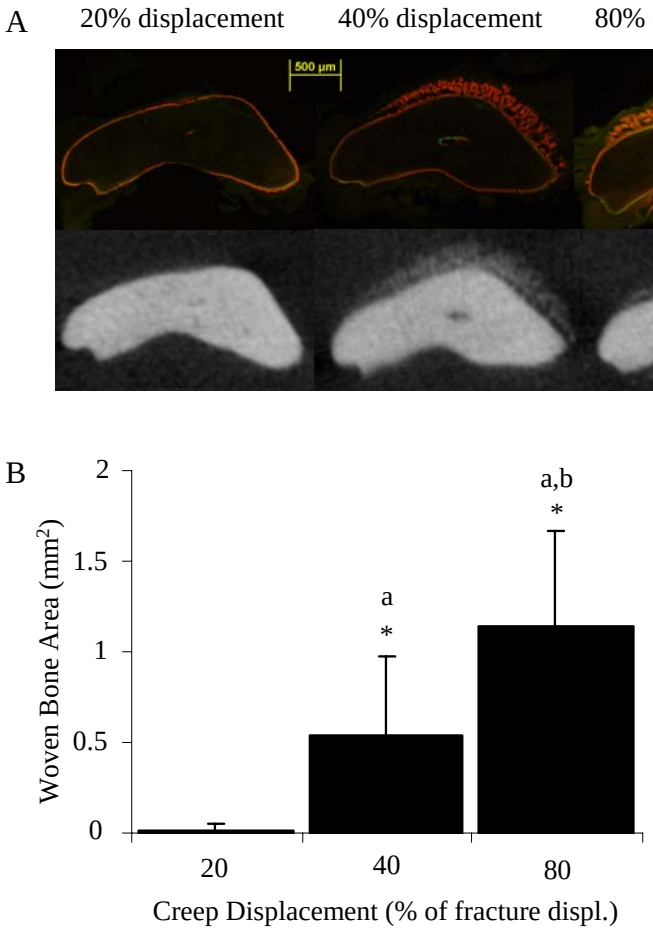

Figure 5.3. A clear dose-response was seen in the total amount of woven bone formed after creep loading. (A) Histological and microCT images illustrate increasing amounts of periosteal woven bone formation 1 mm distal to the midpoint of the bone for low (20%), medium (40%) and high (80%) displacement groups. (B) Quantification of woven bone area (totaled from all histomorphometry slides at five locations) demonstrates significant differences between displacement groups. ($P<0.05$: * vs. control; a vs. 20%; b vs. 40%)

Table 5.3. MicroCT (n=5-10/group) and histological (n=8-10/group) parameters (mean ± SD) measured 7 days post loading. The last four parameters (BMC, B.Ar, Wo.B.Ar and LS/BS) were measured 2 mm proximal to the midpoint of the ulna. The loaded (Right) ulnae are compared to a pooled control (Left) ulnae group.

Displacement Group	Visible Crack (% of ulnae)	Visible Wo.B. (% of ulnae)	Wo. B. Extent (mm)	BMC (mg/cm)	B.Ar (mm^2)	Wo.B.Ar (mm^2)	LS/BS (%)
Control	0	0	0.00 ±0.00	1.85 + 0.09	1.74 + 0.06	0.00 ±0.00	66 ±17
20%	0	30	0.37 ±0.88	1.85 ±0.05	1.79 ±0.04	0.00 ±0.00	89* ±9
40%	50	90	3.70*[a] ±1.7	2.01*[a] ±0.17	2.11*[a] ±0.33	0.10*[a] ±0.13	92* ±8
80%	80	100	5.25*[ab] ±0.98	2.25*[ab] ±0.29	2.71*[ab] ±0.65	0.18*[a] ±0.12	96* ±4

P<0.05: * vs. control; a vs. 20%, b vs. 40%

Woven bone formed near the midpoint of the ulnae in each of the three displacement groups. Sections taken 1 mm distal to the midpoint (D1) showed a clear dose-response with progressively larger amounts of woven bone in proportion to initial displacement. The dose-response at P2 was similar to that of D1, but without a significant increase from medium to high displacement (P = 0.053). Furthermore, there was a dose-response in woven bone labeled surface at D1 and P2. MicroCT data confirmed the changes in woven bone area seen using histology.

The distribution of bone formation varied along the length of the ulna (Figure 5.4). The largest amount of woven bone formed in the area of highest strain (Kotha 2004), near the midpoint (MP) of the ulna. Bone mineral content and mineral density were significantly different from control at the midpoint and 2 mm proximal to the midpoint (P2) for the 40 and 80% displacement groups (data not shown). Outside of the region of high strain (away from the midpoint) woven bone transitioned into lamellar bone. Woven bone was absent in sections 5 mm proximal to the midpoint (P5) and comprised less than 1% of the total bone area at sections 4 and 7 mm distal to the midpoint (D4 and D7, respectively). Loaded ulnae (from all displacement groups) had significantly more labeled surface compared to controls at all locations with the exception of the low displacement group (20% displacement) at P5. In the low displacement group there were no significant changes in BMC or BMD over the entire region of interest (P6-D8).

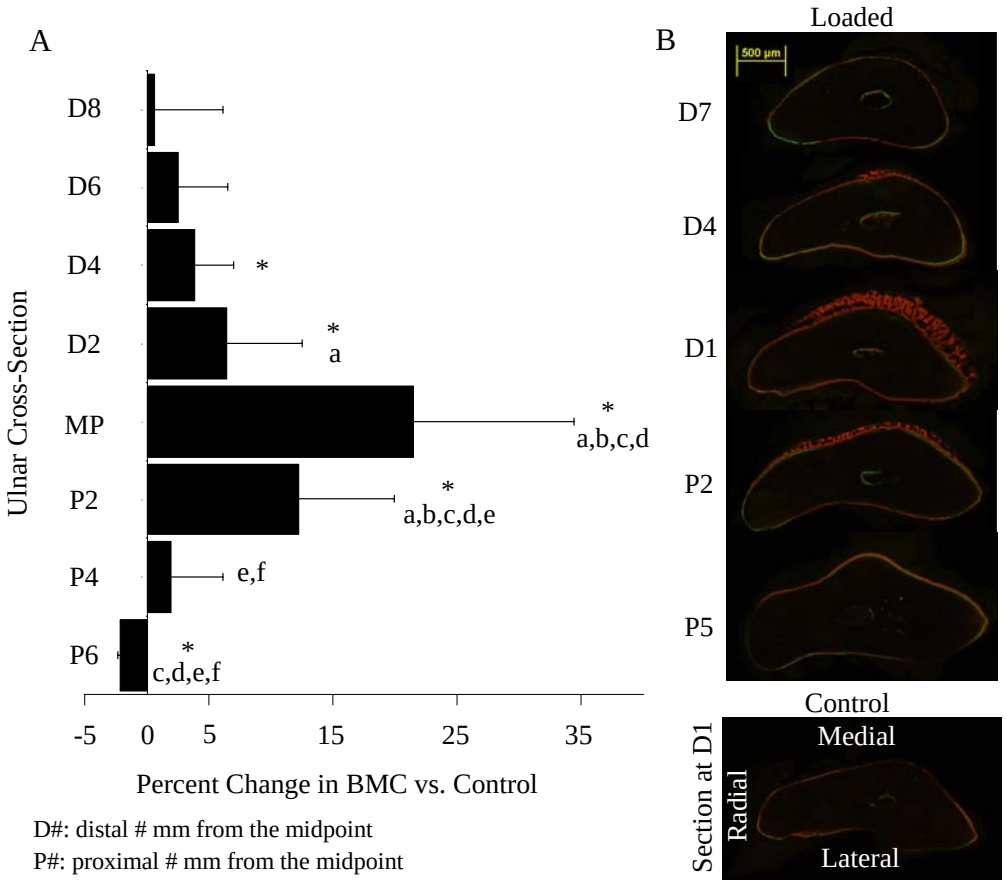

Figure 5.4. The magnitude and type of bone formed in response to creep loading varies longitudinally, similar to the pattern observed after fatigue loading (Uthgenannt 2007a). (Data from 40% displacement group shown; other groups had similar distributions) (A) The percentage change in BMC peaks at the midpoint (MP) and decreases both in the proximal and distal directions away from the midpoint. (B) Histological images illustrate labeled surfaces at five locations along the ulna. Woven bone is greatest 1 mm distal to the midpoint (D1) on the medial side of the bone. ($P<0.05$: * vs. control; a vs. D8; b vs. D6; c vs. D4; d vs. D2; e vs. MP; f vs. P2)

5.5.3 Recovery of mechanical properties

Ulnae from forelimbs loaded to high (80%) displacement demonstrated improvement in several mechanical properties compared to controls at 14 days (Table 5.4, Figure 5.5). Three-point bending tests revealed that the loaded ulnae had significantly greater values of ultimate

force, post-yield displacement and fracture energy than control. The stiffness of loaded limbs recovered to the level of control. Micro-computed tomography data showed visible cracks in 8 out of 9 ulnae. The woven bone density significantly increased between 7 and 14 days (7 days: 394 ± 21.5 mg HA/mm^3; 14 days: 710 ± 32 mg HA/mm^3; P < 0.0001), while woven bone extent was unchanged (7 days: 5.25 ±0.98 mm; 14 days: 5.34 ±0.94 mm; P = 0.84).

Table 5.4. Day 14 mechanical properties of isolated ulnae determined using 3-point bending after in vivo creep loading of the right forelimb (mean ± SD; n = 9). There were significant increases in the loaded (Right) ulnae in ultimate force, fracture energy and post-yield displacement compared to control (Left). (*p<0.05 vs. control)

Displacement Group	Stiffness (N/mm)		Ultimate force (N)		Fracture energy (Nmm)		Post-yield displacement (mm)	
	Left	Right	Left	Right	Left	Right	Left	Right
80%	23.9 ± 2.9	24.5 ± 3.7	14.9 ± 1.6	19.2* ± 1.5	21.1 ± 3.4	33.9* ± 6.0	1.2 ± 0.2	1.6* ± 0.3

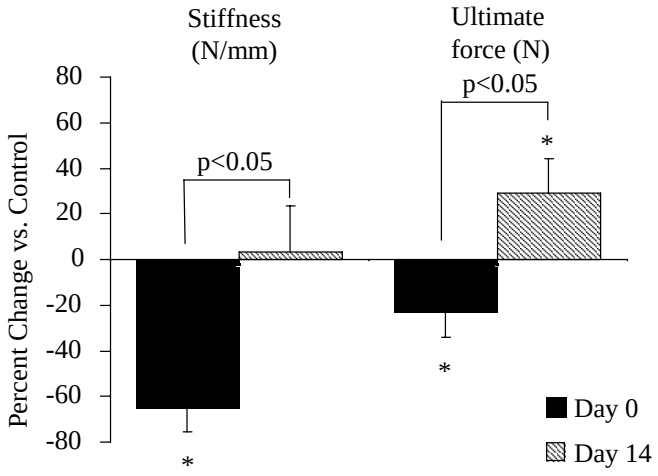

Figure 5.5. Initial significant decreases in stiffness and ultimate force were recovered 14 days after loading. Percentage change is based on comparison to contralateral controls. There were significant increases over the 14 day recovery period in both of these parameters. The ultimate force of the loaded (Right) limb was significantly higher compared to control (Left) at 14 days post loading. (*P<0.05 vs. control)

5.6 Discussion

Our objectives were to use static creep loading of the rat forelimb to produce discrete levels of ulnar damage and subsequently to determine the in vivo bone response to creep damage. In support of our first hypothesis, microCT and mechanical testing indicated that a single bout of creep loading can lead to reduced structural properties at time-zero. Generally, increased displacement produced a higher percentage of visible cracks, along with increased crack length and extent and greater loss of stiffness. In support of our second hypothesis, creep damage stimulated a dose-response in woven bone formation. This woven bone response led to an enhancement of mechanical properties 14 days after loading. These findings demonstrate that even without dynamic strain, bone damage triggers a woven bone response that leads to a functional repair of whole-bone strength.

Previous studies of bone response to creep loading have reported mixed findings. Positive osteogenic effects associated with static loading were reported in dog femora (Meade 1984) and rabbit calvariae (Hassler 1980). These studies both used long term loading protocols that involved invasive surgical procedures to implant continuous loading devices. The bone growth seen in these models could be due to an injury response, rather than an adaptation response (Hassler 1980). Our study produced an osteogenic response using a short-term non-invasive, damaging loading protocol. More commonly, studies have shown no osteogenic response to static loading, although these studies used loading protocols that probably did not produce bone damage. Comparisons between static versus dynamic loading protocols applied to the rabbit tibia (Hert 1969), the turkey ulna (Lanyon 1984) and the rat ulna (Robling 2001b) demonstrated that static loading produced no osteogenic response whereas dynamic loading was osteogenic. In growing rats, brief-duration static loading had an inhibitory effect on appositional bone formation while dynamic loading triggered an adaptive formation response (Robling 2001b). In addition, dynamic loading did not stimulate bone formation at frequencies below 0.5 Hz in the rat tibia (Turner 1994a). Our findings clearly demonstrate that when static loading produces measurable bone damage, woven bone formation is activated. While we also observed lamellar bone formation, this occurred between sites where woven bone was activated and sites where

there was no response. We hypothesize that this lamellar formation is part of a coordinated damage response rather than a primary response to short-term static loading.

Creep displacement is a component of the total displacement that occurs during fatigue loading in cortical (Carter 1985, Cotton JR 2005) and trabecular (Bowman 1998) bone. Moreover, it is well established that static loading by itself leads to progressive creep of bone (Bowman 1994, Caler 1989). While there are several reports on the degradation of bone mechanical properties during fatigue (dynamic) loading both in vivo and ex vivo, with reported decreases in modulus (Pattin 1996), strength (Carter 1977) and stiffness (Carter 1977, Danova 2003, Uthgenannt 2007b), similar data for in vivo creep (static) loading are lacking. Fondrk et al (Fondrk 1988) demonstrated bone stiffness degradation during tensile creep, but they used multiple cycle tests. Our results indicate that while creep loading of the rat ulna often produced visible cracks on microCT (i.e., a stress fracture) and reductions in mechanical properties, there were important differences between creep and fatigue damage. (Note that these comparisons are being made between studies done in the same lab, using the same age and sex of rats, and the same microCT and mechanical testing protocols. In both studies actuator displacement was used to produce discrete levels of damage based on a percentage of the displacement to fracture.) Fatigue loading more consistently created ulnar cracks that were visible on microCT (Uthgenannt 2007b), whereas creep-loaded ulnae did not always have a visible crack even at high values of displacement. Overall, there were fewer cracks and lower crack length density for creep compared to fatigue loading. Reductions in ultimate force, although significant for creep loading, were smaller than those reported for fatigue loading ($P<0.001$) (Uthgenannt 2007b). The two types of loading produced similar reductions in stiffness, and in both cases stiffness loss was detected in the absence of large cracks. We hypothesize that diffuse damage or cracks not visible at 16 μm resolution contribute to the loss of stiffness in both creep and fatigue. We further hypothesize that the loss of strength (ultimate force) is more strongly related to the formation of large cracks than to diffuse damage or microcracks. In summary, creep and fatigue loading of the rat ulna both produce bone damage but there are some notable differences between the two loading models.

Our motivation for examining the response of bone to damaging creep loading was to follow up on previous studies that showed woven bone formation after damaging fatigue loading (Colopy 2004, Hsieh 2002, Tami 2003, Uthgenannt 2007a). Consistent with fatigue loading (Uthgenannt 2007a), there is a dose-response in woven bone formation after creep loading whereby woven bone area increases with increasing damage. This strongly suggests that the damage component of fatigue is the predominant stimulus for the woven bone formation we and others have observed. Direct comparisons between the amount of woven bone formed for fatigue versus creep are difficult because of the differences in damage between the two loading modes as discussed above. Nonetheless, some qualified comparisons are worth considering. The “low” (20%), “medium” (40%) and “high” (80%) creep displacement groups were chosen for the survival experiments in this study because they produced equivalent loss of stiffness as the 30, 45 and 65% fatigue displacement groups (Uthgenannt 2007b) (~15, 40 and 60% loss of ulnar stiffness, respectively). If stiffness loss is taken as the measure of structural damage, our data indicate that creep produced a diminished woven bone response compared to damage-equivalent fatigue loading. The center of woven bone formation was similar between the two loading modes, at the ulnar midpoint (creep) or 1 mm distal to the midpoint (fatigue). Yet microCT analysis revealed consistently less woven bone extent for bones loaded in creep – 4 mm shorter (92% decrease) for the low-displacement group, and 2 mm shorter (35% and 25% decrease) for the medium- and high-displacement groups. In addition, total woven bone area (summed over five histology slides from P5 to D7) was reduced 94, 59 and 27% compared to fatigued loaded ulnae for low, medium and high displacement groups, respectively. By day 14 the mechanical properties of ulnae loaded in creep had recovered, similar to the response to fatigue loading (Colopy 2004, Hsieh 2002, Uthgenannt 2007a), indicating a functional repair of the structural damage in both cases. There are two possible explanations for the relatively greater woven bone formation after fatigue loading compared to creep. First, the more severe crack formation in fatigue may have stimulated a greater repair response. Second, the dynamic strain that occurs with fatigue may have an additive effect on top of damage. The latter possibility is consistent with the fact that supraphysiological levels of strain can stimulate woven bone formation in the

absence of damage (Turner 1994a), and the likelihood that the dynamic strain in the region of fatigue damage is supraphysiological.

There are several limitations to this study. First, our servohydraulic loading machines did not always hold a constant force when the forelimb was displacing (creeping) slowly. Thus, during creep loading, some forelimbs experienced a small, superimposed sinusoidal variation in strain (less than 1% of the total strain). We do not believe this influenced the creep response, as mouse forelimbs statically loaded with superimposed vibration were not stimulated to form new cortical bone (Castillo 2006), and the frequency of the superimposed variation (0.1 Hz) is less than that required to stimulate an adaptive bone response (Turner 1994a). Second, the applied force was not equal for all animals. We found there were variations between different batches of rats and the time it took them to reach their pre-determined displacement, so we adjusted the force magnitude in an attempt to keep loading time in a target range of 10-60 minutes. Although this may have added variance to our data, post hoc statistical analysis revealed no force dependence on any of the parameters of interest. Third, it is possible that dynamic strain produced during normal cage activities in the days following the bout of creep loading may have contributed to the bone formation response. Future studies are planned to examine this possibility. Fourth, the resolution of microCT is not high enough to detect true microcracks nor can it detect diffuse damage. Additional studies are needed to better characterize and distinguish the microdamage associated with creep versus fatigue loading. Finally, the bone formation response and mechanical property assessment tests were not run at both 7 and 14 days. Previous work in our lab has demonstrated that the total woven bone area does not increase from 7 to 14 days (Uthgenannt 2007a), thus 7 days is a suitable time to characterize bone formation. Moreover, full recovery of mechanical properties after fatigue loading takes 12-14 days (Hsieh 2002, Uthgenannt 2007a); thus we chose 14 days to assess mechanical properties.

The results of our study may have clinical implications. We have demonstrated that creep loading can lead to progressive bone damage, which suggests that the accumulation of bone microdamage with age (Schaffler 1995) or disease may not be entirely due to dynamic loading. Static loading, especially in the axial skeleton, may contribute importantly to bone

deformation and damage, as has been suggested previously (Bowman 1994). Regardless of the mechanical loading history that produces damage, our results indicate that when the damage leads to measurable structural degradation, a woven bone repair response is activated.

In summary, creep loading results in decreased mechanical properties at time-zero and a robust woven bone response 7 days after loading. We observed a clear dose-response with progressively larger amounts of woven bone in proportion to initial creep displacement (damage). This study provides an assessment of the bone damage response in the (near) absence of dynamic strain. Comparisons between creep and fatigue demonstrate that the effects of creep loading are similar to fatigue loading. We conclude that the woven bone response seen after the creation of a stress fracture is largely a response to localized bone damage.

5.7 Acknowledgements

This work was supported by the National Institutes of Health/NIAMS Grant AR050211

6 Conclusions

Mechanical loading is a powerful osteogenic stimulus and can be used to initiate woven or lamellar bone formation. The rat forelimb loading model applies a controlled waveform that distributes high magnitude compressive and tensile strains on the medial and lateral surfaces of the ulna, respectively. The changes in the strain environment, perhaps coupled with increased fluid flow in the bone increase periosteal bone formation. By controlling the applied waveform, the loading can be damaging or non-damaging to the structure of the bone. Thus, in a single-bout of loading we can stimulate formation of woven or lamellar bone near the ulnar midpoint.

The synchronization of the timelines between damaging and non-damaging loading protocols allowed us to study the gene expression changes caused by the induction of woven and lamellar bone. Both the timing and magnitude of gene expression changes were different between the formation of woven and lamellar bone. After damaging loading, there was a significant upregulation of genes associated with cell proliferation and angiogenesis followed by a robust upregulation of osteogenic genes. In contrast, non-damaging loading did not induce large changes in gene expression at any timepoint. An increase in vascular support precedes woven, but not lamellar bone formation. The early differences in magnitude of angiogenic and osteogenic gene expression between woven and lamellar bone are reflected in the physical changes in vasculature and bone formation at 3 and 10 days, respectively.

Expanding our subset of target genes using a whole genome microarray allowed us to simultaneously measure the expression of thousands of genes. There was differential expression of hundreds of genes 1 hr after loading between woven and lamellar bone formation, and thousands of genes on days 1 and 3. Because we did not pre-select target genes for the microarray, we were able to expand our previous findings on angiogenesis and strengthen our understanding of the role of osteogenic pathways. In addition, use of the microarray brought to light many inflammatory factors not previously investigated in our model. After confirming select microarray genes using qRT-PCR we concluded that woven bone formation required a significant early inflammation response prior to an increase in angiogenic and osteogenic gene expression. Additionally, mechanisms for the attenuation of the inflammatory, angiogenic and osteogenic

responses were also active at various timepoints. Analysis of the microarray demonstrated the complexities in gene expression that are required to promote the sequential events of bone formation.

Our data suggested that angiogenesis was critical to woven bone formation. However, our attempts to show that an inhibition of angiogenesis led to a reduction in woven bone formation were unsuccessful. We had moderate success using a widely published angiogenic inhibitor, TNP-470. In spite of its predicted inhibitory affects, we saw no change in vasculature following administration of TNP-470. Despite this, TNP-470 impaired woven bone formation. Moreover, administration of vascular inhibitors SU5416 and YC-1 did not decrease bone formation (although their effect on the vasculature was not investigated). These studies made it clear that in order to determine the role of angiogenesis we need to validate the delivery of the drug to the periosteal midshaft of the ulna and ensure that the drug is affecting its target.

Finally, as studies had shown that the magnitude of applied strain was not the key regulator of woven bone formation, we sought to separate the effects of bone damage from dynamic strain. We assessed damage following creep loading and compared those results to historical fatigue loading groups. Using discrete damage-matched levels of forelimb loading we were able to stimulate a dose-response in woven bone formation following creep loading. Because of the absence of dynamic strain in creep loading, our findings demonstrate that bone damage triggers the woven bone response. We also demonstrated that after creep or fatigue loading, the woven bone response leads to a functional repair of whole-bone strength.

In summary, using the rat forelimb loading model we have advanced our understanding of the formation of woven and lamellar bone. Ulnar damage is a key trigger for woven bone formation, not dynamic strain. In contrast, lamellar bone formation does not require bone damage. The molecular response varies between the two types of bone formation. Prior to woven bone formation there is a large inflammation response that is not present prior to lamellar bone formation. An increase in vascularity precedes woven, but not lamellar bone formation. In addition, both the angiogenic and osteogenic responses are greater for woven bone formation than for lamellar bone formation.

7 Future Directions

The role of angiogenesis needs to be investigated further to determine the link between vascular changes and bone formation. We hypothesized that woven bone formation is dependent on increases in angiogenesis. Microarray results demonstrated that factors involved in vessel dilation were upregulated in response to damaging loading. By further characterization of angiogenesis using this model, we will improve our understanding of the vascular role in new bone formation. A feasible first step in this investigation would be to characterize the blood flow following damaging and non-damaging loading. If blood flow is increased following forelimb loading, a future angiogenic inhibition study could attempt to target both the increased blood flow as well as new blood vessel formation.

Additionally, there are still large amounts of data available for analysis in the microarray. One shortcoming to our analysis was that based on our stringent significance criteria, we had very few genes that were upregulated between lamellar and control. It would be advantageous to relax the significance criteria and determine which genes are promoting lamellar bone formation.

Finally, while the rat has been an excellent animal model for this system, forelimb loading using mouse models can take advantage of genetically altered animals to help us understand the difference between woven and lamellar bone formation. It would be very interesting to investigate the bone formation response to forelimb loading, particularly in mouse models of immune deficiency, alterations in vasculature or bone formation defects. These could be very powerful tools to manipulate our model system without using any type of drug inhibition.

Appendix A – Blood Vessel Quantification

A.1 Introduction

MicroCT is commonly used to image bone. Normally, on a two-dimensional cross section of an imaged specimen, a threshold is used to segment bone from soft tissue to yield a binary image. Typically, blood vessels are impossible to discern from the surrounding soft tissue. However, by filling the vasculature with a radio-opaque substance (Microfil) we were able to image the vessels in the tissue surrounding the bone. In order to calculate the vessel volume in the tissue surrounding the bone, a modified analysis method had to be devised. Then we used standard histological techniques to verify the location of blood vessels and to obtain quantitative analysis of vessel number and area.

A.2 Methods

A.2.1 MicroCT Analysis

A 1.6 mm section (100 slices) of the ulna (with surrounding muscle intact) was scanned at 16 μm resolution. On the two-dimensional images contours were drawn that outlined the ulna on all 100 slices. Using the manufacturer's software the bone volume was calculated (sigma 1.2, support 2, threshold 345). Then, the ulna contour was dilated 20 pixels away from the bone surface (Figure A.1). A three-dimensional analysis was performed again to calculate the total volume of both the bone and surrounding vessels. To obtain the vessel volume, the total bone volume from the small (ulna only) contour was subtracted from the larger dilated volume. Finally, a three-dimensional reconstruction with the outer and inner contours was made (Figure A.2).

Figure A.1. A microCT two-dimensional cross section showing the ulna, radius and surrounding muscle tissue. The ulna and vessels were quantified inside of the green contour, while surrounding muscle was excluded from analysis. The entire forelimb takes up most of the 16 mm diameter of the scanning tube (shown as light gray circle).

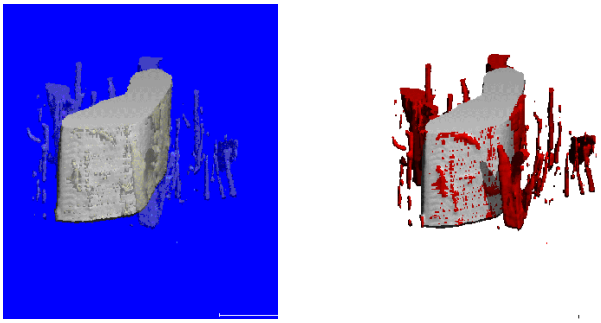

Figure A. 2. MicroCT three-dimensional reconstructions of ulna midshaft and surrounding vasculature. On the left-hand side is the reconstruction prior to color manipulation. The image on the right-hand side shows the vessels in red, the bone in grey and the background as white.

A.2.2 Histological Analysis

After scanning with microCT, the forelimbs were decalcified for three weeks using EDTA. The bones (and surrounding tissue) were embedded in paraffin and sections 5 μm thick were cut. Then, sections were stained using H&E to help visualize morphology (Figure A.3). Using Bioquant software, bone area and perimeter were quantified (threshold [255,0]). Then, a larger tissue volume was drawn intersecting the expanded periosteum and muscle cuff. The area was

re-analyzed (threshold [135,0]; smoothing; low filter = 0) after erasing any vessels inside of the bone. From this analysis, vessel number, vessel area, and mean vessel area were calculated for each sample.

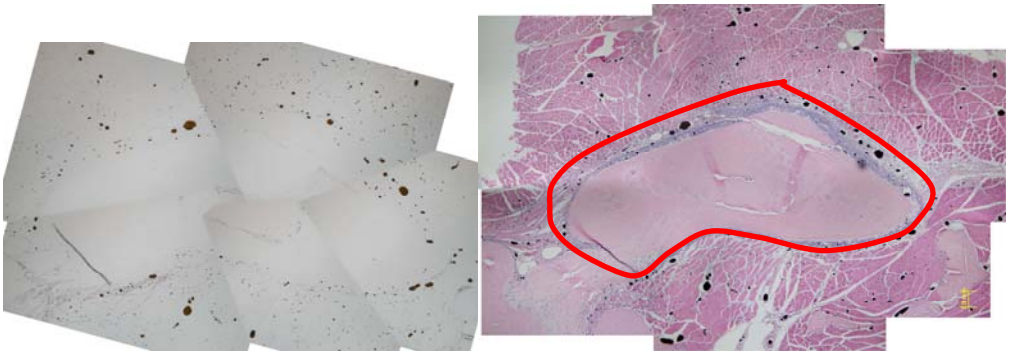

Figure A.3. Non-stained (left) and H&E stained (right) paraffin sections of loaded ulnae and surrounding tissue that has been perfused with microfil. The area inside of the red contour was analyzed for vessel number and area.

A.3 Results

Using microCT and standard histological techniques the vessels surrounding the ulna were analyzed. There are large blood vessels on the medial side of the ulna in control and loaded sections shown both on microCT and histologically. The specific applied thresholds (for both microCT and histology) attempted to reflect the actual vessel and bone area. Analysis results are in Chapters 2 and 4.

A.4 Conclusions

Vascular perfusion with microfil can be used to determine vessel volume, number and area in the periosteum of the rat ulna. Because the blood vessels in our model were on the periosteal surface, it permitted separation of the bone from the surrounding vasculature. If the vasculature inside the bone needed to be quantified, a calcified bone could not have been used, as it is impossible to separate vessels from bone using standard microCT thresholding techniques. A standard histological section (on decalcified bone) allows a much higher resolution image of vessels and allows a more accurate quantification of vessel number and area.

Appendix B Microarray Sample Setup

B.1 Introduction

Microarrays are becoming a common tool used in scientific research. A number of papers have been written on the subject of microarray sample size. In order to ensure we were able to obtain statistically relevant results using the smallest number of microarray's, we did a complete power analysis prior to beginning our experiment. Microarray variation can be classified into three categories; array variation, non-array-technical variation and biological variation (Shih 2004). Although we have little control over array variation, we can control non-array-technical variation, and we can investigate biological variation using pooled or non-pooled data in our array analysis (Agrawal 2002, Kendziorski 2005). Pooling would average the data from multiple animals onto one chip and require fewer microarrays per group, but would potentially have a higher animal-to-animal variability that could not be sorted out. Single microarrays (without pooling) could potentially have a higher cost, as more arrays would need to be done to get the same statistical significance.

B.2 Methods

Relevant microarray literature was surveyed to determine whether or not pooling would be beneficial in our model. It has been shown that pooling is advantageous when biological variability is large compared to technical variability (replicates) (Kendziorski 2005). This could potentially hide biological variance and give false confidence concerning the data significance (Zhang 2005). Also, it was reported that increasing the sample size did not change the accuracy of the array beyond a certain point (Figure B.1) (Kendziorski 2005). If there is enough RNA from each individual animal to run an array, the non-pooled design is recommended (Shih 2004).

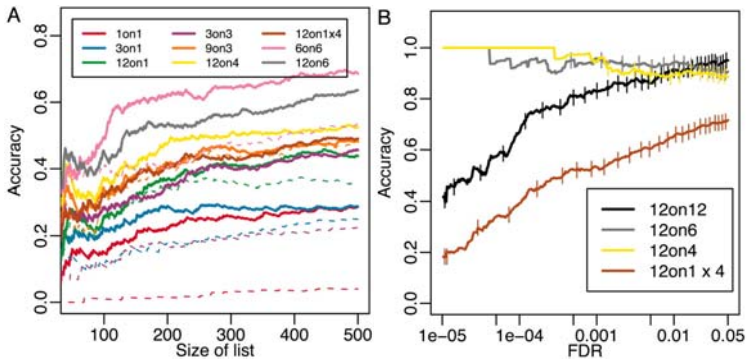

Figure B.1. Microarray design accuracy. (*A*) Using lists of fixed size, the accuracy of the microarray was calculated. The solid lines give the average performer across 100 subsets, while the dashed lines give the worst case performer. The top (pink) line shows the results from 6 animals on 6 separate arrays, which was higher than the yellow line (12 animals split into pools of 3 on 4 arrays). (*B*) In a different type of analysis, the false discovery rate (FDR) was varied and the accuracy calculated. Each vertical tick on the FDR plot marks 100 genes identified at the specified level of FDR. As the FDR increases, the accuracy of the animals per array converge. (Kendziorski 2005).

We then needed to determine how many samples would be necessary for statistically significant results. We used a power function (S) (Zhang 2005), which reads

$$S = \int_0^\infty P_{n_c+n_t-2}(Y)\Phi\left[\frac{-|\xi|\sqrt{Y}}{\sqrt{n_c+n_t-2}} + \frac{|\mu|}{\sigma_D}\right]dY. \qquad \text{(B.1)}$$

A detailed description of the variables in the equation can be found in (Zhang 2005). Using a variety of user input, the formula determined statistical power (Table B.1)

Table B.1. The variable inputs for use in the power function (Zhang 2005). The application can be accessed at http://wads.le.ac.uk/htox/WadsSoftware/MrcStats/SCal4Poolings.jnlp.

Variable name	Variable description	Values used
Nc	number of pools for the control population	4, 5 or 6
Nt	number of pools for the treatment population	4, 5 or 6
R	number of biological subjects used to form a pool	1 or 3
M	number of measurements made on each pool	1
var_bio	biological variance at individual subject level	0.05
Pth	threshold p value; or false positive rate which is sometimes denoted by the symbol alpha	0.00001-0.01
Mu	magnitude of difference between the two populations	1
Ns	total number of biological subjects from the two populations	r=1: 8, 10 or 12
Nm	total number of measurements in the experiment	r=3: 24, 30 or 36

Finally, the cost considerations between pooling and non-pooling were considered. We took into account the cost of animals (baseline cost plus housing), tissue processing and fees associated with microarray chips and reagents.

B.3 Results

One of the main strengths of pooling samples was to obtain a certain quantity of RNA. Since we knew exactly how much RNA to expect from both loaded and normal samples (based on our gene expression study in Chapter 2) there was no question that each animal would provide enough RNA for a single microarray. Our power study showed us that using a non-pooled microarray with a sample size of 6 or greater would yield statistically significant results at a variety of p-values (Table B.2). Our cost analysis was $12,330 for non-pooled samples and $15,630 for pooled samples. Because the rat chips we were using came in sets of 12 arrays, in order to get the most arrays done (and therefore be most efficient) we decided to use a total of 7 arrays per loading protocol and timepoint along with 6 normal controls.

Table B.2. The results of power analysis for select p-values and array numbers. We looked at both non-pooling and pooling scenarios of 6 and 4 arrays, respectively.

P-value	S (no pooling; 6 arrays)	S (pooling; 4 arrays)
P = 0.005	0.998	0.994
P = 0.001	0.980	0.900
P = 0.0005	0.953	0.796

B.4 Conclusions

A microarray requires a significant investment in time and resources. Considerations are taken based on published data, the volume of tissue processed for each rat ulna and the overall cost of the microarray experiment. A thorough look into pooled vs. non-pooled samples prior to microarray completion gave us a better indication of how to get the most statistically relevant information out of our experimental model. We found that using non-pooled distribution would actually lower cost without reducing the power of our results. A pooled experimental design does not necessarily guarantee savings of cost unless the subject cost is low relative to the array cost (Shih 2004). Based on all of the above data, we decided to do a non-pooled microarray study.

8 References

1. Osteoporosis prevention, diagnosis, and therapy. NIH Consens Statement2000. p. 1-45.

2. Agrawal D, Chen T, Irby R, Quackenbush J, Chambers AF, Szabo M, et al. Osteopontin identified as lead marker of colon cancer progression, using pooled sample expression profiling. J Natl Cancer Inst. 2002;94(7):513-21.

3. Ai-Aql ZS, Alagl AS, Graves DT, Gerstenfeld LC, Einhorn TA. Molecular mechanisms controlling bone formation during fracture healing and distraction osteogenesis. J Dent Res. 2008;87(2):107-18.

4. Akhter MP, Cullen DM, Pedersen EA, Kimmel DB, Recker RR. Bone response to in vivo mechanical loading in two breeds of mice. Calcif Tissue Int. 1998;63(5):442-9.

5. Alagiakrishnan K, Juby A, Hanley D, Tymchak W, Sclater A. Role of vascular factors in osteoporosis. J Gerontol A Biol Sci Med Sci. 2003;58(4):362-6.

6. Alam I, Warden SJ, Robling AG, Turner CH. Mechanotransduction in bone does not require a functional cyclooxygenase-2 (COX-2) gene. J Bone Miner Res. 2005;20(3):438-46.

7. Arany Z, Foo SY, Ma Y, Ruas JL, Bommi-Reddy A, Girnun G, et al. HIF-independent regulation of VEGF and angiogenesis by the transcriptional coactivator PGC-1alpha. Nature. 2008;451(7181):1008-12.

8. Armstrong VJ, Muzylak M, Sunters A, Zaman G, Saxon LK, Price JS, et al. Wnt/beta-catenin signaling is a component of osteoblastic bone cell early responses to load-bearing and requires estrogen receptor alpha. J Biol Chem. 2007;282(28):20715-27.

9. Beck TJ, Ruff CB, Mourtada FA, Shaffer RA, Maxwell-Williams K, Kao GL, et al. Dual-energy X-ray absorptiometry derived structural geometry for stress fracture prediction in male U.S. Marine Corps recruits. J Bone Miner Res. 1996;11(5):645-53.

10. Bentolila V, Boyce TM, Fyhrie DP, Drumb R, Skerry TM, Schaffler MB. Intracortical remodeling in adult rat long bones after fatigue loading. Bone. 1998;23(3):275-81.

11. Berchner-Pfannschmidt U, Frede S, Wotzlaw C, Fandrey J. Imaging of the hypoxia-inducible factor pathway: insights into oxygen sensing. Eur Respir J. 2008;32(1):210-7.

12. Blau M, Ganatra R, Bender MA. 18 F-fluoride for bone imaging. Semin Nucl Med. 1972;2(1):31-7.

13. Bonewald LF, Johnson ML. Osteocytes, mechanosensing and Wnt signaling. Bone. 2008;42(4):606-15.

14. Bowman S, Guo XE, Cheng DW, Keaveny TM, Gibson LJ, Hayes WC, McMahon TA. Creep contributes to the fatigue behavior of bovine trabecular bone. J Biomech Eng. 1998;120(5):647-54.

15. Bowman SM, Keaveny TM, Gibson LJ, Hayes WC, McMahon TA. Compressive creep behavior of bovine trabecular bone. J Biomech. 1994;27(3):301-10.

16. Brandi ML, Collin-Osdoby P. Vascular biology and the skeleton. J Bone Miner Res. 2006;21(2):183-92.

17. Burkhardt R, Kettner G, Bohm W, Schmidmeier M, Schlag R, Frisch B, et al. Changes in trabecular bone, hematopoiesis and bone marrow vessels in aplastic anemia, primary osteoporosis, and old age: a comparative histomorphometric study. Bone. 1987;8(3):157-64.

18. Burr DB. Bone, exercise, and stress fractures. Exerc Sport Sci Rev. 1997;25:171-94.

19. Burr DB, Hooser M. Alterations to the en bloc basic fuchsin staining protocol for the demonstration of microdamage produced in vivo. Bone. 1995;17(4):431-3.

20. Caler WE, Carter DR. Bone creep-fatigue damage accumulation. J Biomech. 1989;22(6-7):625-35.

21. Carter DR, Caler WE. A cumulative damage model for bone fracture. J Orthop Res. 1985;3(1):84-90.

22. Carter DR, Hayes WC. Fatigue life of compact bone--I. Effects of stress amplitude, temperature and density. J Biomech. 1976;9(1):27-34.

23. Carter DR, Hayes WC. Compact bone fatigue damage--I. Residual strength and stiffness. J Biomech. 1977;10(5-6):325-37.

24. Carvalho RS, Einhorn TA, Lehmann W, Edgar C, Al-Yamani A, Apazidis A, et al. The role of angiogenesis in a murine tibial model of distraction osteogenesis. Bone. 2004;34(5):849-61.

25. Castillo AB, Alam I, Tanaka SM, Levenda J, Li J, Warden SJ, et al. Low-amplitude, broad-frequency vibration effects on cortical bone formation in mice. Bone. 2006;39(5):1087.

26. Chen XY, Zhang XZ, Guo Y, Li RX, Lin JJ, Wei Y. The establishment of a mechanobiology model of bone and functional adaptation in response to mechanical loading. Clin Biomech (Bristol, Avon). 2008;23 Suppl 1:S88-95.

27. Cho TJ, Gerstenfeld LC, Einhorn TA. Differential temporal expression of members of the transforming growth factor beta superfamily during murine fracture healing. J Bone Miner Res. 2002;17(3):513-20.

28. Colnot CI, Helms JA. A molecular analysis of matrix remodeling and angiogenesis during long bone development. Mech Dev. 2001;100(2):245-50.

29. Colopy SA, Benz-Dean J, Barrett JG, Sample SJ, Lu Y, Danova NA, et al. Response of the osteocyte syncytium adjacent to and distant from linear microcracks during adaptation to cyclic fatigue loading. Bone. 2004;35(4):881-91.

30. Cooper C. The crippling consequences of fractures and their impact on quality of life. Am J Med. 1997;103(2A):12S-7S; discussion 7S-9S.

31. Cotton JR WK, Zioupos P, Taylor M. Damage rate is a predictor of fatigue life and creep strain rate in tensile fatigue of human cortical bone samples. J Biomech Eng. 2005;127(2):213-9.

32. Cowin SC, Weinbaum S, Zeng Y. A case for bone canaliculi as the anatomical site of strain generated potentials. J Biomech. 1995;28(11):1281-97.

33. Danova NA, Colopy SA, Radtke CL, Kalscheur VL, Markel MD, Vanderby R, et al. Degradation of bone structural properties by accumulation and coalescence of microcracks. Bone. 2003;33(2):197-205.

34. Dean DB, Watson JT, Moed BR, Zhang Z. Role of bone morphogenetic proteins and their antagonists in healing of bone fracture. Front Biosci. 2009;14:2878-88.

35. Deckers MM, van Bezooijen RL, van der Horst G, Hoogendam J, van Der Bent C, Papapoulos SE, et al. Bone morphogenetic proteins stimulate angiogenesis through osteoblast-derived vascular endothelial growth factor A. Endocrinology. 2002;143(4):1545-53.

36. Dimitriou ID, Clemenza L, Scotter AJ, Chen G, Guerra FM, Rottapel R. Putting out the fire: coordinated suppression of the innate and adaptive immune systems by SOCS1 and SOCS3 proteins. Immunol Rev. 2008;224:265-83.

37. Dimitriou R, Tsiridis E, Giannoudis PV. Current concepts of molecular aspects of bone healing. Injury. 2005;36(12):1392-404.

38. Dinarello CA. Immunological and inflammatory functions of the interleukin-1 family. Annu Rev Immunol. 2009;27:519-50.

39. Einhorn TA. The cell and molecular biology of fracture healing. Clin Orthop Relat Res. 1998(355 Suppl):S7-21.

40. Fang TD, Salim A, Xia W, Nacamuli RP, Guccione S, Song HM, et al. Angiogenesis is required for successful bone induction during distraction osteogenesis. J Bone Miner Res. 2005;20(7):1114-24.

41. Ferrara N. Role of vascular endothelial growth factor in regulation of physiological angiogenesis. Am J Physiol Cell Physiol. 2001;280(6):C1358-66.

42. Fondrk M, Bahniuk E, Davy DT, Michaels C. Some viscoplastic characteristics of bovine and human cortical bone. J Biomech. 1988;21(8):623-30.

43. Fong TA, Shawver LK, Sun L, Tang C, App H, Powell TJ, et al. SU5416 is a potent and selective inhibitor of the vascular endothelial growth factor receptor (Flk-1/KDR) that inhibits tyrosine kinase catalysis, tumor vascularization, and growth of multiple tumor types. Cancer Res. 1999;59(1):99-106.

44. Forwood MR, Turner CH. The response of rat tibiae to incremental bouts of mechanical loading: a quantum concept for bone formation. Bone. 1994;15(6):603-9.

45. Forwood MRaT, C.H. Skeletal adaptations to mechanical usage: results from tibial loading studies in rats. Bone. 1995;17(197S-205S).

46. Friis T, Hansen AB, Houen G, Engel AM. Influence of angiogenesis inhibitors on endothelial cell morphology in vitro. Apmis. 2006;114(3):211-24.

47. Frost H. Bone "mass" and the "mechanostat": a proposal. Anat Record. 1987a;219:1-9.

48. Frost HM. Mechanical determinants of bone modeling. Metab Bone Dis Relat Res. 1982;4(4):217-29.

49. Frost HM. Bone "mass" and the "mechanostat": a proposal. Anat Record. 1987b;219:1-9.

50. Frost HM. Perspectives: bone's mechanical usage windows. . Bone Miner. 1992;19:257-71.

51. Frost HM. The Utah paradigm of skeletal physiology: an overview of its insights for bone, cartilage and collagenous tissue organs. J Bone Miner Metab. 2000;18(6):305-16.

52. Genant HK, Bautovich GJ, Singh M, Lathrop KA, Harper PV. Bone-seeking radionuclides: an in vivo study of factors affecting skeletal uptake. Radiology. 1974;113(2):373-82.

53. Georges S, Ruiz Velasco C, Trichet V, Fortun Y, Heymann D, Padrines M. Proteases and bone remodelling. Cytokine Growth Factor Rev. 2009;20(1):29-41.

54. Gerber HP, Vu TH, Ryan AM, Kowalski J, Werb Z, Ferrara N. VEGF couples hypertrophic cartilage remodeling, ossification and angiogenesis during endochondral bone formation. Nat Med. 1999;5(6):623-8.

55. Gerstenfeld LC, Cullinane DM, Barnes GL, Graves DT, Einhorn TA. Fracture healing as a post-natal developmental process: molecular, spatial, and temporal aspects of its regulation. J Cell Biochem. 2003a;88(5):873-84.

56. Gerstenfeld LC, Einhorn TA. Developmental aspects of fracture healing and the use of pharmacological agents to alter healing. J Musculoskelet Neuronal Interact. 2003b;3(4):297-303; discussion 20-1.

57. Ghadjar P, Rubie C, Aebersold DM, Keilholz U. The chemokine CCL20 and its receptor CCR6 in human malignancy with focus on colorectal cancer. Int J Cancer. 2009;125(4):741-5.

58. Glowacki J. Angiogenesis in fracture repair. Clin Orthop Relat Res. 1998(355 Suppl):S82-9.

59. Goodship AE, Lanyon LE, McFie H. Functional adaptation of bone to increased stress. An experimental study. J Bone Joint Surg Am. 1979;61(4):539-46.

60. Haroon ZA, Amin K, Saito W, Wilson W, Greenberg CS, Dewhirst MW. SU5416 delays wound healing through inhibition of TGF-beta 1 activation. Cancer Biol Ther. 2002;1(2):121-6.

61. Hassler CR, Rybicki EF, Cummings KD, Clark LC. Quantification of bone stresses during remodeling. J Biomech. 1980;13(2):185-90.

62. Hausman MR, Schaffler MB, Majeska RJ. Prevention of fracture healing in rats by an inhibitor of angiogenesis. Bone. 2001;29(6):560-4.

63. Heiner DE, Meyer MH, Frick SL, Kellam JF, Fiechtl J, Meyer RA, Jr. Gene expression during fracture healing in rats comparing intramedullary fixation to plate fixation by DNA microarray. J Orthop Trauma. 2006;20(1):27-38.

64. Hert J, Liskova M, Landrgot B. Influence of the long-term, continuous bending on the bone. An experimental study on the tibia of the rabbit. Folia Morphol (Praha). 1969;17(4):389-99.

65. Hsieh YF, Robling AG, Ambrosius WT, Burr DB, Turner CH. Mechanical loading of diaphyseal bone in vivo: the strain threshold for an osteogenic response varies with location. J Bone Miner Res. 2001a;16(12):2291-7.

66. Hsieh YF, Silva MJ. In vivo fatigue loading of the rat ulna induces both bone formation and resorption and leads to time-related changes in bone mechanical properties and density. J Orthop Res. 2002;20(4):764-71.

67. Hsieh YF, Turner CH. Effects of loading frequency on mechanically induced bone formation. J Bone Miner Res. 2001b;16(5):918-24.

68. Huss WJ, Barrios RJ, Greenberg NM. SU5416 selectively impairs angiogenesis to induce prostate cancer-specific apoptosis. Mol Cancer Ther. 2003;2(7):611-6.

69. Iqbal J, Zaidi M. Molecular regulation of mechanotransduction. Biochem Biophys Res Commun. 2005;328(3):751-5.

70. Jacobsen KA, Al-Aql ZS, Wan C, Fitch JL, Stapleton SN, Mason ZD, et al. Bone formation during distraction osteogenesis is dependent on both VEGFR1 and VEGFR2 signaling. J Bone Miner Res. 2008;23(5):596-609.

71. Jazrawi LM, Majeska RJ, Klein ML, Kagel E, Stromberg L, Einhorn TA. Bone and cartilage formation in an experimental model of distraction osteogenesis. J Orthop Trauma. 1998;12(2):111-6.

72. Johnson LC, Stradford HT, Geis RW, Dineen JR, Kerley E. Histogenesis of stress fractures. Journal of Bone and Joint Surgery. 1963;45A:1542.

73. Jones BH, Harris JM, Vinh TN, Rubin C. Exercise-induced stress fractures and stress reactions of bone: epidemiology, etiology, and classification. Exerc Sport Sci Rev. 1989;17:379-422.

74. Katanasaka Y, Ida T, Asai T, Shimizu K, Koizumi F, Maeda N, et al. Antiangiogenic cancer therapy using tumor vasculature-targeted liposomes encapsulating 3-(3,5-dimethyl-1H-pyrrol-2-ylmethylene)-1,3-dihydro-indol-2-one, SU5416. Cancer Lett. 2008;270(2):260-8.

75. Kawamoto K, Matsuda H. Nerve growth factor and wound healing. Prog Brain Res. 2004;146:369-84.

76. Kendziorski C, Irizarry RA, Chen KS, Haag JD, Gould MN. On the utility of pooling biological samples in microarray experiments. Proc Natl Acad Sci U S A. 2005;102(12):4252-7.

77. Kesavan C, Mohan S, Oberholtzer S, Wergedal JE, Baylink DJ. Mechanical loading-induced gene expression and BMD changes are different in two inbred mouse strains. J Appl Physiol. 2005;99(5):1951-7.

78. Khan SN, Solaris J, Ramsey KE, Yang X, Bostrom MP, Stephan D, et al. Identification of novel gene expression in healing fracture callus tissue by DNA microarray. Hss J. 2008;4(2):149-60.

79. Knothe Tate ML, Knothe U. An ex vivo model to study transport processes and fluid flow in loaded bone. J Biomech. 2000a;33(2):247-54.

80. Knothe Tate ML, Niederer P. A theoretical FE-based model developed to predict the relative contribution of convective and diffusive transport mechanisms for the maintenance of local equilibria within cortical bone. Clegg S, editor. New York: The American Society of Mechanical Engineers; 1998.

81. Knothe Tate ML, Steck R, Forwood MR, Niederer P. In vivo demonstration of load-induced fluid flow in the rat tibia and its potential implications for processes associated with functional adaptation. J Exp Biol. 2000b;203(Pt 18):2737-45.

82. Ko FN, Wu CC, Kuo SC, Lee FY, Teng CM. YC-1, a novel activator of platelet guanylate cyclase. Blood. 1994;84(12):4226-33.

83. Komori T. Regulation of bone development and maintenance by Runx2. Front Biosci. 2008;13:898-903.

84. Kotha SP, Hsieh YF, Strigel RM, Muller R, Silva MJ. Experimental and finite element analysis of the rat ulnar loading model-correlations between strain and bone formation following fatigue loading. J Biomech. 2004;37(4):541-8.

85. Krishnan V, Ma Y, Moseley J, Geiser A, Friant S, Frolik C. Bone anabolic effects of sonic/indian hedgehog are mediated by bmp-2/4-dependent pathways in the neonatal rat metatarsal model. Endocrinology. 2001;142(2):940-7.

86. Kubota T, Michigami T, Ozono K. Wnt signaling in bone metabolism. J Bone Miner Metab. 2009;27(3):265-71.

87. Lanyon LE, Magee PT, Baggott DG. The relationship of functional stress and strain to the processes of bone remodelling. An experimental study on the sheep radius. J Biomech. 1979;12(8):593-600.

88. Lanyon LE, Rubin CT. Static vs dynamic loads as an influence on bone remodelling. Journal of Biomechanics. 1984;17(12):897.

89. Lau KH, Kapur S, Kesavan C, Baylink DJ. Up-regulation of the Wnt, estrogen receptor, insulin-like growth factor-I, and bone morphogenetic protein pathways in C57BL/6J osteoblasts as opposed to C3H/HeJ osteoblasts in part contributes to the differential anabolic response to fluid shear. J Biol Chem. 2006;281(14):9576-88.

90. Lecaille F, Bromme D, Lalmanach G. Biochemical properties and regulation of cathepsin K activity. Biochimie. 2008;90(2):208-26.

91. Li J, Burr DB, Turner CH. Suppression of prostaglandin synthesis with NS-398 has different effects on endocortical and periosteal bone formation induced by mechanical loading. Calcif Tissue Int. 2002;70(4):320-9.

92. Li J, Miller MA, Hutchins GD, Burr DB. Imaging bone microdamage in vivo with positron emission tomography. Bone. 2005;37(6):819-24.

93. Li KC, Zernicke RF, Barnard RJ, Li AF. Effects of a high fat-sucrose diet on cortical bone morphology and biomechanics. Calcif Tissue Int. 1990;47(5):308-13.

94. Liao D, Johnson RS. Hypoxia: a key regulator of angiogenesis in cancer. Cancer Metastasis Rev. 2007;26(2):281-90.

95. Liedert A, Kaspar D, Blakytny R, Claes L, Ignatius A. Signal transduction pathways involved in mechanotransduction in bone cells. Biochem Biophys Res Commun. 2006;349(1):1-5.

96. Lohela M, Bry M, Tammela T, Alitalo K. VEGFs and receptors involved in angiogenesis versus lymphangiogenesis. Curr Opin Cell Biol. 2009;21(2):154-65.

97. Lynch JA, Silva MJ. In vivo static creep loading of the rat forelimb reduces ulnar structural properties at time-zero and induces damage-dependent woven bone formation. Bone. 2008;42(5):942-9.

98. Ma J, Li S, Reed K, Guo P, Gallo JM. Pharmacodynamic-mediated effects of the angiogenesis inhibitor SU5416 on the tumor disposition of temozolomide in subcutaneous and intracerebral glioma xenograft models. J Pharmacol Exp Ther. 2003;305(3):833-9.

99. Maes C, Carmeliet P, Moermans K, Stockmans I, Smets N, Collen D, et al. Impaired angiogenesis and endochondral bone formation in mice lacking the vascular endothelial growth factor isoforms VEGF164 and VEGF188. Mech Dev. 2002;111(1-2):61-73.

100. Maruyama Z, Yoshida CA, Furuichi T, Amizuka N, Ito M, Fukuyama R, et al. Runx2 determines bone maturity and turnover rate in postnatal bone development and is involved in bone loss in estrogen deficiency. Dev Dyn. 2007;236(7):1876-90.

101. Matsuzaki H, Wohl GR, Novack DV, Lynch JA, Silva MJ. Damaging fatigue loading stimulates increases in periosteal vascularity at sites of bone formation in the rat ulna. Calcif Tissue Int. 2007;80(6):391-9.

102. McKenzie J, Silva, MJ. Differences in angiogenesis and cell proliferation distinguish woven and lamellar bone formation following mechanical loading in the rat ulna. Submitted for publication. 2009.

103. Meade JB, Cowin SC, Klawitter JJ, Van Buskirk WC, Skinner HB. Bone remodeling due to continuously applied loads. Calcif Tissue Int. 1984;36 Suppl 1:S25-30.

104. Meyer MH, Etienne W, Meyer RA, Jr. Altered mRNA expression of genes related to nerve cell activity in the fracture callus of older rats: A randomized, controlled, microarray study. BMC Musculoskelet Disord. 2004;5:24.

105. Mollace V, Muscoli C, Masini E, Cuzzocrea S, Salvemini D. Modulation of prostaglandin biosynthesis by nitric oxide and nitric oxide donors. Pharmacol Rev. 2005;57(2):217-52.

106. Mori S LJ, Kawaguchi Y. The histological appearance of stress fractures. In: Burr D, Milgrom C, editor. Musculoskeletal fatigue and stress fractures: Boca Raton: CRC Press; 2001. p. 151-9.

107. Mosley JR, Lanyon LE. Growth rate rather than gender determines the size of the adaptive response of the growing skeleton to mechanical strain. Bone. 2002;30(1):314-9.

108. Mosley JR, March BM, Lynch J, Lanyon LE. Strain magnitude related changes in whole bone architecture in growing rats. Bone. 1997;20(3):191-8.

109. Ono M. Molecular links between tumor angiogenesis and inflammation: inflammatory stimuli of macrophages and cancer cells as targets for therapeutic strategy. Cancer Sci. 2008;99(8):1501-6.

110. Pacicca DM, Patel N, Lee C, Salisbury K, Lehmann W, Carvalho R, et al. Expression of angiogenic factors during distraction osteogenesis. Bone. 2003;33(6):889-98.

111. Pattin CA, Caler WE, Carter DR. Cyclic mechanical property degradation during fatigue loading of cortical bone. Journal of Biomechanics. 1996;29(1):69.

112. Pechak DG, Kujawa MJ, Caplan AI. Morphology of bone development and bone remodeling in embryonic chick limbs. Bone. 1986;7(6):459-72.

113. Powis G, Kirkpatrick L. Hypoxia inducible factor-1alpha as a cancer drug target. Mol Cancer Ther. 2004;3(5):647-54.

114. Pramer A, Furner S, Rice DP. Musculoskeletal Conditions in the United States American Academy of Orthopaedic Surgeons1999.

115. Renner F, Schmitz ML. Autoregulatory feedback loops terminating the NF-kappaB response. Trends Biochem Sci. 2009;34(3):128-35.

116. Robling A, Castillo AB, Turner CH. Biomechanical and Molecular Regulation of Bone Remodeling. Annu Rev Biomed Eng. 2006a.

117. Robling AG, Burr DB, Turner CH. Partitioning a daily mechanical stimulus into discrete loading bouts improves the osteogenic response to loading. J Bone Miner Res. 2000;15(8):1596-602.

118. Robling AG, Burr DB, Turner CH. Recovery periods restore mechanosensitivity to dynamically loaded bone. J Exp Biol. 2001a;204(Pt 19):3389-99.

119. Robling AG, Castillo AB, Turner CH. Biomechanical and Molecular Regulation of Bone Remodeling. Annu Rev Biomed Eng. 2006b.

120. Robling AG, Duijvelaar KM, Geevers JV, Ohashi N, Turner CH. Modulation of appositional and longitudinal bone growth in the rat ulna by applied static and dynamic force. Bone. 2001b;29(2):105-13.

121. Rosenkilde MM, Schwartz TW. The chemokine system -- a major regulator of angiogenesis in health and disease. Apmis. 2004;112(7-8):481-95.

122. Rubin CT, Gross TS, McLeod KJ, Bain SD. Morphologic stages in lamellar bone formation stimulated by a potent mechanical stimulus. J Bone Miner Res. 1995;10(3):488-95.

123. Rubin CT, Lanyon LE. Regulation of bone formation by applied dynamic loads. J Bone Joint Surg Am. 1984;66(3):397-402.

124. Rubin CT, Lanyon LE. Regulation of bone mass by mechanical strain magnitude. Calcif Tissue Int. 1985;37(4):411-7.

125. Rubin CT, Lanyon LE. Kappa Delta Award paper. Osteoregulatory nature of mechanical stimuli: function as a determinant for adaptive remodeling in bone. J Orthop Res. 1987;5(2):300-10.

126. Rundle CH, Wang H, Yu H, Chadwick RB, Davis EI, Wergedal JE, et al. Microarray analysis of gene expression during the inflammation and endochondral bone formation stages of rat femur fracture repair. Bone. 2006;38(4):521-9.

127. Salcedo R, Oppenheim JJ. Role of chemokines in angiogenesis: CXCL12/SDF-1 and CXCR4 interaction, a key regulator of endothelial cell responses. Microcirculation. 2003;10(3-4):359-70.

128. Sato M, Ochi T, Nakase T, Hirota S, Kitamura Y, Nomura S, et al. Mechanical tension-stress induces expression of bone morphogenetic protein (BMP)-2 and BMP-4, but not BMP-6, BMP-7, and GDF-5 mRNA, during distraction osteogenesis. J Bone Miner Res. 1999;14(7):1084-95.

129. Schaffler MB, Choi K, Milgrom C. Aging and matrix microdamage accumulation in human compact bone. Bone. 1995;17(6):521-25.

130. Seedhom BB, Takeda T, Tsubuku M, Wright V. Mechanical factors and patellofemoral osteoarthrosis. Annals of the Rheumatic Diseases. 1979;38(4):307-16.

131. Shaffer RA. Incidence and prevalence of stress fractures in military and athletic populations. In: Burr DB, Milgrom C, editors. Musculoskeletal fatigue and stress fractures: CRC Press; 2001. p. 1-14.

132. Shih JH, Michalowska AM, Dobbin K, Ye Y, Qiu TH, Green JE. Effects of pooling mRNA in microarray class comparisons. Bioinformatics. 2004;20(18):3318-25.

133. Shin DH, Kim JH, Jung YJ, Kim KE, Jeong JM, Chun YS, et al. Preclinical evaluation of YC-1, a HIF inhibitor, for the prevention of tumor spreading. Cancer Lett. 2007;255(1):107-16.

134. Silva M, Uthgenannt BA, Rutlin JR, Wohl GR, Lewis JS, Welch MJ. In vivo skeletal imaging of (18)F-fluoride with positron emission tomography reveals damage- and time-dependent responses to fatigue loading in the rat ulna. Bone. 2006a;39(2):229-36.

135. Silva MJ, Uthgenannt BA, Rutlin JR, Wohl GR, Lewis JS, Welch MJ. In vivo skeletal imaging of (18)F-fluoride with positron emission tomography reveals damage- and time-dependent responses to fatigue loading in the rat ulna. Bone. 2006b;39(2):229-36.

136. Simon AM, Manigrasso MB, O'Connor JP. Cyclo-oxygenase 2 function is essential for bone fracture healing. J Bone Miner Res. 2002;17(6):963-76.

137. Sin N, Meng L, Wang MQ, Wen JJ, Bornmann WG, Crews CM. The anti-angiogenic agent fumagillin covalently binds and inhibits the methionine aminopeptidase, MetAP-2. Proc Natl Acad Sci U S A. 1997;94(12):6099-103.

138. Sirois I, Cheung AM, Ward WE. Biomechanical bone strength and bone mass in young male and female rats fed a fish oil diet. Prostaglandins Leukot Essent Fatty Acids. 2003;68(6):415-21.

139. Smith EL, Gilligan C. Dose-response relationship between physical loading and mechanical competence of bone. Bone. 1996;18(1 Suppl):455-505.

140. Srinivasan S, Agans SC, King KA, Moy NY, Poliachik SL, Gross TS. Enabling bone formation in the aged skeleton via rest-inserted mechanical loading. Bone. 2003;33(6):946-55.

141. Sterling JC, Edelstein DW, Calvo RD, Webb R, 2nd. Stress fractures in the athlete. Diagnosis and management. Sports Med. 1992;14(5):336-46.

142. Street J, Bao M, deGuzman L, Bunting S, Peale FV, Jr., Ferrara N, et al. Vascular endothelial growth factor stimulates bone repair by promoting angiogenesis and bone turnover. Proc Natl Acad Sci U S A. 2002;99(15):9656-61.

143. Takamoto T, Sasaki M, Kuno T, Tamaki N. Flk-1 specific kinase inhibitor (SU5416) inhibited the growth of GS-9L glioma in rat brain and prolonged the survival. Kobe J Med Sci. 2001;47(4):181-91.

144. Tami AE, Nasser P, Schaffler MB, Knothe Tate ML. Noninvasive fatigue fracture model of the rat ulna. J Orthop Res. 2003;21(6):1018-24.

145. Torrance AG, Mosley JR, Suswillo RF, Lanyon LE. Noninvasive loading of the rat ulna in vivo induces a strain-related modeling response uncomplicated by trauma or periostal pressure. Calcif Tissue Int. 1994;54(3):241-7.

146. Trevino V, Falciani F, Barrera-Saldana HA. DNA microarrays: a powerful genomic tool for biomedical and clinical research. Mol Med. 2007;13(9-10):527-41.

147. Tsuji K, Bandyopadhyay A, Harfe BD, Cox K, Kakar S, Gerstenfeld L, et al. BMP2 activity, although dispensable for bone formation, is required for the initiation of fracture healing. Nat Genet. 2006;38(12):1424-9.

148. Turner CH, Forwood MR, Otter MW. Mechanotransduction in bone: do bone cells act as sensors of fluid flow? Faseb J. 1994a;8(11):875-8.

149. Turner CH, Forwood MR, Rho JY, Yoshikawa T. Mechanical loading thresholds for lamellar and woven bone formation. J Bone Miner Res. 1994b;9(1):87-97.

150. Turner CH, Owan I, Alvey T, Hulman J, Hock JM. Recruitment and proliferative responses of osteoblasts after mechanical loading in vivo determined using sustained-release bromodeoxyuridine. Bone. 1998;22(5):463-9.

151. Turner CH, Takano Y, Owan I, Murrell GA. Nitric oxide inhibitor L-NAME suppresses mechanically induced bone formation in rats. Am J Physiol. 1996;270(4 Pt 1):E634-9.

152. Turner CH, Warden SJ, Bellido T, Plotkin LI, Kumar N, Jasiuk I, et al. Mechanobiology of the skeleton. Sci Signal. 2009;2(68):pt3.

153. Uthgenannt BA, Kramer MH, Hwu JA, Wopenka B, Silva MJ. Skeletal self-repair: Stress fracture healing by rapid formation and densification of woven bone. J Bone Miner Res. 2007a;22(10):1548-56.

154. Uthgenannt BA, Silva MJ. Use of the rat forelimb compression model to create discrete levels of bone damage in vivo. J Biomech. 2007b;40(2):317-24.

155. van der Schaft DW, Seftor RE, Seftor EA, Hess AR, Gruman LM, Kirschmann DA, et al. Effects of angiogenesis inhibitors on vascular network formation by human endothelial and melanoma cells. J Natl Cancer Inst. 2004;96(19):1473-7.

156. van Hinsbergh VW, Koolwijk P. Endothelial sprouting and angiogenesis: matrix metalloproteinases in the lead. Cardiovasc Res. 2008;78(2):203-12.

157. Verborgt O, Gibson GJ, Schaffler MB. Loss of osteocyte integrity in association with microdamage and bone remodeling after fatigue in vivo. J Bone Miner Res. 2000;15(1):60-7.

158. Wang FS, Yang KD, Kuo YR, Wang CJ, Sheen-Chen SM, Huang HC, et al. Temporal and spatial expression of bone morphogenetic proteins in extracorporeal shock wave-promoted healing of segmental defect. Bone. 2003;32(4):387-96.

159. Wang J, Lou P, Henkin J. Selective inhibition of endothelial cell proliferation by fumagillin is not due to differential expression of methionine aminopeptidases. J Cell Biochem. 2000;77(3):465-73.

160. Weinbaum S, Cowin SC, Zeng Y. A model for the excitation of osteocytes by mechanical loading-induced bone fluid shear stresses. J Biomech. 1994;27(3):339-60.

161. Wohl GR, Towler DA, Silva MJ. Stress fracture healing: fatigue loading of the rat ulna induces upregulation in expression of osteogenic and angiogenic genes that mimic the intramembranous portion of fracture repair. Bone. 2009;44(2):320-30.

162. Wozney JM, Rosen V. Bone morphogenetic protein and bone morphogenetic protein gene family in bone formation and repair. Clin Orthop Relat Res. 1998(346):26-37.

163. Wu Q, Sample SJ, Baker TA, Thomas CF, Behan M, Muir P. Mechanical loading of a long bone induces plasticity in sensory input to the central nervous system. Neurosci Lett. 2009;463(3):254-7.

164. Xing W, Baylink D, Kesavan C, Hu Y, Kapoor S, Chadwick RB, et al. Global gene expression analysis in the bones reveals involvement of several novel genes and pathways in mediating an anabolic response of mechanical loading in mice. J Cell Biochem. 2005;96(5):1049-60.

165. Yao Z, Lafage-Proust MH, Plouet J, Bloomfield S, Alexandre C, Vico L. Increase of both angiogenesis and bone mass in response to exercise depends on VEGF. J Bone Miner Res. 2004;19(9):1471-80.

166. Yeo EJ, Chun YS, Cho YS, Kim J, Lee JC, Kim MS, et al. YC-1: a potential anticancer drug targeting hypoxia-inducible factor 1. J Natl Cancer Inst. 2003;95(7):516-25.

167. Zelzer E, McLean W, Ng YS, Fukai N, Reginato AM, Lovejoy S, et al. Skeletal defects in VEGF(120/120) mice reveal multiple roles for VEGF in skeletogenesis. Development. 2002;129(8):1893-904.

168. Zhang SD, Gant TW. Effect of pooling samples on the efficiency of comparative studies using microarrays. Bioinformatics. 2005;21(24):4378-83.

169. Zhao Q, Jia Y, Xiao Y. Cathepsin K: a therapeutic target for bone diseases. Biochem Biophys Res Commun. 2009;380(4):721-3.

170. Zhong XS, Zheng JZ, Reed E, Jiang BH. SU5416 inhibited VEGF and HIF-1alpha expression through the PI3K/AKT/p70S6K1 signaling pathway. Biochem Biophys Res Commun. 2004;324(2):471-80.

171. Zimmerman LB, De Jesus-Escobar JM, Harland RM. The Spemann organizer signal noggin binds and inactivates bone morphogenetic protein 4. Cell. 1996;86(4):599-606.